



**IChF**

Institute of Physical Chemistry PAS

# **Equilibrium constants determination for anthracycline-DNA interactions: from aqueous solution to single cell study**

Doctoral thesis

Ying Zhou

**Supervisor:** prof. dr hab. Robert Hołyst

The dissertation was prepared within the International PhD Studies at  
the Institute of Physical Chemistry of the Polish Academy of Sciences

Department of Soft Condensed Matter and Fluids

Kasprzaka 44/52, 01-224 Warsaw

Warsaw, March 2021

# Acknowledgements

This work can not be finished without the help of people around, I would like to show my sincere and great thanks to them.

**Prof. Robert Hołyst**, who supervises me in my whole Ph.D. study. With his guide, I start solving the biological problems in a more physical way. Also, with his training, I gain the confidence and skills to present my work in front of unfamiliar audiences. His enthusiasm, curiosity, and imagination in science will always encourage me in the future.

**Dr. Karina Kwapiszewska**, who teaches me everything related to cells. Whenever I meet problems, she is always there to help me.

**Dr. Xuzhu Zhang** and **dr. Haijing Meng**, who help me to adapt to the work and life in Poland at the beginning of my study.

**Dr. Krzysztof Sozański**, who passes me all of the knowledge about microscopes and fluorescence, from theory to practice.

**Krzysztof Bielec**, who helps me in experiment designing, problem discussions, and article writing.

My dearest friends **Yu-Ting Kao** and **Airit Agasty**, who help me to get through the tough time and always make me happy. **Dr. Pasitsuparoad Pakorn**, **dr. Grzegorz Bubak** and **dr. Tomasz Kalwarczyk**, who provide me with valuable suggestions and support in work. All of the members from the soft matter group, who are always there

to offer me help, either at work or in daily life.

In addition, my auxiliary supervisor **prof. Wilhelm Huck**, who offers me a one-year internship in his lab and gives me a chance to study the origin of life. **Mahesh Vibhute** and **Ludo Schoenmakers**, who help me in working with synthetic cells. All of the lab members from the Huck group at Radboud University Nijmegen in the Netherlands, who create a friendly atmosphere for me to work there.

The last but not the least, my **parents** and **friends** in China, their endless support is my power to pursue light and truth.

This research is part of a project that has received funding from the European Union's Horizon 2020 research and innovation programme under the Marie Skłodowska-Curie grant agreement No. 711859 and scientific work funded from the financial resources for science in the years 2017-2022 awarded by the Polish Ministry of Science and Higher Education for the implementation of an international co-financed project.



# List of publications

## Publications related to this work:

1. **Y. Zhou**, K. Bielec, P. Pasitsuparoad, and R. Holyst, "Single molecule brightness analysis for determination of anticancer drugs interactions with DNA," *The Analyst*, vol. 145, no. 20, pp. 6600–6606, 2020.
2. X. Zhang, A. Poniewierski, K. Sozański, **Y. Zhou**, A. Brzozowska-Elliott, R. Holyst. "Fluorescence correlation spectroscopy for multiple-site equilibrium binding: a case of doxorubicin-DNA interaction," *Phys Chem Chem Phys*, vol. 21, no. 3, pp. 1572-1577, 2019.

## Other publications:

1. **Y. Zhou**, J. Chen, Z. Wang, and H. Liu, "Evaluating the risk of tumors diseases based on measurement of urinary and serumal antioxidants using the new agar diffusion methods," *Oxidative Medicine and Cellular Longevity*, vol. 2017, no. 2017, pp. 6578453, 2017.
2. **Y. Zhou**, N. Xu, M. Zhang, and H. Liu, "A new method for measuring total antioxidant capacity in urine using the iodine starch agar based on agar diffusion," *Current Analytical Chemistry*, vol. 12, no. 5, pp. 425–430, 2016.
3. **Y. Zhou**, M. Zhang, and H. Liu, "Total antioxidant capacity of serum determined using the potassium permanganate agar method based on serum diffusion in agar," *Bioinorganic Chemistry and Applications*, vol. 2015, no. 2015, pp. 406071, 2015.

# Abstract

Anthracyclines are the most effective and important chemical compounds used in cancer treatment. Among them, doxorubicin hydrochloride (DOX), daunorubicin hydrochloride (DNR), epirubicin hydrochloride (EPR), and idarubicin hydrochloride (IDR) are the most widely used ones. They induce the apoptosis of cancer cells by binding with deoxyribonucleic acid (DNA). In novel anticancer drug discoveries or cancer treatment, scientists are always seeking an anticancer drug with a tight binding with DNA. The equilibrium constants ( $K$ ) of anthracycline-DNA interactions are determined to quantify how strong the anthracyclines can bind with DNA. Association constant ( $K_a$ ) and dissociation constant ( $K_d$ ) are two special cases of  $K$ .  $K_a$  is the inverse of  $K_d$ . The larger the  $K_a$  value, the smaller the  $K_d$  value, the stronger the drug binding, and vice versa. However, currently, there are few issues to determine the  $K$  accurately.

First of all, the  $K$  values for reported anthracyclines vary from  $10^4 \text{ M}^{-1}$  to  $10^8 \text{ M}^{-1}$ . As a result, a 4-order of magnitude error occurs in determining the effective anthracycline concentration to form anthracycline-DNA complexes. The second issue is the detection limit. Most of the experiments are conducted with an anthracycline concentration at the micromolar level. However, anthracyclines may aggregate with each other at such a high concentration. The self-aggregation of anthracyclines can compete with anthracycline-DNA interactions, leading the equilibrium of anthracycline-DNA interactions to be shifted. Consequently, the  $K$  values of anthracycline-DNA interactions

are altered. Thirdly, the action mechanisms of anthracyclines are still full of debates. Researchers have widely accepted that anthracyclines react with DNA through intercalation. However, my recent reports have shown an additional reaction occurring between anthracyclines and anthracycline-DNA complexes. The reaction is dominated when the amount of anthracyclines is in large excess to DNA binding sites. The  $K$  value in such a reaction is 2-order smaller than that in the intercalation. Fourthly, the macromolecular crowding effect on  $K$  values. The previous reported  $K$  values are obtained in aqueous solution. However, the cell nucleus, where anthracycline-DNA interactions take place, is packed with macromolecules. The macromolecular crowding can shift the equilibrium of anthracycline-DNA interactions and further change the  $K$  values. Accordingly, the  $K$  values determined in aqueous solution may differ significantly from their values from *in vivo* experiments. The last issue is that there are fewer reports concerning the  $K$  values for DOX analogs: DNR, EPR, and IDR. Therefore, we addressed these issues by studying the fluorescence property changes of anthracyclines in interactions.

At the beginning of my research, I cleared the self-aggregation issue of anthracyclines. By using UV-Visible (Uv-Vis) spectroscopic techniques, I found anthracyclines had no self-aggregations at the micromolar level (see chapter 2). Next, I determined the  $K$  for anthracycline-DNA interactions at the nanomolar scale with fluorescence correlation spectroscopy (FCS) and single-molecule brightness (MB) analysis methods. Moreover, with the single-MB analysis method, I confirmed the formation of DOX-(DOX-DNA) complexes and determined the  $K$  for DOX analogs (see chapter 3). Lastly, I developed a method based on the photobleaching of DOX to determine the  $K$  of DOX-DNA interaction in single cells, and I discussed the possible reasons for the smaller  $K$  determined in cells (see chapter 4). In chapter 5, I concluded for the whole study. In

chapter 6, I showed the future work to do to have a more accurate  $K$  determination in cells.

Overall, the thesis provides the vision of anthracycline-DNA interactions at the single-molecular level, and gives a clue in new drug development and cancer treatment.

# Contents

<b>Acknowledgements</b>	<b>iii</b>
<b>List of publications</b>	<b>iv</b>
<b>Abstract</b>	<b>vii</b>
<b>1 Introduction</b>	<b>1</b>
1.1 Anthracyclines and mechanisms of anthracycline-DNA interactions . . . . .	1
1.1.1 Structure of anthracyclines . . . . .	1
1.1.2 Mechanisms of anthracycline-DNA interactions . . . . .	2
1.2 Equilibrium constants of anthracycline-DNA interactions . . . . .	5
1.2.1 Basic definitions and equations . . . . .	5
1.2.2 Approaches to determine the equilibrium constants in anthracycline-DNA interactions . . . . .	6
1.2.3 Reported equilibrium constants for anthracycline-DNA interactions in aqueous solution . . . . .	8
1.3 Equilibrium constants in crowded environment . . . . .	9
1.3.1 Macromolecules and macromolecular crowding . . . . .	10
1.3.2 Macromolecular crowding and equilibrium constant . . . . .	10

CONTENTS	ix
1.3.3 Equilibrium constant determined in crowded environment . . .	17
1.4 Techniques used to determine the equilibrium constants in this work .	19
1.4.1 Fluorescence . . . . .	19
1.4.2 FCS method . . . . .	21
1.4.3 Single-MB analysis method . . . . .	30
1.4.4 Fluorescence decay fitting for the photobleached anthracyclines	34
<b>2 Aggregation of anthracyclines</b>	<b>39</b>
2.1 Materials and instruments . . . . .	39
2.1.1 Materials . . . . .	39
2.1.2 Instruments . . . . .	40
2.2 Results and discussions . . . . .	40
2.3 Summary . . . . .	42
<b>3 Equilibrium constants determination in aqueous solution</b>	<b>43</b>
3.1 Materials, instruments, methods, and working flow . . . . .	44
3.1.1 Materials . . . . .	44
3.1.2 Instruments . . . . .	45
3.1.3 Methods . . . . .	45
3.1.4 Working flow . . . . .	46
3.2 Results and discussions . . . . .	47
3.2.1 Equilibrium constants determination with FCS method . . . .	47

CONTENTS	x
3.2.2 Equilibrium constants determination with single-MB analysis method . . . . .	52
3.3 Summary . . . . .	62
<b>4 Equilibrium constants determination in single living cells</b>	<b>64</b>
4.1 Materials, instruments, methods, and working flow . . . . .	65
4.1.1 Materials . . . . .	65
4.1.2 Instruments . . . . .	67
4.1.3 Methods . . . . .	67
4.1.4 Working flow . . . . .	67
4.2 Results and discussions . . . . .	68
4.2.1 Cell selection . . . . .	68
4.2.2 Equilibrium constants determination in single living cells . . .	68
4.2.3 Possible mechanisms for the smaller equilibrium constants de- termined in cells . . . . .	70
4.2.4 Spatial equilibrium constants determination within an individ- ual cell . . . . .	74
4.3 Summary . . . . .	75
<b>5 Conclusions</b>	<b>77</b>
<b>6 Outlook</b>	<b>79</b>
<b>Bibliography</b>	<b>82</b>

CONTENTS	xi
<b>A List of abbreviations</b>	<b>A-1</b>
<b>B Parameters in a typical measurement</b>	<b>B-1</b>
B.1 Equilibrium constants determination with FCS method . . . . .	B-1
B.2 Equilibrium constants determination with single-MB analysis method	B-2
B.3 DNA concentration calculation in the single cells . . . . .	B-3

# Introduction

---

## 1.1 Anthracyclines and mechanisms of anthracycline-DNA interactions

According to the therapeutic targets, anticancer drugs are divided into 5 groups [1]. Those anticancer drugs which directly kill cancer cells or inhibit the growth of cancer cells are called chemotherapeutic agents. Among them, anthracyclines are the most effective ones.

### 1.1.1 Structure of anthracyclines

In clinical, [DOX](#), [DNR](#), [EPR](#) and [IDR](#) are four of the most important anthracyclines [2, 3, 4]. Basically, they contain three domains: an aromatic backbone (blue background), an amino sugar on the side chain (yellow background), and substituents on the aromatic ring (red background) (see figure 1.1).

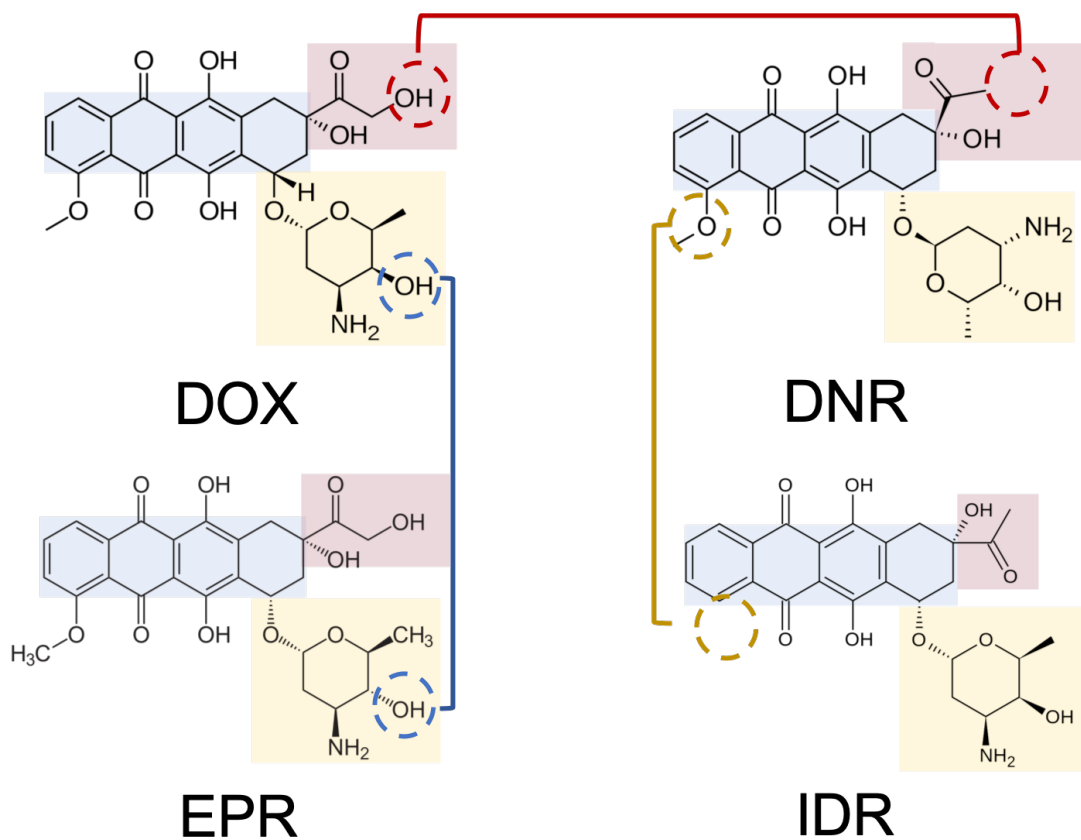


Figure 1.1: Structures of the most important anthracyclines. **DOX** and **DNR** contain a tetracyclic aglycone structure of four cyclohexane chains with a daunosamine sugar moiety. However, **DNR** is in absence of a hydroxyl group (red circle). Compared with **DOX**, **EPR** has an opposite chirality of hydroxyl group in daunosamine moiety (blue circle). **IDR** is identical to daunorubicin except the lack of 4-methoxy group on the ring (yellow circle).

### 1.1.2 Mechanisms of anthracycline-DNA interactions

Because of the three domains, anthracyclines can interact with **DNA** in different ways (see figure 1.2).

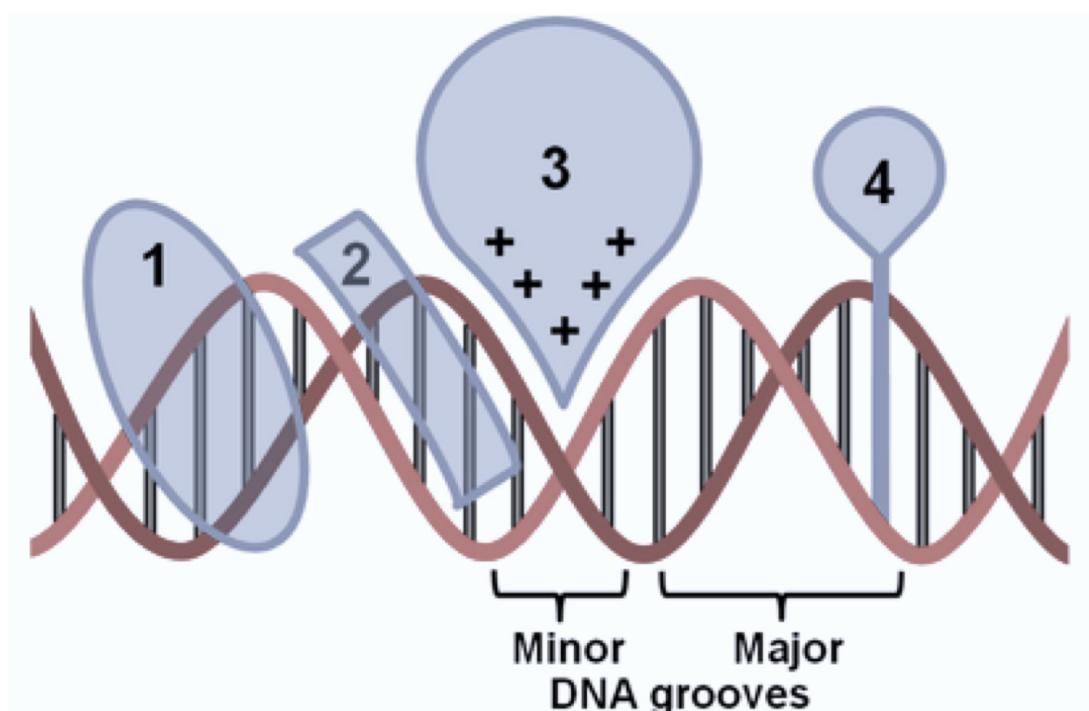


Figure 1.2: The action mechanisms of anthracyclines in the interactions with DNA. 1 and 2 are groove bindings, 3 is electrostatic binding, and 4 is intercalation. The figure is from Almaqwashi [5].

### A. Intercalation

The aromatic ring allows anthracyclines to intercalate into the base pair (bp) of DNA through  $\pi - \pi$  stacking, preferentially at 5'-pyrimidinepurine- 3' GC-rich sites. Because of intercalation, the polynucleotide structure of DNA is distorted, further the replication and transcription of DNA is inhibited. Intercalation is the most widely accepted mechanism in anthracycline-DNA interactions [6, 7, 8, 9, 10, 11, 12, 13].

### **B. Electrostatic binding**

In recent years, researchers also report the formation of external DOX-(DOX-DNA) aggregates in DOX-DNA interaction. When all of the intercalative sites on DNA are occupied, the excess DOX molecules overhang from the intercalated core of DOX-DNA complexes and form external aggregates [14]. In the formation of external aggregates, an electrostatic interaction could be involved, since the amino sugar group of DOX is positively charged while the DNA is negatively charged [5, 15]. Though currently, the formation of external aggregates is only reported in DOX-DNA interaction, the interaction mode could also apply to DNR-, EPR- and IDR-DNA interactions, because these anthracyclines share a similar structure with DOX.

### **C. Groove binding**

Anthracyclines can also stay in the minor groove of DNA through electrostatic interaction [5, 12, 14, 16, 17]. It is an intermediate step in the intercalation process, which helps anthracycline-DNA complexes to be stabilized.

### **D. Hydrogen bonding**

The substituents on the aromatic ring can also form hydrogen bonds with the bp of DNA, serving as an anchor to stabilize the anthracycline-DNA complexes. This type of interaction is identified by crystallographic and vibrational spectroscopic in previous reports [12, 18].

## 1.2 Equilibrium constants of anthracycline-DNA interactions

In the synthesis of novel anticancer drugs or cancer treatment, scientists are always looking for some anticancer drugs which can tightly bind with their targets. The strength of binding is quantified by two special cases of equilibrium constant ( $K$ ): association constant ( $K_a$ ) or dissociation constant ( $K_d$ ).  $K_a$  is the inverse of  $K_d$ . The larger the  $K_a$  value in interaction, the stronger the drug binding, and the higher the drug affinity. The opposite occurs when an anticancer has a low drug affinity [19, 20, 21]. The correct determination of  $K$  value is very important in pharmacodynamic (PD), because some important parameters (for instance, fractional occupancy– the fraction of all receptors that are bound to ligand) are calculated according to  $K_d$  [19].

### 1.2.1 Basic definitions and equations

If we consider the interaction between anthracycline and DNA as a simple reversible binding reaction. According to the simple model of law of mass action, the interaction between DNA and anthracycline (represented as "ANT" in formulas and equations in the following content) is [19, 22]:



where  $k_a$  and  $k_d$  is the association and dissociation rate constant respectively. At equilibrium state (eq), the association rate equals to the dissociation rate:

$$C_{ANT}^{eq} \cdot C_{DNA}^{eq} \cdot k_a = C_{ANT-DNA}^{eq} \cdot k_d \quad (1.2)$$

where  $C_{ANT}^{eq}$ ,  $C_{DNA}^{eq}$ , and  $C_{ANT-DNA}^{eq}$  are the concentration of anthracycline, DNA, and anthracycline-DNA complexes at equilibrium state respectively. Thus,  $K_a$  is given by:

$$K_a = \frac{1}{K_d} = \frac{k_a}{k_d} = \frac{C_{ANT-DNA}^{eq}}{C_{ANT}^{eq} \cdot C_{DNA}^{eq}} \quad (1.3)$$

### 1.2.2 Approaches to determine the equilibrium constants in anthracycline-DNA interactions

Currently, we can determine  $K$  by several experimental methods. We have listed the main experimental approaches in table 1.1. As each method has its pros and cons, to get a more accurate  $K$  value, researchers usually determine the  $K$  value with several methods based on different principles [14, 23]. Also, with the development of optic techniques, more and more rapid, simple and non-destructive techniques are used in  $K$  determination, especially in living cells [24, 25]. With the single-MB analysis method, the sensitivity of measurement can even reach a sub-picomolar level [26].

Table 1.1: Typical techniques used in equilibrium constants determination.

Categories	Typical techniques	Principles	Detection limits
Calorimetric	Isothermal titration calorimetry (ITC) [14, 27, 28, 29, 30]	Heat releasing	$\mu\text{M}$
measurements		or absorption	

**Table 1.1 continued from previous page**

	Differential scanning calorimetry (DSC) [14, 27, 31]		$\mu\text{M}$
Spectroscopic measurements	Circular dichroism spectroscopy (CD) [23, 32, 33]	Ellipticity changes	$\mu\text{M}$
	Surface plasmon resonance spectroscopy (SPR) [33, 34]	Refractive index changes	mM
	Resonance light scattering spectroscopy (RLS) [35, 36, 37, 38, 39]	Molecular size or shape change	mM
	UV-Visible (Uv-Vis) spectroscopy [14, 23, 40, 41, 42, 43, 44]	Florescence absorbance	$\mu\text{M}$
	Fluorescence spectroscopy [45, 46]	Florescence emission	$\mu\text{M}$
		FCS [47, 48]	Diffusion coefficient change
Fluorescence based techniques	Fluorescence recovery after photobleaching (FRAP) [49, 50]	Photon bleaching	$\mu\text{M}$
	Single-MB analysis [26]	MB change	pM

**Table 1.1 continued from previous page**

	Continuous photobleaching [51, 52]	Photon bleaching	nM
Potentiometric measurements	Cyclic voltammetry (CV) [42, 53, 54, 55]	Electrons transfer	$\mu$ M
Nuclear magnetic resonance chemical shift measurements	Nuclear magnetic resonance spectroscopy (NMR) [16, 56]	Chemical shift	$\mu$ M

### 1.2.3 Reported equilibrium constants for anthracycline-DNA interactions in aqueous solution

In table 1.2, we list the previously reported  $K$  values of anthracycline-DNA interactions in aqueous solution. However, as the  $K$  values vary orders of magnitude from report to report, there are debates regarding the accurate  $K$  values in anthracycline-DNA interactions. Some researchers consider the difference is caused by the measuring conditions, especially the ionic strength [15]; while other researchers propose the difference is brought by the novel action mechanism of anthracyclines [14]. Moreover, there are fewer reports concerning the  $K$  values for DOX analogs: DNR, EPR, and IDR.

Table 1.2: Association constants reported for anthracycline-DNA interactions.

<b>Anthracyclines</b>	<b>Methods</b>	<b>Ionic strength (mM)</b>	$K_a$ ( $\times 10^6 M^{-1}$ )
DOX	Fluorescence spectroscopy [16]	100	0.01
	ITC [57]	100	0.3
	FCS [47]	10	1.0
	Fluorescence spectroscopy [16]	63	13
	Fluorescence spectroscopy [14]	2.5	230
DNR	RLS [36]	200	0.02
	Second harmonic generation [58]	not mentioned	0.2
	CV[42]	200	1.2
EPR	Uv-Vis spectroscopy [41]	not mentioned	0.03
	Uv-Vis spectroscopy[44]	20	0.4
IDR	Uv-Vis spectroscopy [59]	not mentioned	0.02
	Fluorescence spectroscopy [9]	200	0.6

To make clear which  $K$  value is accurate for anthracycline-DNA interactions in table 1.2, we need to know the exact action mechanism of anthracyclines. Also, to exclude the influence of ionic strength, we need to conduct the experiment under physiological conditions.

### 1.3 Equilibrium constants in crowded environment

From table 1.2, we know the  $K$  values determined in aqueous solution are not accurate. The  $K$  value determined in cell nucleus is even unknown. However, *in vivo*, anthracycline-DNA interactions take place in cell nucleus. As the background macromolecules in cell nucleus may shift the equilibrium of anthracycline-DNA interactions, and further alter anthracycline affinity, the  $K$  values determined in aqueous solution can differ with that determined in cell nucleus. To get a more accurate anthracycline affinity *in vivo*, we should determine the  $K$  value of anthracycline-DNA interactions in

cell nucleus directly.

### 1.3.1 Macromolecules and macromolecular crowding

The nucleus is packed with macromolecules, including high-molecular chromatin, ribonucleo particles, and associated proteins. The concentrations of the macromolecules reach as high as 100-200 mg mL<sup>-1</sup>. Macromolecular crowding refers to an environments where various macromolecules are present at high total concentrations (see figure 1.3) [60, 61].

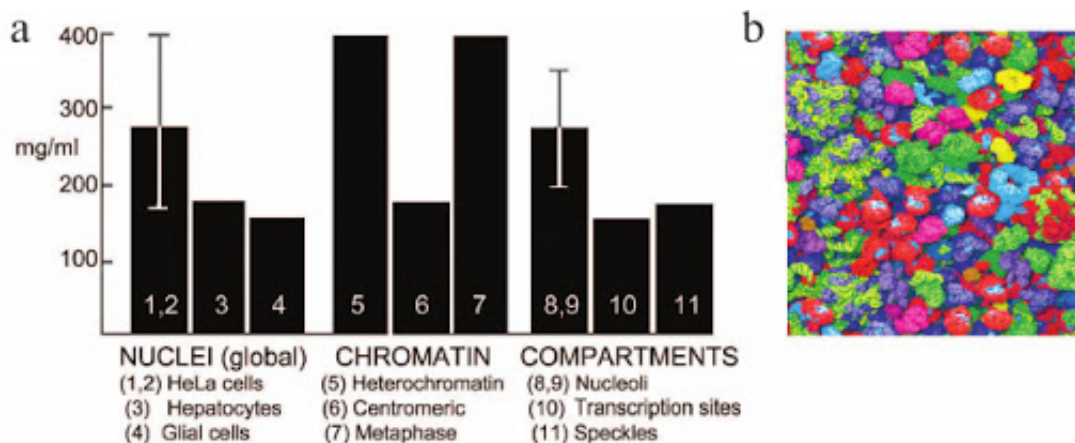


Figure 1.3: Concentrations of macromolecules in nucleus (left) and the simulation of crowded environment in cells (right). The graph is from R. Hancock [60].

### 1.3.2 Macromolecular crowding and equilibrium constant

In a crowded environment, the background macromolecules can affect the equilibrium and the rate of a chemical reaction. The constituents of the local environment can react with a particular reactant through 4 ways: nonspecific intermolecular interactions,

side reactions, partitioning between microenvironments, and surface interactions (see figure 1.4) [62, 63, 64].

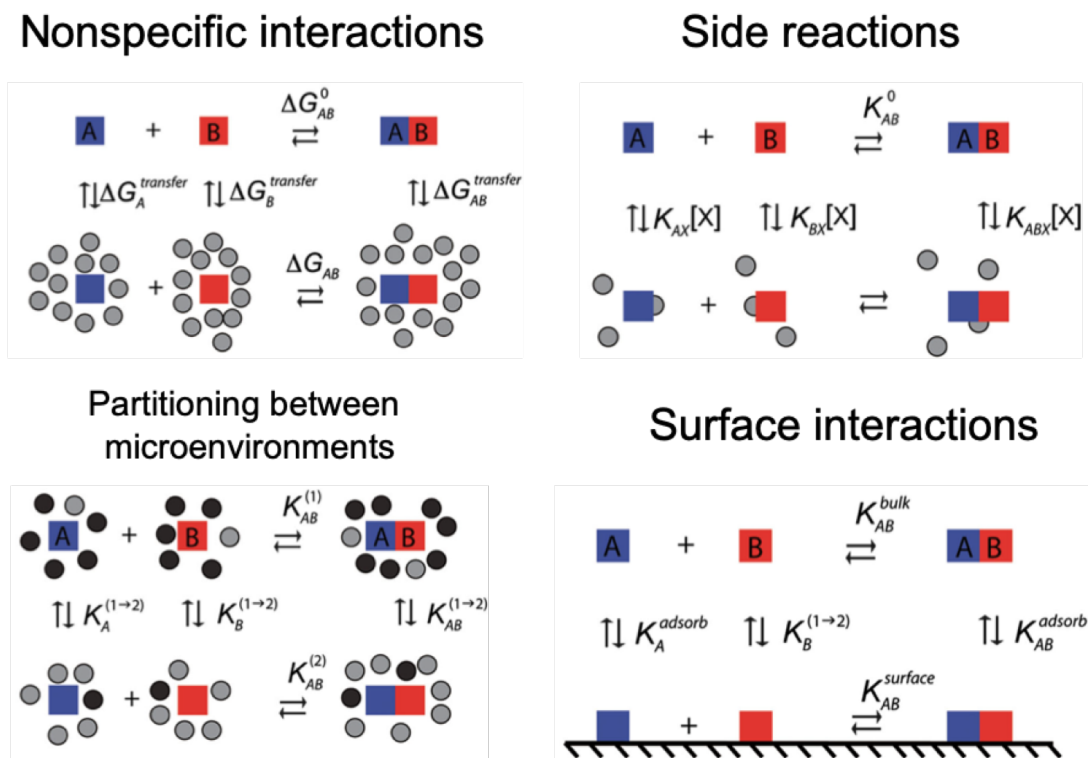


Figure 1.4: The crowded environment can affect the equilibrium of a reaction through 4 ways: nonspecific intermolecular interactions, side reactions, partitioning between microenvironments, and surface interactions. The graph is from Rivas [62].

### A. Nonspecific intermolecular interactions

For a reaction involving reactant A and B:



the free energies of association in the dilute solution and crowded environment are:

$$\Delta G_{AB}^0 = -RT \ln K_{AB}^0 \quad (1.5)$$

and

$$\Delta G_{AB} = -RT \ln K_{AB} \quad (1.6)$$

respectively. Where R denotes the molar gas constant, T is the absolute temperature. The equilibrium constants in these two environment are linked as:

$$\begin{aligned} -RT \ln \left( \frac{K_{AB}}{K_{AB}^0} \right) &= \Delta G_{AB} - \Delta G_{AB}^0 \\ &= \Delta G_A^{transfer} + \Delta G_B^{transfer} - \Delta G_{AB}^{transfer} \end{aligned} \quad (1.7)$$

where  $\Delta G_i^{transfer}$  is the standard free energy required to transfer molecule i from bulk solution to the crowded environment, and i can either represent A, B or AB respectively.

As the reactants can react with the background molecules through attractive force (electrostatic attraction or hydrogen-binding, and solvent-mediated interactions) or repulsive force (volume exclusion or electrostatic repulsion), the total free energy of transfer is accordingly partitioned into contributions from various types of interactions [64]:

$$\Delta G_i^{transfer} = \Delta G_i^{excludedvolume} + \Delta G_i^{electrostatic} + \Delta G_i^{H-bonding} + \Delta G_i^{solventmediated} \quad (1.8)$$

As a result, the free energy required for molecule transferring is altered, and the rate

and/or the equilibrium of a reaction is changed. The impacts of nonspecific interactions on the kinetics of a reaction are listed in figure 1.5.

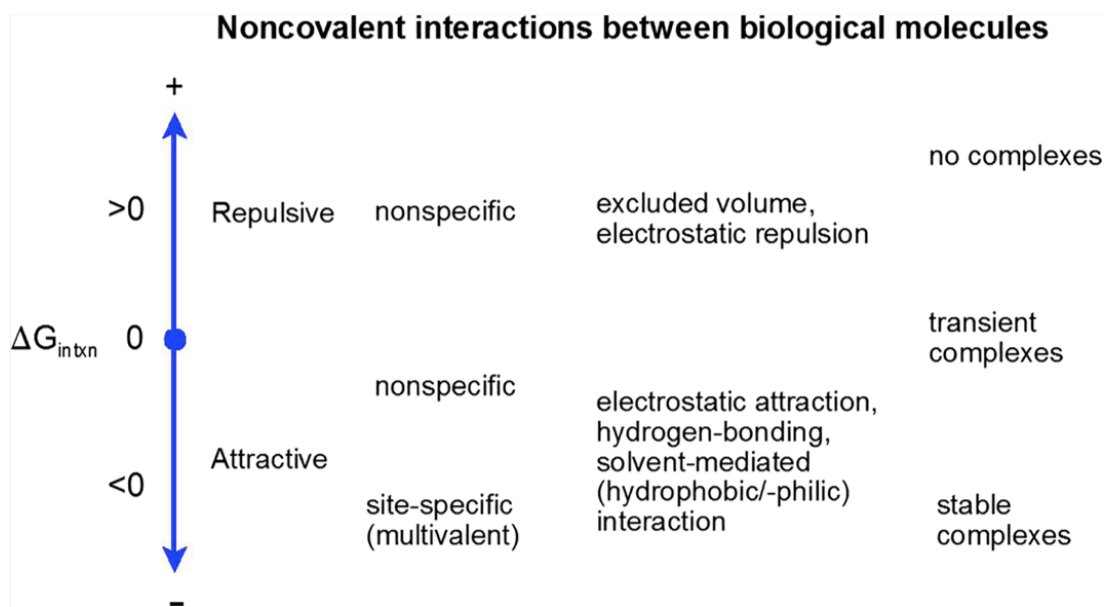


Figure 1.5: The types of nonspecific interactions and their impact on the change of free energy. The graph is from Rivas [62].

With the increase of background macromolecules (namely a larger volume fraction of background macromolecules), the  $K$  value of a reaction increases at first and decreases finally (see figure 1.6) [65, 66, 67, 68]. Among these nonspecific interactions, the most basic and dominant contribution is the volume exclusion ( $\Delta G_i^{\text{excluded volume}}$ ) [68, 69].

However, Minton points out that the equilibrium of a reaction is not affected by macromolecular crowding if the reaction is not accompanied by a significant change in the volume excluded to background solutes. In other words, the equilibrium of an interaction between a small molecule and a macromolecule (for instance, the interaction between DOX and genomic DNA) is not affected by macromolecular crowding, because there is no major conformation or state change of the macromolecules during

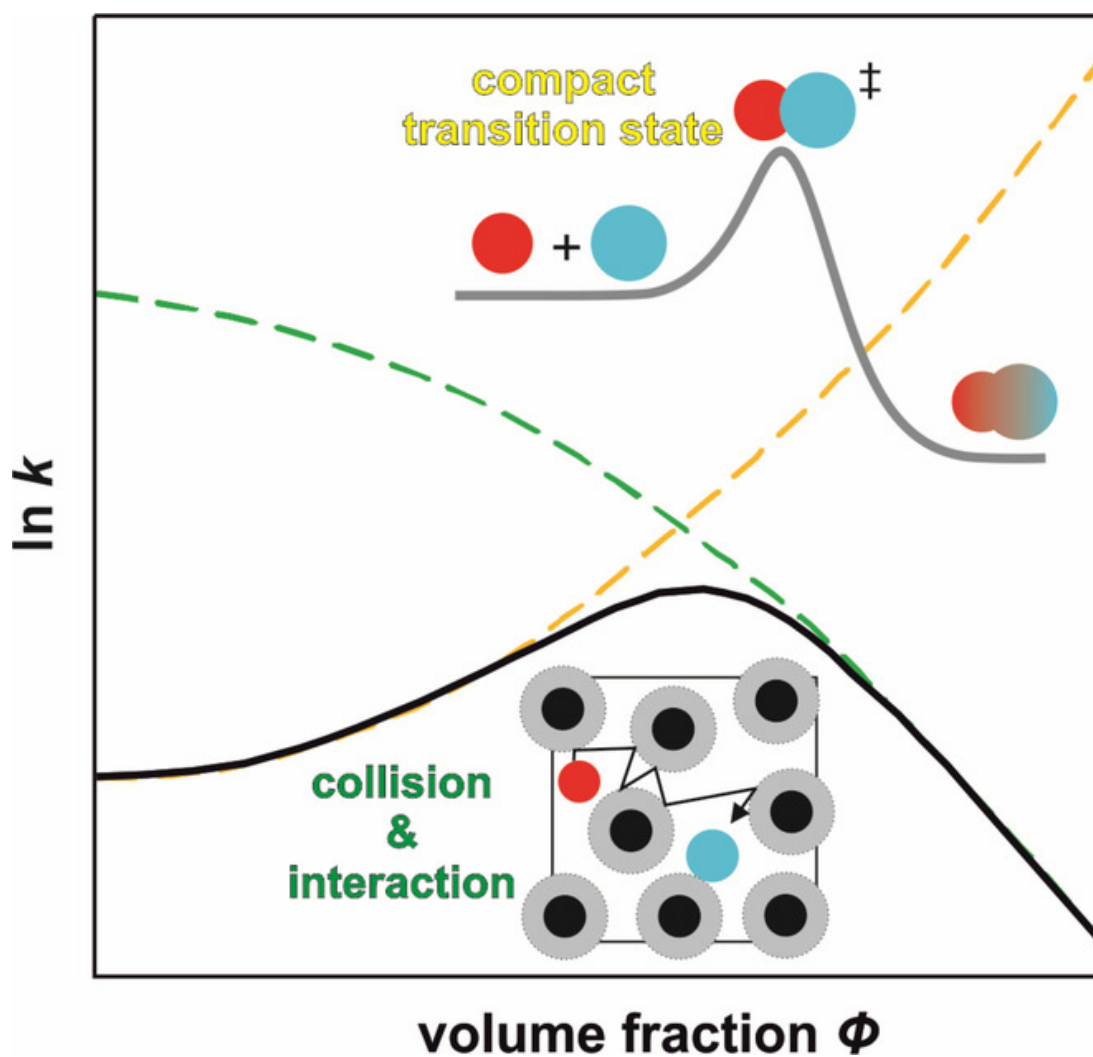


Figure 1.6: How the equilibrium constant of reaction will be affected by the nonspecific intermolecular interactions. The graph is from Gao [65].

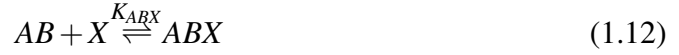
the binding event by the small molecule [70].

### B. Side reactions

For a reaction without side reactants, the association equilibrium is specified by the relation:



If each of the reactant or product is reacting with a single molecule of the background species X respectively, the additional side reactions are:



where  $K_{AX}$ ,  $K_{BX}$ , and  $K_{ABX}$  are the equilibrium constant in A-X, B-X, and AB-X interaction respectively. Combine equation 1.9, 1.10, 1.11, and 1.12 together, we get the experimentally determined ratio of product to reactant concentrations:

$$K_{ABX} \equiv \frac{C_{AB}}{C_A \cdot C_B} = K_{AB}^0 \cdot \frac{1 + K_{ABX} \cdot C_X}{(1 + K_{AX} \cdot C_X)(1 + K_{BX} \cdot C_X)} \quad (1.13)$$

where  $C_A$ ,  $C_B$ ,  $C_{AB}$ , and  $C_X$  are the concentrations of A, B, AB, and X at equilibrium state respectively.  $K_{AB}$  is not a true equilibrium constant, it varies with  $C_X$ , unless the binding of reactants or products to X is negligible (namely  $K_{AX}C_X$ ,  $K_{BX}C_X$ , and  $K_{ABX}C_X \ll 1$ ).

### C. Partitioning between microenvironments

If each reactant distributes between two microenvironments 1 and 2 (for instance, microenvironment 1 is aqueous phase and microenvironment 2 is lipid phase), the partition coefficients of each reactant is defined as:

$$K_Z^{(1 \rightarrow 2)} \equiv \frac{C_{Z(2)}}{C_{Z(1)}} \quad (1.14)$$

where  $C_{Z(i)}$  is the equilibrium concentration of reactant Z in microenvironment  $i$ . The free energy to transfer molecule Z from microenvironment  $i$  to microenvironment  $j$  is related to the partition coefficient of species Z:

$$\Delta G_Z^{(i \rightarrow j)} = -RT \ln K_Z^{(i \rightarrow j)} \quad (1.15)$$

Combine equation 1.14 and 1.15, we get the experimentally measured ratio of the concentrations of product and reactants:

$$K_{AB} \equiv \frac{C_{AB}}{C_A C_B} = K_{AB}^{(1)} \frac{1 + f_2(K_{12,AB} - 1)}{[1 + f_2(K_{12,A} - 1)][1 + f_2(K_{12,B} - 1)]} \quad (1.16)$$

where  $f_2$  is the fraction of the total system volume occupied by microenvironment 2.  $K_{AB}$  is not the true equilibrium constant, it varies with  $f_2$  and depends on the distribution of reactants and products between the compartments.  $K_{AB}$  follows from equation 1.16:

$$\frac{K_{AB}^{(2)}}{K_{AB}^{(1)}} = \frac{K_{AB}^{(1 \rightarrow 2)}}{K_A^{(1 \rightarrow 2)} K_B^{(1 \rightarrow 2)}} \quad (1.17)$$

### D. Surface interactions

Surface interactions are special cases of partitioning. In the ideal limit, the adsorption coefficient is defined as the concentrations of a given species X in the bulk and on the surface:

$$K_X^{adsorb} = \frac{C_{X_{surface}}}{C_{X_{bulk}}} \quad (1.18)$$

A macromolecule in a membrane surface is at a "surface microenvironment", which is different with the remote molecules far from the surface. In a medium with significant surface area, the measured product to reactant concentration ratio can not reflect the true equilibrium constant, it varies with the amount(s) and type(s) of accessible surface. In heterogeneous environments, the macromolecular associations are more rapidly on surfaces than in solution.

### 1.3.3 Equilibrium constant determined in crowded environment

In table 1.3, we compared the association constants determined in crowded environment ( $K_a$ ) and in diluted environment ( $K_a^0$ ). The association constant of a reaction can be altered 2 orders of magnitude with the presence of macormolecules.

Table 1.3: The association constants of a chemical reaction in diluted solution ( $K_a^0$ ) and in crowded environment ( $K_a$ ).

Reactions	Crowders	$K_a^0/K_a$
TEM1- $\beta$ -lactamase and $\beta$ -lactamase inhibitor protein [71]	Polyethylene glycol (PEG)	0.04
Barnase and barstar [71]	Ethylene glycol (EG)	0.1
Xanthine oxidase and bovine erythrocyte copper, zinc-superoxide dismutase [72]	Dextran	9.8
Protein RepA and DNA sequences [73]	Bovine serum albumin or ovalbumin	10
DNA and T7 RNA polymerase [74]	PEG	83.3

However, the  $K$  values displayed in table 1.3 are determined for protein-protein interactions (PPIs) or protein-DNA interactions (PDIs). The  $K$  values may not change for anthracycline-DNA interactions in crowded environment, because anthracycline-DNA interactions are not accompanied by a significant change in the volume excluded to background solutes. As there are no reports concerning the kinetics of anthracycline-DNA interactions in crowded environment, we need to determine the  $K$  values of anthracycline-DNA interactions with the presence of macromolecules. Also, in previous reports, to analyze how the macromolecules can affect the equilibrium of a reaction, researchers only choose one specific crowder (such as PEG, serum albumin) to create the crowded environment. In recent years, to mimic the heterogeneity of the intracellular environment, the mixed crowders are recommended to be used [69, 75]. Instead of creating an artificial crowded environment, we decided to determine  $K$  directly in the cell nucleus.

## 1.4 Techniques used to determine the equilibrium constants in this work

Since all of the anthracyclines contain aromatic rings with delocalized  $\pi$ -electrons, they can absorb and emit photons without any external fluorescent labels. Thus, in our work, we mainly determined the  $K$  of anthracycline-DNA interactions through three techniques. All of the techniques are based on the fluorescence change of anthracyclines in the interaction with DNA.

### 1.4.1 Fluorescence

#### A. Jablonski diagram

The Jablonski diagram illustrates the electronic states of a molecule and the transitions between them (see figure 1.7). When a molecule at the singlet ground state ( $S_0$ ) absorbs light with an energy of  $h\nu_A$ , it will transfer to one of the singlet excited states ( $S_1$  or  $S_2$ ) within  $10^{-15}$  s. The molecule at the excited state is not at an equilibrium state, it will return to  $S_0$  by dissipating the absorbed energy through nonradiative transitions (internal conversion or intersystem crossing) or radiative transitions (fluorescence or phosphorescence). The internal conversion takes place from  $10^{-14}$  to  $10^{-11}$  s, while the timescale of intersystem crossing is  $10^{-8}$  to  $10^{-3}$  s. The photon emission from  $S_1$  to  $S_0$  is known as fluorescence, occurring at the timescale of  $10^{-9}$  to  $10^{-7}$  s, while the photon emission from  $T_1$  to  $S_0$  is known as phosphorescence, occurring from  $10^{-4}$  to  $10^{-1}$  s.

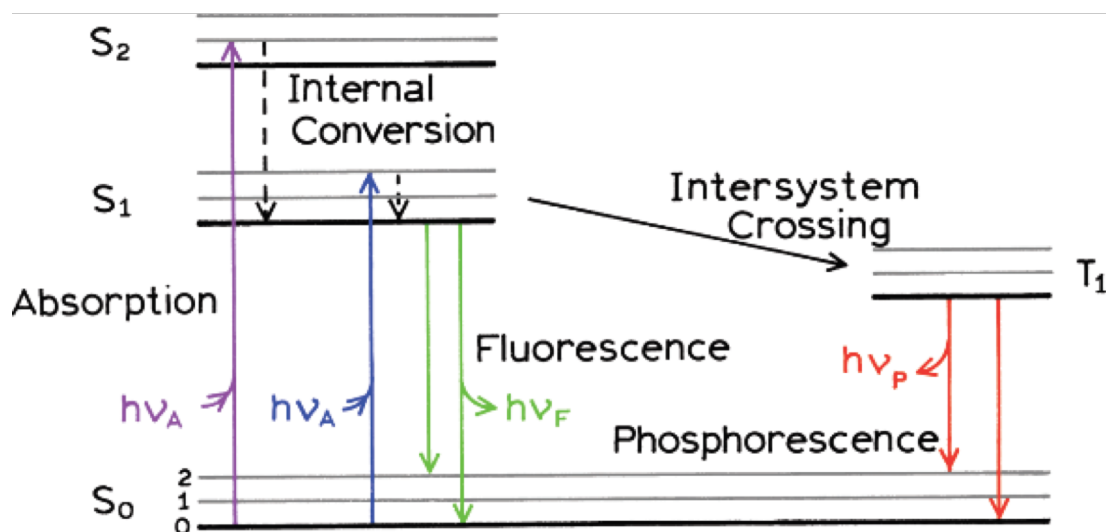


Figure 1.7: A typical Jablonski diagram illustrates how a molecule absorbs and emits photons. The figure is from Jameson [76].

## B. Fluorescence quantum yield

The fluorescence quantum yield ( $q$ ) is defined as the ratio of the number of photons emitted ( $n_{\text{emitted}}$ ) to the number of photons absorbed ( $n_{\text{absorbed}}$ ) by a fluorescent molecule:

$$q = \frac{n_{\text{emitted}}}{n_{\text{absorbed}}} \times 100\% \quad (1.19)$$

According to previous reports [77, 78], the quantum yield of DOX (9%) is 10 times smaller than the reference dye Rhodamine 6G (95%).

## C. Fluorescence quenching

Fluorescence quenching refers to any process which can decrease the fluorescence intensity of a given sample. It is caused by molecular interactions, including excited-

state reactions, molecular rearrangements, energy transfer, ground-state complex formation, and collisional quenching [76]. Anthracyclines are reported to be quenched in the interactions with DNA [9, 79, 80, 81].

#### **D. Photobleaching**

Photobleaching is the photochemical destruction of a fluorophore. As a result, the fluorophore is unable to fluoresce permanently. The mechanisms are involved in photo-oxidation, organic reaction, and multi-photon events. Photobleaching is a severe problem for fluorescence fluctuation experiments, because the obtained autocorrelation curve (ACF) curves are distorted due to the reduced diffusion time or the decreased fluorophore concentration [82, 83]. In practice, we can avoid photobleaching either by reducing the laser power or correcting the ACF with analytical function [51, 52]. If both of the solutions can not work, usually, the bleached curves are discarded for downstream analysis [84, 85].

#### **1.4.2 FCS method**

FCS is a technique used to investigate the temporal fluctuations of fluorescence signals within a small detecting volume [86]. It provides the physical information which causes the rise of fluctuations, including local concentrations of compounds in the confocal volume, diffusion coefficients or characteristic rate constants of inter- or intramolecular reactions of fluorescent molecules [25, 87]. As a sensitive method, it allows the measurements at the nanomolar level. Also, due to its non-invasivity, it is an ideal tool to analyze the minute quantities inside living cells [25]. The basic theory of FCS and the setup required for a FCS measurement are illustrated in figure 1.8.

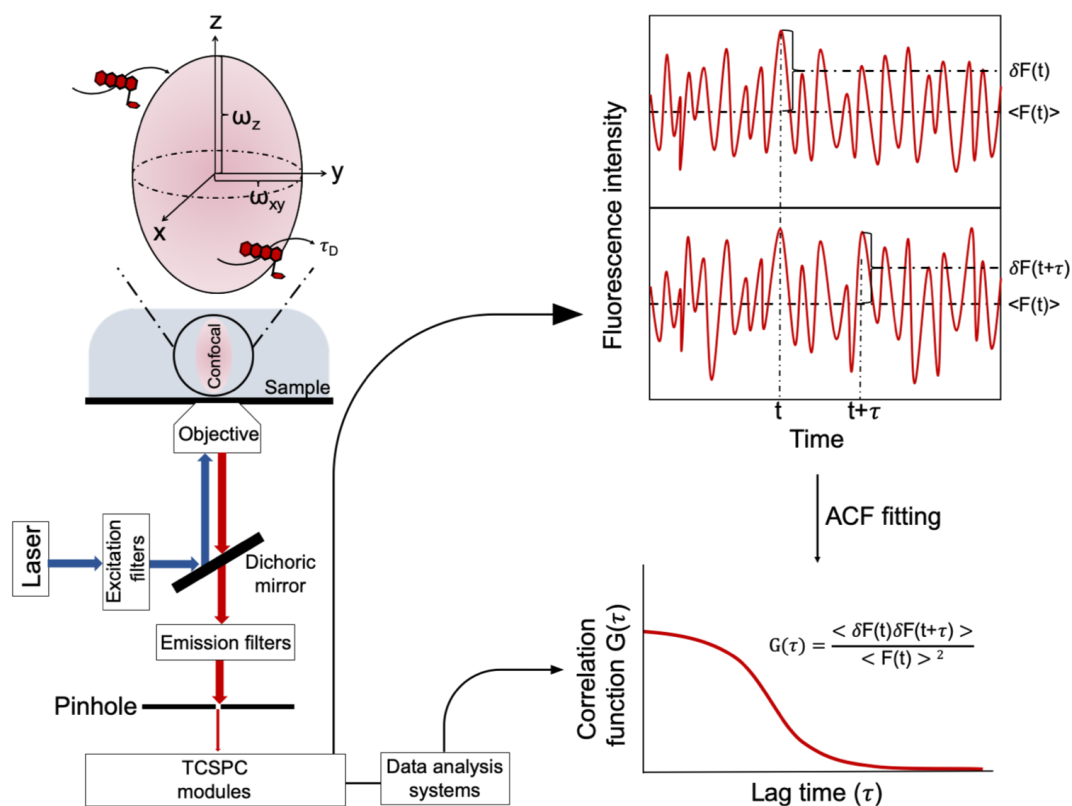


Figure 1.8: The theory behinds **FCS** and the setups required for a **FCS** measurement.

### A. Theoretical concepts

For a chemical reaction at equilibrium state, the macroscopic concentrations of molecules are constant in space and time for infinite time-periods. However, due to Brownian motion of fluorescent molecules in space and the Poisson process of chemical reaction, the local concentrations of molecules in the confocal volume fluctuate, so does the fluorescence intensity (namely the number of photons recorded by the Time-correlated single photon counting (**TCSPC**) module) in the confocal volume. The fluctuations of the fluorescence intensity are defined as:

$$\delta F(t) = F(t) - \langle F(t) \rangle \quad (1.20)$$

where  $F(t)$  is the instantaneous fluorescence intensity at a given time  $t$ ,  $\langle F(t) \rangle$  denotes to the average fluorescence intensity over a period of time  $t$ . To quantify how much the fluorescence intensity is still similar to itself after a given delay, the normalized ACF is applied [86, 88]:

$$G(\tau) = \frac{\langle \delta F(t) \cdot \delta F(t + \tau) \rangle}{\langle F(t) \rangle^2} \quad (1.21)$$

where  $F(t+\tau)$  is the instantaneous fluorescence intensity at a later time  $t+\tau$ , the brackets  $\langle \rangle$  indicates a time average.

To describe the fluorescence signal  $F(t)$  in a more detailed way, some experimental details are required to be considered. The FCS experiment is conducted in a confocal microscope. If all of the fluctuations arise only from changes in the local concentration ( $\delta C$ ) within the effective volume ( $V_{eff}$ ) of the focal spot, the variation of  $F(t)$  is [25, 89]:

$$\delta F(t) = \kappa \int_V I_{ex}(\mathbf{r}) \cdot S(\mathbf{r}) \cdot \delta(\sigma \cdot q \cdot C(\mathbf{r}, t)) dV \quad (1.22)$$

The parameters in equation 1.22 describe the probability to excite a fluorophore within the focal volume and detect the emitted photon afterwards due to the final detection efficiency of the setup. More specifically,  $\kappa$  is the overall detection efficiency,  $I_{ex}(\mathbf{r})$  is the spatial distribution of the exciting laser beam with the maximum amplitude  $I_0$ ,  $S(\mathbf{r})$  is the fluorescence detection probability,  $\delta(\sigma \cdot q \cdot C(\mathbf{r}, t))$  is the dynamics of fluorophore on the single-particle level ( $\sigma$  represents the molar extinction coefficient of

the fluorophore, and  $q$  refers to the quantum yield of the fluorophore). Since it is very hard to determine all of the parameters individually, to simplify equation 1.22, some parameters are integrated. The product  $W(\mathbf{r}) = \frac{I_{ex}(\mathbf{r}) \cdot S(\mathbf{r})}{I_0}$  describes the shape of the confocal detection efficiency profile, and it is approximated by a 3D Gaussian [90]:

$$W(\mathbf{r}) = \exp \left[ -\frac{2(x^2 + y^2)}{\omega_{xy}^2} - \frac{2z^2}{\omega_z^2} \right] \quad (1.23)$$

where  $\omega_{xy}$  and  $\omega_z$  are the  $1/e^2$  radius of the confocal in lateral and axial direction respectively. The remaining parameters can be combined with  $I_0$  to determine the photon count rate per molecule per second:

$$\eta_0 = I_0 \cdot \kappa \cdot \sigma \cdot q \quad (1.24)$$

Finally, equation 1.22 becomes:

$$\delta F(t) = \int_V W(\mathbf{r}) \cdot \delta(\eta_0 \cdot C(\mathbf{r}, t)) dV \quad (1.25)$$

where  $\delta C(r, t)$  is the fluctuation of the local particle concentration at time  $t$ , and  $V$  is the confocal volume. Substituting equation 1.25 into equation 1.21, the ACF becomes:

$$G(\tau) = \frac{\int \int W(\mathbf{r}) W(\mathbf{r}') \langle \delta(\eta_0 \cdot C(\mathbf{r}, t)) \delta(\eta_0 \cdot C(\mathbf{r}', t + \tau)) \rangle dV dV'}{(\int W(\mathbf{r}) \langle \delta(\eta_0 \cdot C(\mathbf{r}, t)) \rangle dV)^2} \quad (1.26)$$

If we only consider the fluorescent molecules are diffusing in the confocal volume with a diffusion coefficient of  $D$ , and either the concentration ( $C$ ) or the parameter  $\eta_0$  is constant for a given system, equation 1.26 is simplified as:

$$\begin{aligned}
G(\tau) &= \frac{1}{V_{eff} \cdot C} \cdot \left(1 + \frac{\tau}{\tau_D}\right)^{-1} \cdot \left(1 + \frac{\tau}{\omega^2 \cdot \tau_D}\right)^{-\frac{1}{2}} \\
&= \frac{1}{N} \cdot \left(1 + \frac{\tau}{\tau_D}\right)^{-1} \cdot \left(1 + \frac{\tau}{\omega^2 \cdot \tau_D}\right)^{-\frac{1}{2}}
\end{aligned} \tag{1.27}$$

where  $N$  is the average number of fluorescent molecules in the confocal,  $\omega$  denotes to the structure of the confocal, and  $\tau_D$  represents the diffusion time of fluorescent molecules in the confocal. In equation 1.27,  $V_{eff}$  can be calculated with:

$$V_{eff} = \pi^{3/2} \cdot \omega_{xy}^2 \cdot \omega_z \tag{1.28}$$

the parameter  $\omega$  is determined with:

$$\omega = \frac{\omega_z}{\omega_{xy}} \tag{1.29}$$

$\tau_D$  is calculated according to:

$$\tau_D = \frac{\omega_{xy}^2}{4D} \tag{1.30}$$

In formula 1.30,  $D$  is the diffusion coefficient of the fluorescent molecules, it is determined by:

$$D = \frac{k_b \cdot T}{6 \cdot \pi \cdot \eta \cdot R_h} \tag{1.31}$$

where  $k_b$  is the Boltzmann's constant,  $T$  is the absolute temperature,  $\eta$  is the viscosity of the medium the fluorescent molecules diffuse in, and  $R_h$  is the hydrodynamic radius of the fluorescent molecules. At zero lag time, equation 1.27 changes to:

$$G(\tau \rightarrow 0) = \frac{1}{N} \quad (1.32)$$

However, equation 1.27 is based on the assumption that the fluorescence fluctuations are only caused by the motion of chromophores. In reality, the fluorescent properties of chromophores can change during the traverse of the laser beam (for instance, intra- or inter-molecular reactions), namely,  $\delta\eta_0$  is not constant. In this case, we should consider a general form of ACF. If the fluorescence fluctuation caused by the properties change is much faster than the motion of fluorescent molecules on time-scales, the ACF (equation 1.27) changes to:

$$G_{total}(\tau) = G_{motion}(\tau) \cdot X_{kinetics}(\tau) \quad (1.33)$$

The transition of chromophores to the first excited triplet state is the most common cause of fluorescence properties change ( $S_1$  to  $T_1$ , see figure 1.7), and the triplet blinking can be described by an exponential decay:

$$X_{triplet}(\tau) = 1 + \frac{p}{1-p} \cdot e^{-\frac{\tau}{\tau_{triplet}}} \quad (1.34)$$

where  $p$  is the average fraction of fluorescent molecules in triplet state, and  $\tau_t$  is the lifetime of triplet state (usually between  $10^{-8}$  and  $10^{-3}$ s). Finally, equation 1.33 becomes:

$$G(\tau) = \left(1 + \frac{p}{1-p} \cdot e^{-\frac{\tau}{\tau_t}}\right) \cdot \frac{1}{N} \cdot \left(1 + \frac{\tau}{\tau_D}\right)^{-1} \cdot \left(1 + \frac{\tau}{\omega^2 \cdot \tau_D}\right)^{-\frac{1}{2}} \quad (1.35)$$

If the fluorescence signals are contributed by  $i$  types of non-interacting fluorescent

molecules, equation 1.27 changes to the formula [25]:

$$G_{multi}(\tau) = \frac{1}{V_{eff}} \cdot \frac{\sum_{i=1}^{\infty} \eta_i \cdot \langle C_i \rangle \cdot M_i(\tau)}{(\sum_i \eta_i \cdot \langle C_i \rangle)^2} \quad (1.36)$$

where  $M_i(\tau)$  is the mobility term of i-th component, and it is expressed as:

$$M_i(\tau) = \left(1 + \frac{\tau}{\tau_{D_i}}\right)^{-1} \cdot \left(1 + \frac{\tau}{\omega^2 \cdot \tau_{D_i}}\right)^{-\frac{1}{2}} \quad (1.37)$$

## B. Experimental setups

To conduct the FCS experiment, an excitation laser, filters, an objective, pinholes, photon counting modules such as avalanche photodiodes (APDs), and data analysis systems are required. To have the maximum detection efficiency, some key parameters should be considered [88].

- Laser power. If the laser power is too low, no photons can be detected, while too high laser power induces the photobleaching of a fluorescent molecule. The maximum number of photons we can detect in our system is  $10^5$ . To avoid the saturation of detectors, the laser power should be set in a proper range.
- The number of numerical aperture (NA). To ensure the maximum collection efficiency, an objective with a high NA is preferable. Usually, the number of NA in experiment is 1.2.
- Size of pinholes. To collect the maximum fluorescent signals, the pinhole size should be set properly. The larger the pinhole size, the more fluorescent signals are detected, but the more the background noises are also collected.

- Quantum yield ( $q$ ). It affects the parameter  $\eta_0$ , and further affects the number of photons collected in APDs.
- Fitting model. To fit the ACF precisely, a proper mathematical model should be considered. For instance, to interpret the ACF curve with a diffusion dominant model or a reaction dominant model [49]. The advanced data analysis is usually dealt with software such as Origin, Python, Matlab, Gnuplot, etc.

### C. Equilibrium constant determination

In anthracycline-DNA interactions, it is widely accepted that the anthracycline molecules intercalate into the bp of DNA chains [91]. To determine the  $K$  in formula 1.3, it is crucial to know  $C_{ANT-DNA}^{eq}$ ,  $C_{ANT}^{eq}$ , and  $C_{DNA}^{eq}$  respectively.

If we only let the fluorescent anthracycline molecules with a known concentration ( $C_{ANT}$ ) diffuse inside the confocal, the average fluorescence intensity of anthracycline molecules in a period of time  $t$  is recorded as  $\langle F(t) \rangle_{ANT}$ . The number ( $N_{ANT}$ ) and the diffusing time ( $\tau_{ANT}$ ) of anthracycline molecules are determined by fitting the ACF with the 1-component model:

$$G(\tau) = \frac{1}{N_{ANT}} \cdot \left(1 + \frac{t}{\tau_{ANT}}\right)^{-1} \cdot \left(1 + \frac{t}{\omega^2 \tau_{ANT}}\right)^{-1/2} \cdot \left(1 + \frac{P}{1-P} \cdot e^{-t/\tau_i}\right) \quad (1.38)$$

Also, we can calculate the corresponding diffusion coefficient of anthracycline molecules ( $D_{ANT}$ ) according to equation 1.31. When DNA molecules are added to the pure anthracycline solution, anthracycline molecules bind with these DNA. Now, the average fluorescence intensity recorded in confocal changes to  $\langle F(t) \rangle_{ANT-DNA}$ . In

the confocal volume, there are two types of anthracycline molecules: the free diffusing one with a diffusing coefficient of  $D_{ANT}$ , and the bound one with a diffusing coefficient of  $D_{ANT-DNA}$ . With the parameter  $\tau_{ANT}$  fit from equation 1.38, by fitting the ACF with the 2-component model [92]:

$$G(\tau) = \frac{1}{N_{ANT}} \cdot \left[ A_{ANT-DNA} \cdot \left(1 + \frac{t}{\tau_{ANT-DNA}}\right)^{-1} \cdot \left(1 + \frac{t}{\omega^2 \cdot \tau_{ANT-DNA}}\right)^{-1/2} + A_{ANT} \cdot \left(1 + \frac{t}{\tau_{ANT}}\right)^{-1} \cdot \left(1 + \frac{t}{\omega^2 \cdot \tau_{ANT}}\right)^{-1/2} \right] \cdot \left(1 + \frac{P}{1-p} \cdot e^{-t/\tau_i}\right) \quad (1.39)$$

we can know the fraction of unbound anthracycline ( $A_{ANT}$ ) and bound anthracycline ( $A_{ANT-DNA}$ ) respectively. Once the parameter  $\frac{A_{ANT-DNA}}{A_{ANT}}$  is determined, with the multiple-site equilibrium binding model [47], we can determine the  $K$ :

$$\begin{aligned} \frac{C_{ANT-DNA}^{eq}}{C_{ANT}^{eq}} &= \frac{A_{ANT-DNA}}{A_{ANT}} \cdot \left(\frac{MB_{ANT}}{MB_{ANT-DNA}}\right)^2 \\ &= \frac{n \cdot K \cdot C_{DNA} \cdot \left(1 + n \cdot K \cdot C_{DNA} + n \cdot K \cdot C_{ANT}\right)}{1 + n \cdot K \cdot C_{DNA}} \end{aligned} \quad (1.40)$$

In formula 1.40  $n$  is the number of binding sites on DNA, it depends on the total bp number of the DNA chain.  $MB_{ANT}$  is the MB of anthracyclines, and  $MB_{ANT-DNA}$  represents the MB of anthracycline-DNA complexes.

The parameter MB characterizes the number of photons emitted by a molecule in a time of period  $t$ . The value of MB is not constant, it depends on the molecular properties (such as quantum yield), excitation conditions (such as laser power), and measurement instruments (detector efficiency). Under a given experimental environment, it is proportional to the average fluorescence intensity over a period of  $t$  and the number of

fluorescent molecules (N):

$$MB = \frac{\langle F(t) \rangle}{N} \quad (1.41)$$

Thus, the parameter  $\left(\frac{MB_{ANT}}{MB_{ANT-DNA}}\right)^2$  is expressed as:

$$\left(\frac{MB_{ANT}}{MB_{ANT-DNA}}\right)^2 = \left(\frac{\frac{\langle F(t) \rangle_{ANT}}{N_{ANT}}}{\frac{\langle F(t) \rangle_{ANT-DNA}}{N_{ANT}}}\right)^2 = \left(\frac{\langle F(t) \rangle_{ANT}}{\langle F(t) \rangle_{ANT-DNA}}\right)^2 \quad (1.42)$$

where  $\langle F(t) \rangle_{ANT}$  is the fluorescence intensity recorded when there are only anthracycline molecules in the confocal volume, while  $\langle F(t) \rangle_{ANT-DNA}$  is the fluorescence intensity recorded when all of the anthracycline molecules are reacting with DNA in the confocal volume.

### 1.4.3 Single-MB analysis method

Recently, to determine the  $K$  for a reaction, Bielec has proposed a method based on the single-MB change of a fluorescent molecule in reaction [26]. As mentioned in section 1.4.2, to determine the  $K$ , we need to know  $C_{ANT-DNA}^{eq}$ ,  $C_{ANT}^{eq}$ , and  $C_{DNA}^{eq}$  respectively. Within a confocal with a volume  $V_{eff}$ , if there are only anthracycline molecules containing a MB of  $\alpha$ , the average fluorescence intensity of anthracycline molecules over time  $t$  ( $\langle F(t) \rangle_{ANT}$ ) is:

$$V_{eff} \cdot N_A \cdot C_{ANT} \cdot \alpha = N_{ANT} \cdot \alpha = \langle F(t) \rangle_{ANT} \quad (1.43)$$

where  $N_A$  is the Avogadro constant, and  $N_{ANT}$  is the number of anthracycline molecules.

When DNA molecules are added in the pure anthracycline solution, anthracycline molecules bind with these DNA molecules, the average fluorescence intensity recorded in the confocal changes to  $\langle F(t) \rangle_{ANT-DNA}$ . There are three types of molecules in the system: unbound anthracycline molecules with a MB of  $\alpha$ , DNA with a MB of  $\beta$ , and anthracycline-DNA complexes with a MB of  $\gamma_1$ . The average fluorescence intensity recorded is:

$$V_{eff} \cdot N_A \cdot ( \alpha \cdot C_{ANT}^{eq} + \beta \cdot C_{DNA}^{eq} + \gamma_1 \cdot C_{ANT-DNA}^{eq} ) = \langle F(t) \rangle_{ANT-DNA} \quad (1.44)$$

At chosen experimental conditions, the fluorescence intensity of DNA is negligible (proportional to background noise). In the reaction, only anthracycline molecules and anthracycline-DNA complexes are fluorescent, thus, equation 1.44 simplifies as:

$$V_{eff} \cdot N_A \cdot ( \alpha \cdot C_{ANT}^{eq} + \gamma_1 \cdot C_{ANT-DNA}^{eq} ) = \langle F(t) \rangle_{ANT-DNA} \quad (1.45)$$

As  $K$  can be expressed as:

$$K = \frac{C_{ANT-DNA}^{eq}}{C_{ANT}^{eq} \cdot C_{DNA}^{eq}} = \frac{C_{ANT-DNA}^{eq}}{(C_{ANT} - C_{ANT-DNA}^{eq}) \cdot (C_{DNA} - C_{ANT-DNA}^{eq})} \quad (1.46)$$

where  $C_{ANT}$  is the initial anthracycline concentration, and  $C_{DNA}$  is the initial DNA concentration. Now, equation 1.46 can be re-written as:

$$C_{ANT-DNA}^{eq} = \frac{1}{2} \cdot \left[ C_{ANT} + C_{DNA} + \frac{1}{K} - \sqrt{\left( -C_{ANT} - C_{DNA} - \frac{1}{K} \right)^2 - 4 \cdot C_{ANT} \cdot C_{DNA}} \right] \quad (1.47)$$

With equation 1.47 and the relation  $C_{DNA} = C_{DNA}^{eq} + C_{ANT-DNA}^{eq}$ , equation 1.45 can be written as:

$$V_{eff} \cdot N_A \cdot \alpha \left[ C_{ANT} - C_{ANT-DNA}^{eq} \right] \cdot \left[ 1 + \frac{\gamma_1}{\alpha} \cdot K \cdot \left( C_{DNA} - C_{ANT-DNA}^{eq} \right) \right] = \langle F(t) \rangle_{ANT-DNA} \quad (1.48)$$

We name equation 1.48 as the 1-reaction model.

Recent works have shown that except for intercalation, the excess anthracycline molecules overhang from the intercalated core of DOX-DNA complexes and form external aggregates [8, 12, 23]. The mechanism of this reaction is illustrated as:



where  $K_2$  is the corresponding equilibrium constant. The intrinsic MB of anthracycline-(anthracycline-DNA) complexes is  $\gamma_2$ , which is different from  $\alpha$  and  $\gamma_1$ . With the increase of anthracycline molecules, the third fluorescent complexes are present in the reaction system (there is no formation of transition state), but the fluorescence intensity in measurement remains the same. Now equation 1.45 changes to:

$$V_{eff} \cdot N_A \cdot \left( \alpha \cdot C_{ANT}^{eq} + \gamma_1 \cdot C_{ANT-DNA}^{eq} + \gamma_2 \cdot C_{ANT-(ANT-DNA)}^{eq} \right) = \langle F(t) \rangle_{ANT-DNA} \quad (1.50)$$

where  $C_{ANT-(ANT-DNA)}^{eq}$  is the concentration of complexes anthracycline-(anthracycline-DNA) at equilibrium state.  $K_2$  is given by:

$$K_2 = \frac{C_{ANT-(ANT-DNA)}^{eq}}{C_{ANT}^{eq} \cdot C_{ANT-DNA}^{eq}} \quad (1.51)$$

Finally, the average fluorescence intensity is transformed into:

$$V_{eff} \cdot N_A \cdot \alpha \left\{ \left( C_{ANT} - C_{ANT-DNA}^{eq} \right) \cdot \left[ 1 + \left( \frac{\gamma_1}{\alpha} \right) \cdot K_1 \cdot \left( C_{DNA} - C_{ANT-DNA}^{eq} \right) + \left( \frac{\gamma_2}{\alpha} \right) \cdot K_2 \cdot C_{ANT-DNA}^{eq} \right] \right\} = \langle F(t) \rangle_{ANT-DNA} \quad (1.52)$$

We name equation 1.52 as the 2-reaction model. For a clear understanding, in the following content, when we use single-MB analysis method, we represent the  $K$  determined in equation 1.48 as  $K_1$ . To determine the equilibrium constants with single-MB analysis method, we need to calculate  $\alpha$ ,  $\gamma_1$  and  $\gamma_2$  with the assistant of FCS method. The working flow is illustrated in figure 1.9.

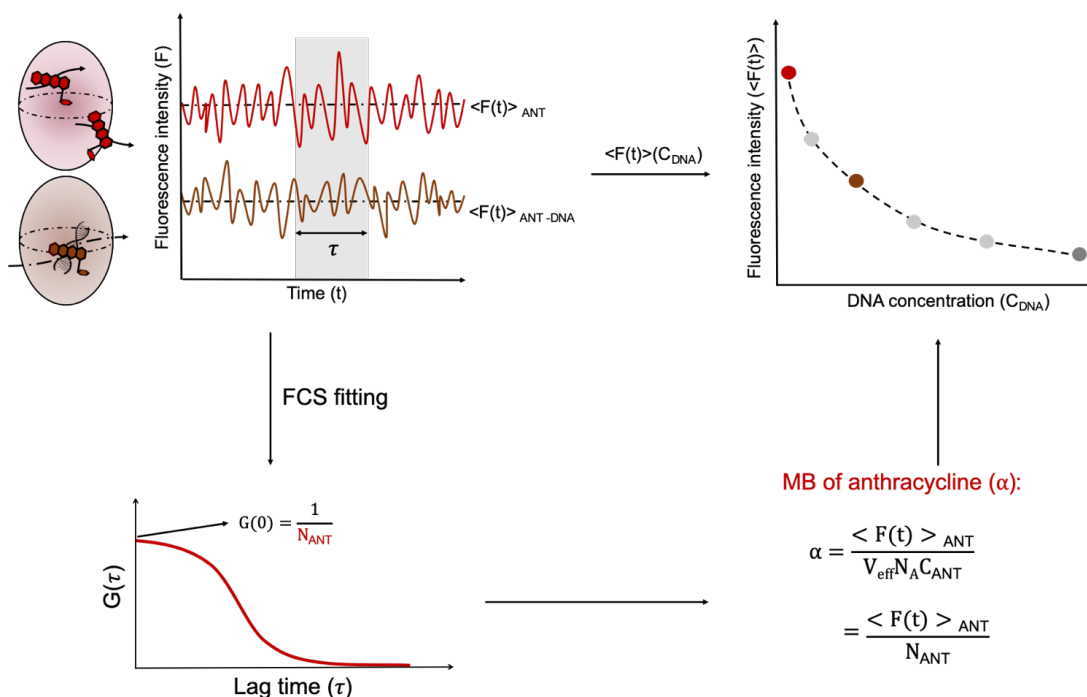


Figure 1.9: The working flow to determine  $K$  with single-MB analysis method. With the help of FCS, the number of anthracycline molecules ( $N_{ANT}$ ) inside the confocal is determined. Also, the MB of anthracycline ( $\alpha$ ) is calculated. By titrating anthracyclines with a constant concentration into a series of DNA solutions with various concentrations, the average fluorescence intensity of each titration point is recorded, and  $\gamma_1$  and  $\gamma_2$  are calculated. The average fluorescence intensity over a period time of  $t$  is plotted against DNA concentrations. By fitting these titration points with equation 1.48 and 1.52, the equilibrium constants ( $K_1$  and  $K_2$ ) are determined.

#### 1.4.4 Fluorescence decay fitting for the photobleached anthracyclines

Though FCS is an ideal tool to determine the  $K$  for bio-samples, it is restricted to rapidly diffusing particles. For immobilized molecules, it is conceptually blind [93].

In cell nucleus, the genomic DNA is relatively static over long periods of time [94]. When anthracyclines bind with the genomic DNA, they also become immobile. Within the confocal volume, due to the immobilization, the bound anthracyclines experience photobleaching with a very high probability [51]. In contrast, unbound anthracyclines are replaced with the fresh anthracyclines rapidly, they have a very low probability to be bleached. In this case, the fluorescence signals are the sum of immobilized components ( $F_{imm}(t)$ ) and freely diffusing components ( $F_{diff}(t)$ ) [93], and it shows an exponential decay over time (see figure 1.10, upper panel). Correspondingly, the ACF curve is distorted (see figure 1.10, lower panel), and the parameters (such as diffusion coefficients or concentrations of the fluorescent molecules) fit from the ACF curve are not accurate anymore [84].

To address the photobleaching issue in cells, scientists use fluorescence recovery after photobleaching (FRAP), fluorescence loss in photobleaching (FLIP) or the variant of FRAP—continuous fluorescence photobleaching (CP) techniques to deal with the fluorescent signals [51, 93, 95]. However, FRAP and FLIP are not single molecule techniques, they do not permit to get the concentration of the various components to which a fluorophore is attached. In contrast, CP allows us to distinguish the contributions between diffusing molecules and the binding-related molecules [52, 93, 96, 97].

Based on these facts, for anthracycline-DNA interaction in living cells, we used the CP technique to bleach the bound anthracyclines, and we recorded the fluorescence intensity over a period of time. In data analysis, we assume the decay of fluorescence intensity is the contribution of the bound anthracyclines, while the stable part is the contribution of the unbound anthracyclines (see figure 1.11). By fitting the fluorescence signals with a mono-exponential function, we determine the ratio of bound and unbound anthracycline molecules. Further, with the ratio of bound and unbound an-

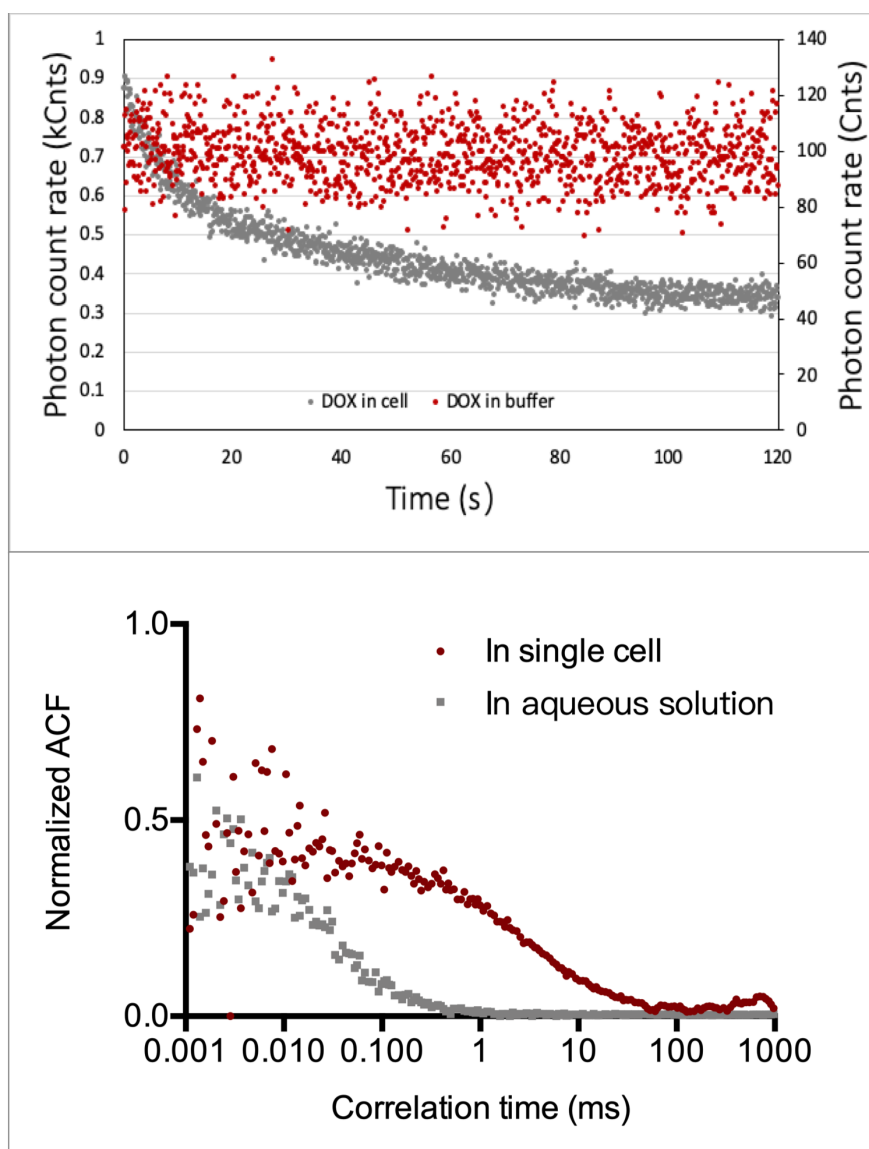


Figure 1.10: Take **DOX** as an example, the time trace of **DOX** fluorescence intensity in aqueous solution and in cell nucleus (upper panel), and the corresponding **ACF** (lower panel). The **ACF** from the cell can not reach to 0 at an infinite correlation time, the parameters fit from the curve are not accurate anymore.

thracycline molecules, we determine the  $K$  for an anthracycline-DNA interaction in cell nucleus.

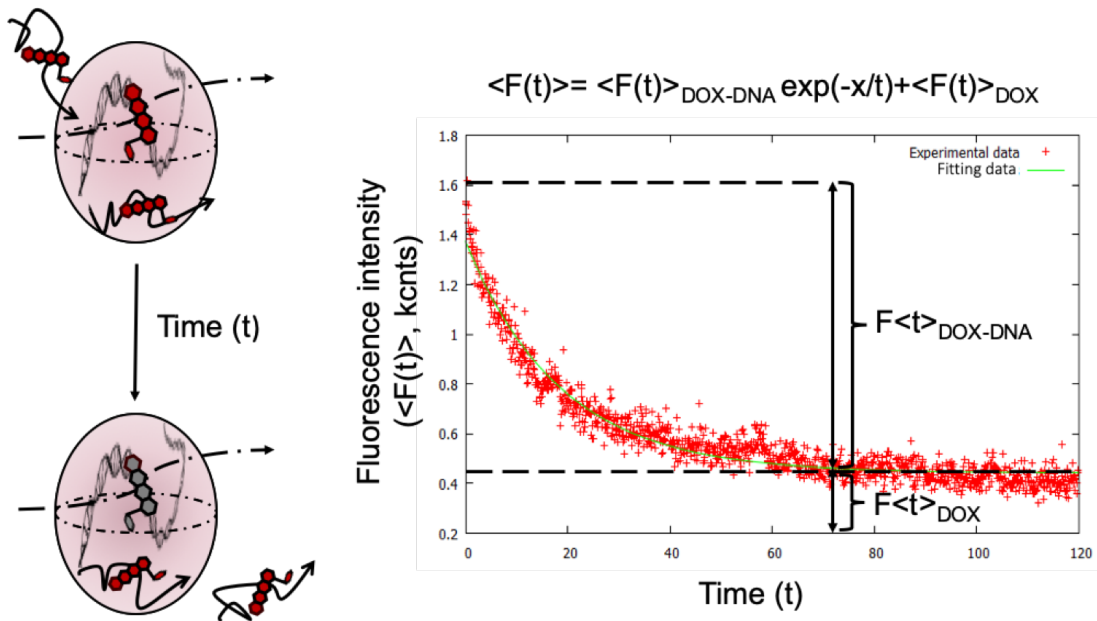


Figure 1.11: The idea behinds the fluorescence decay fitting. Take DOX-DNA interaction as an example. In confocal, the bound DOX molecules can not be replaced with the fresh DOX molecules on time, they are bleached, leading the fluorescence decay over time. In contrast, the free diffusing DOX molecules can be replenished rapidly, their time trace of fluorescence intensity is still stable. Thus, by fitting the whole fluorescence decay curve with a mono-exponential function, the fraction of bound and unbound DOX molecules is determined.

More specifically, within the confocal volume, the concentration of anthracyclines is calculated by:

$$C = \frac{\langle F(t) \rangle}{N_A \cdot V_{eff} \cdot MB} \quad (1.53)$$

Denote equation 1.53 into formula 1.3, we get the equilibrium constant:

$$K = \frac{\frac{\langle F(t) \rangle_{ANT-DNA}^{eq}}{N_A \cdot V_{eff} \cdot MB_{ANT-DNA}}}{\frac{\langle F(t) \rangle_{ANT}^{eq}}{N_A \cdot V_{eff} \cdot MB_{ANT}} \cdot c_{DNA}^{eq}} = \frac{\langle F(t) \rangle_{ANT-DNA}^{eq}}{\langle F(t) \rangle_{ANT}^{eq}} \cdot \frac{MB_{ANT}}{MB_{ANT-DNA}} \cdot \frac{1}{C_{DNA}^{eq}} \quad (1.54)$$

Thus, by simply fitting the intensity ratio of bound and unbound anthracycline molecules, we can determine the  $K$  of anthracycline-DNA in nucleus. The **MB** ratio of unbound and bound anthracycline molecules are calculated with the help of **FCS** measurement.

# Aggregation of anthracyclines

---

The flat aromatic structure of anthracyclines facilitates the formation of dimers or higher aggregates. The self-aggregation process of anthracyclines can compete with anthracycline-DNA interactions, and affect the  $K$  values in anthracycline-DNA interactions. To clear the self-aggregation issue at our working concentrations, we analyzed the fluorescence absorption and emission spectra for all anthracyclines with a series of concentrations.

## 2.1 Materials and instruments

### 2.1.1 Materials

Buffer (Tween 20-EDTA-sodium phosphate, pH= 7.4): the 100 mM stock solution was prepared by diluting 19 mL of 0.2 M  $\text{NaH}_2\text{PO}_4 \cdot \text{H}_2\text{O}$  and 81 mL of 0.2 M  $\text{Na}_2\text{HPO}_4 \cdot 7\text{H}_2\text{O}$  with 100 mL Milli-Q water. The working buffer was prepared by diluting 146.12 mg EDTA and 50 mL of 100 mM sodium phosphate into 450 mL distilled water, 0.002% Tween 20 was used as the surfactant.

Anthracyclines: solid DOX was purchased from Santa Cruz Biotechnology Inc, solid

**DNR**, **EPR**, and **IDR** were purchased from Sigma-Aldrich, Inc. The 100  $\mu\text{M}$  **DOX** stock solution was prepared by dissolving the solid compound into Milli-Q water. After sonication, it was stored at 4°C. Each time before experiment, the stock solution was diluted to a desired working concentration. **DNR**, **EPR**, and **IDR** were prepared the same way as **DOX**.

### 2.1.2 Instruments

UV-2700 spectrophotometer (Shimadzu) and Fluorolog-3 spectrofluorometer (HORIBA Scientific). All of the measurements were conducted at 25°C.

## 2.2 Results and discussions

Due to instrument detection limit, the lowest measuring concentrations of anthracyclines were set at 10000 nM, the absorption and emission spectra of each anthracycline are illustrated in figure 2.1.

Take **DOX** as an example, we inferred that no self-aggregates formed at our measuring concentrations from two aspects.

### A. The shape of absorption and emission spectra

The shapes of **DOX** absorption spectra were totally identical with each other at different concentrations, so did the emission spectra. It was a good evidence of no aggregation. Though at 550 nm of the emission spectra, we can see a decrease of fluorescence intensity with the increase of **DOX** concentration, it was the result of inner filter effects [98, 99]. On one hand, the concentrated sample can let the excitation beam be

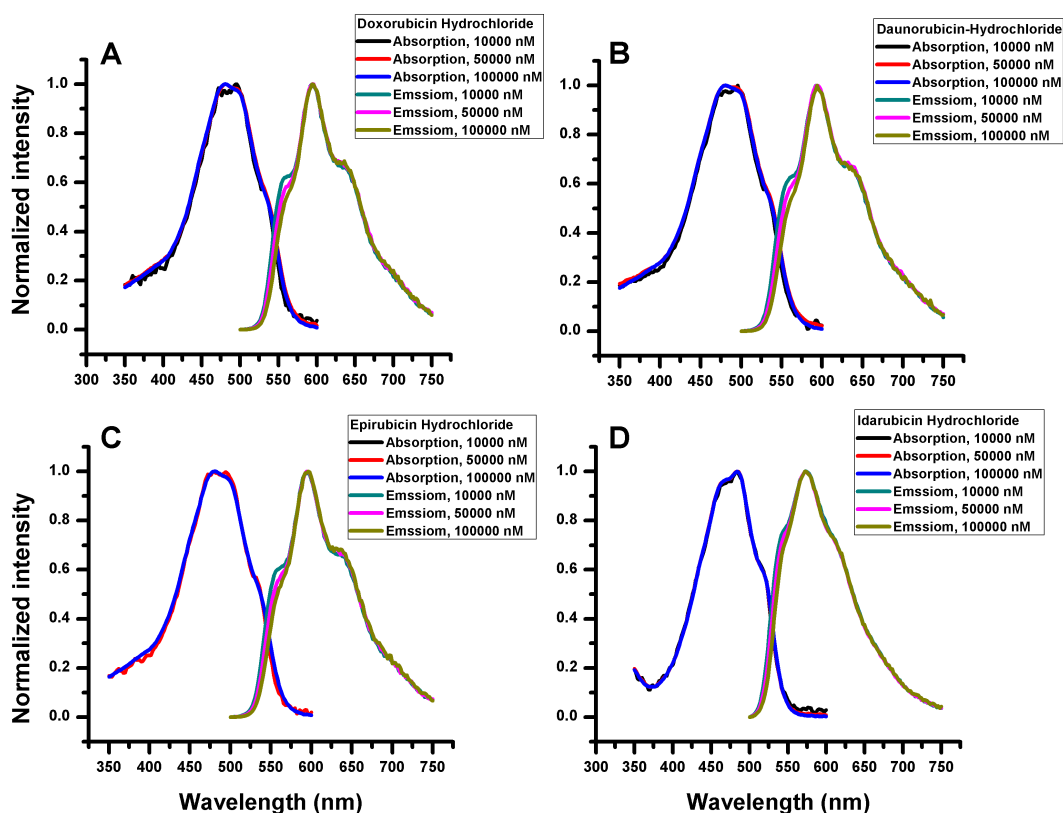


Figure 2.1: Absorption and emission spectra of anthracyclines in PB-EDTA buffer (pH=7.4). A. DOX, B. DNR, C. EPR, D. IDR.

attenuated in the center of the cuvette, thus, less fluorescence emission was detected. On the other hand, the light emitted from the centre of the cuvette was reabsorbed by DOX itself due to the overlapping of excitation and emission spectra.

### B. The peak of fluorescence intensity

According to the previous reference [100], if there are only DOX monomers, one intensity peak should occur at 490 nm in absorption spectra and three distinct peaks should occur at around 560 nm, 594 nm, and 638 nm in emission spectra. If there is the

formation of **DOX** dimers, the monomer spectra will have a 25 nm red shift. From our results, no peak shift occurred, thus no aggregates were formed in the concentration range from 10  $\mu\text{M}$  to 100  $\mu\text{M}$ . Also, according to the reported dimerization constant ( $10^{4.8} \text{ M}^{-1}$ ) of **DOX** molecules, even there are dimers formed, the number of the dimers is negligible when working concentration is below 100 nM.

From the two aspects above, we can also draw similar conclusions that **DNR**, **EPR**, and **IDR** formed no aggregates when their concentrations were in the range between 10  $\mu\text{M}$  to 100  $\mu\text{M}$  [9, 101, 102].

## 2.3 Summary

No self-aggregates were present in anthracycline solutions, when the concentrations of anthracyclines were up to 100  $\mu\text{M}$ . In  $K$  determinations, if the anthracycline concentrations are below 100  $\mu\text{M}$ , the anthracycline-anthracycline interactions do not affect the equilibrium of anthracycline-DNA interactions.

# Equilibrium constants determination in aqueous solution

---

To quantify how strong the anthracyclines can bind with DNA, we determined the  $K$  value for the formation of anthracycline-DNA complexes. To exclude the influence of macromolecules on kinetic study, we conducted our experiments in aqueous solution at first. To make sure the environment in aqueous solution is as close as that in a cell, we performed our experiments at a physiological condition. By using FCS method, we determined the  $K$  at the nanomolar level. To confirm the results acquired by FCS method, we also determined the  $K$  with the single-MB analysis method. Since all anthracyclines share a similar molecular structure, we expect a small difference of action mechanism among these anthracyclines. Thus, we firstly determined the  $K$  for the most studied anticancer drug DOX in the interactions with different types of DNA. Once the  $K$  was determined for DOX, we applied the same way to determine the  $K$  for DOX analogs.

## 3.1 Materials, instruments, methods, and working flow

### 3.1.1 Materials

#### A. Buffer

Buffer was prepared the same way as that in section 2.1.1.

#### B. Anthracyclines

The stock solutions were prepared the same way as that in section 2.1.1. To precisely prepare the working solution at the nanomolar level, before 4°C storing, we aliquoted the stock solution to a concentration of 10  $\mu\text{M}$ . Each time before experiment, the aliquot was diluted to a working concentration of 80 nM.

#### C. DNA

**DNA:** we used different types of DNA, varying in lengths and structures, the details are listed in table 3.1. All types of DNA were stored in standard Tris-EDTA buffer at  $-20^{\circ}\text{C}$ . In a typical experiment for  $K$  determination, DNA was diluted into a series of working concentrations. DNA concentrations varied from 800 nM to 80 nM, 16 concentrations in total. To be noticed, in the following content, all of the DNA concentrations refer to bp concentrations.

#### D. Reference dye

Solid Rhodamine 110 was purchased from Sigma-Aldrich Inc, USA. The stock solution was prepared by dissolving the compound into Milli-Q water with a concentration

Table 3.1: Details of DNA used in our experiment.

Structure	DNA	Length (bp)	Manufacturer
Linear	Oligonucleotide double-strands	20	IBA GmbH, Germany
	Oligonucleotide double-strands	69	IBA GmbH, Germany
	NoLimits Fragment	2500	Thermo Fisher Scientific, US
	Purified calf thymus (ct) DNA	13200	Merck KGaA, Darmstadt, Germany
Circular	$\lambda$ DNA	48502	Thermo Fisher Scientific, US
	pUC 19 plasmid DNA	2686	Thermo Fisher Scientific, US

of 100  $\mu$ M, and it was stored at 4°C. The working solution was diluted from the stock solution and its concentration was about 1 nM.

### E. Sample preparation

The working solution of anthracycline was mixed in an equal volume with the DNA solution. The mixture was incubated over 12 hours at 25°C before measurement. The final anthracycline concentration in experiment was set at 40 nM unless explicitly stated otherwise.

No chemicals were further purified unless specifically stated.

### 3.1.2 Instruments

Experiments were carried on an inverted confocal microscope with a upgraded Laser Scanning Microscopes (LSM) kit, the details of the instruments are listed in table 3.2.

### 3.1.3 Methods

FCS and single-MB analysis methods.

Table 3.2: Details of instruments used in our experiment.

Instruments	Manufacturer	Parameters
Confocal microscope (C1 series)	Nikon	Objective (Nikon Plan Apo): magnification= 60X NA=1.2 immersion Liquid= water
LSM upgrade kit	PicoQuant GmbH, Germany	Excitation sources Wavelength= 485 nm Frequency= 40 MHz
		Single photon counting detectors (MPD and PerkinElmer) Filter: wavelength= 488 nm, long path
		TCSPC modules /
		Software (SymPhoTime 64) /
Power meter (PM100)	Thorlabs, Germany	/
Temperature controller	OkoLab, Italy	/
Glass-bottom container	Thermo Fisher Scientific, US	/

### 3.1.4 Working flow

Every time before experiment, the laser power was set at  $50 \pm 5 \mu\text{W}$  with the laser meter, the temperature was set at  $25 \pm 0.5 \text{ }^\circ\text{C}$  with the temperature controller. Samples were loaded into the well of the glass-bottom chamber and the confocal was at a distance of  $10 \mu\text{m}$  from the edge of the chamber. The volume of the confocal was calibrated with the reference dye Rhodamine 110. Typically, a single measurement lasted 90 s. The control of the system and preliminary data analysis were dealt with the software SymPhoTime 64. Further data analysis was performed by our self-written Python scripts. Each measurement was repeated 3 times within run, 2 runs in total.

## 3.2 Results and discussions

### 3.2.1 Equilibrium constants determination with FCS method

#### A. ACF fitting in DOX-DNA interaction

The ACF curves of DOX-DNA (pUC 19) interactions are displayed in figure 3.1. By fitting the ACF curve of pure DOX solution with the 1-component model (equation 1.38), we got the diffusion time of DOX ( $\tau_{DOX} = 0.023$  ms) and the number of DOX ( $N_{DOX} = 4.9 \pm 0.2$ ) in confocal. With equation 1.30, we calculated DOX diffusion coefficient ( $D_{DOX} = (4.0 \pm 0.3) \times 10^{-10}$  m<sup>2</sup> s<sup>-1</sup>). Compared with DOX diffusion time ( $\tau_{DOX} = 0.023$  ms), the triplet time of DOX ( $\tau_t = 0.6$   $\mu$ s) was two orders smaller, thus, the contribution of triplet state was negligible. With the addition of DNA, the ACF shifted to the long lag time region (from black to red curve in figure 3.1), which meant the occurrence of the second slow component. The more the DNA, the more contribution of the second component. By fitting the ACF curves with the 2-component model (equation 1.39), we got the diffusion time of DOX-DNA complexes ( $\tau_{DOX-DNA} = (0.06 \pm 0.01) \times 10^{-10}$  m<sup>2</sup> s<sup>-1</sup>), and our result was comparable to the reported number [47].

#### B. Equilibrium constant determination for DOX-DNA interaction

Next, to fit  $K$  with equation 1.40, firstly, we set  $n = \frac{2686}{3.1} = 866.5$  for 2686 bp plasmid DNA (according to previous report [103], each DOX can bind with 3.1 bp). Then, by titrating 400 nM DNA into 40 nM DOX solution, we got the parameter  $\frac{MB_{DOX}}{MB_{DOX-DNA}}$  with a value of  $(6.6 \pm 0.1)$  (details can be seen in the reference published by Zhang [47]). In previous reports, the parameter  $\frac{MB_{DOX}}{MB_{DOX-DNA}}$  varied from 5.0-10.0 [43, 47, 79, 104, 105],

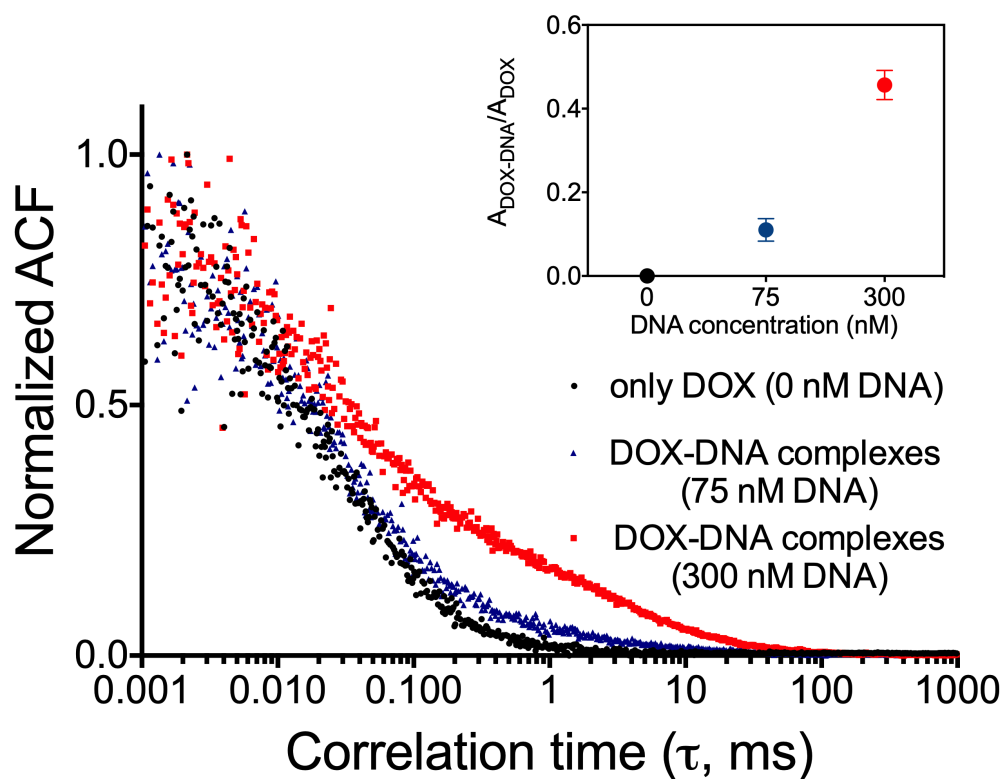


Figure 3.1: The autocorrelation curve of a specific DOX-DNA interaction. With the addition of DNA, the diffusion time of DOX becomes longer, meaning the attachment of DOX to a slow component. The more the DNA, the more obvious to see the attachment of DOX on a slow diffusion component.

our result was comparable with them. Finally, we got the  $K$  with a value of  $(2.3 \pm 0.6) \times 10^6 \text{ M}^{-1}$  (see figure 3.2).

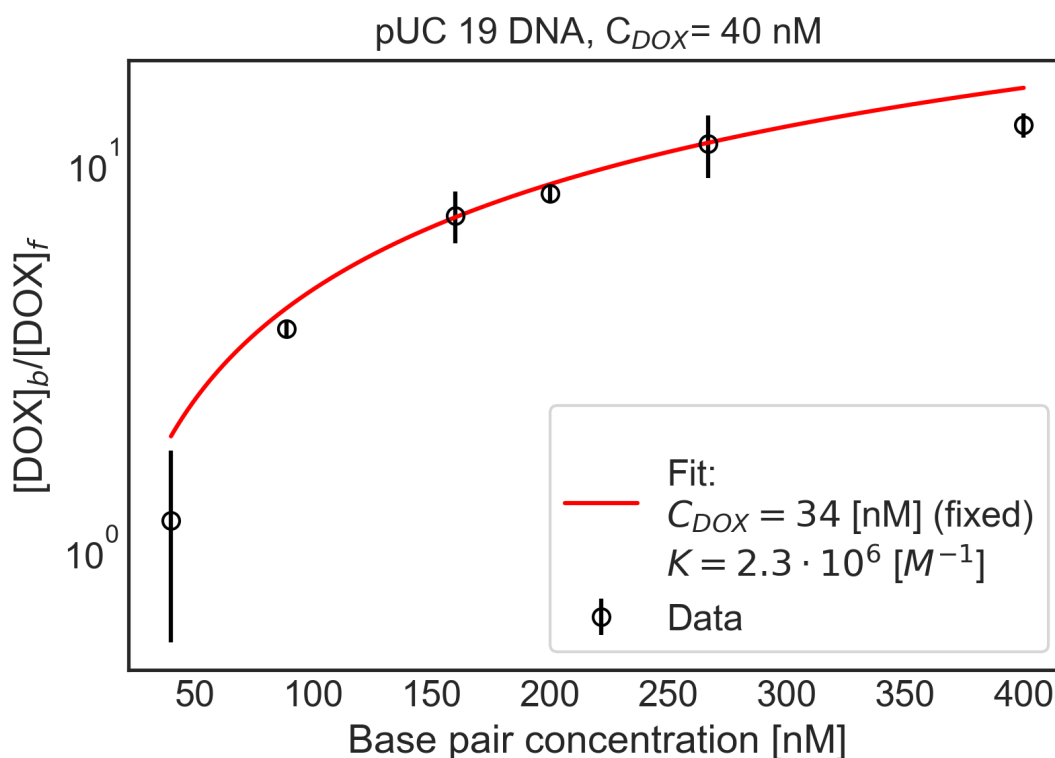


Figure 3.2: The  $K$  fitting in a specific DOX-DNA interaction.

### C. Equilibrium constants determination in the interaction between DOX analogs and DNA

Further, to check whether the DNA structure can affect the value of  $K$ , we determined the  $K$  when DOX was reacting with 2500 bp linear DNA. To check whether the FCS method can be applied for DOX analogs, we determined the  $K$  for DNR- and EPR-DNA interactions. The  $K$  values are displayed in figure 3.3 (other parameters in fitting are listed in appendix B.1). The  $K$  value of DOX-DNA (2500 bp) interaction was  $(1.2 \pm 0.2) \times 10^6 \text{ M}^{-1}$ . While they were  $(1.0 \pm 0.4) \times 10^6 \text{ M}^{-1}$  and  $(3.1 \pm 0.1) \times 10^6 \text{ M}^{-1}$  for DNR-DNA interaction and EPR-DNA interaction respectively. On the average, the  $K$  value of anthracycline-DNA interactions was  $(1.9 \pm 1.0) \times 10^6 \text{ M}^{-1}$ , agreed with the

previous result determined by FCS method (see table 1.2). From the results, we know that DNA structure does not affect anthracycline affinity. We also know DOX analogs share a similar affinity with DOX in the interactions with DNA in aqueous solution.

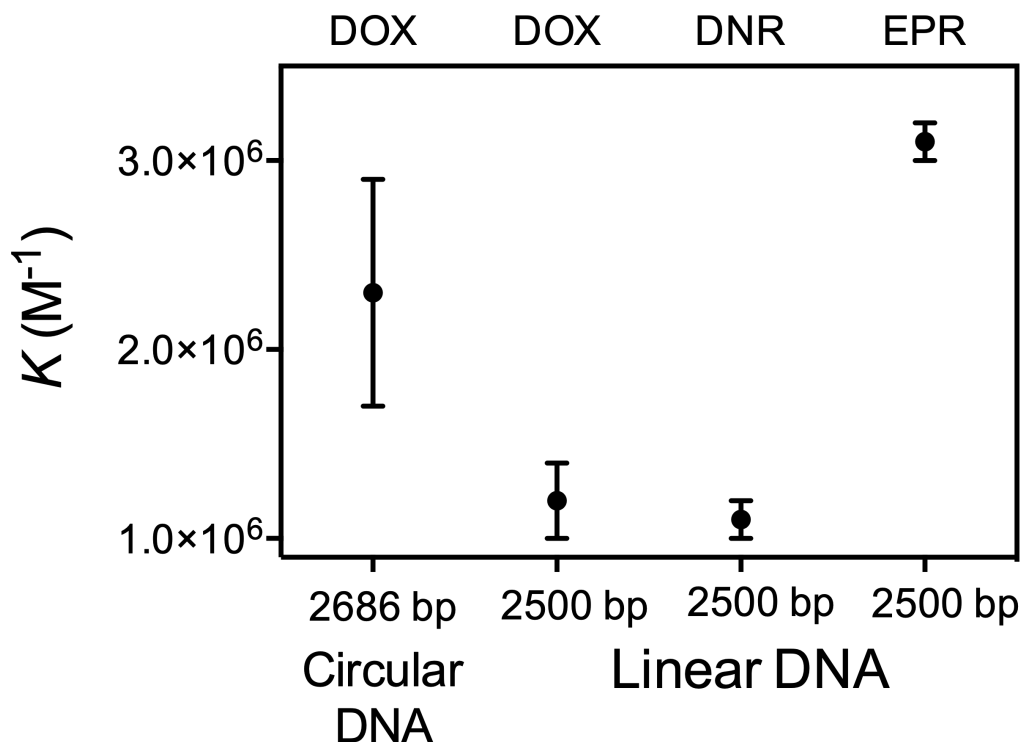


Figure 3.3: Equilibrium constants of anthracycline-DNA interactions in aqueous solution, determined by FCS method.

However, in recent years, for DOX-DNA interaction, a 2-reaction model (intercalation and external aggregates formation) is proposed [12, 14, 23] (see figure 3.4). The intercalation of DOX is a strong reaction, with a  $K$  value at the order of  $10^8 M^{-1}$ . It is apparent when DNA concentration is much larger than DOX concentration (namely,  $C_{DNA} \gg C_{DOX}$ ). When the available bp on DNA are occupied by DOX molecules, the excess DOX molecules suspend on the DNA chain and form external aggregates with

the previously formed DOX-DNA complexes. The formation of external aggregates is a weak reaction, with a  $K$  value at the order of  $10^5 \text{ M}^{-1}$ . It is dominant when DOX concentration is much larger than DNA concentration (namely,  $C_{DNA} \ll C_{DOX}$ ).

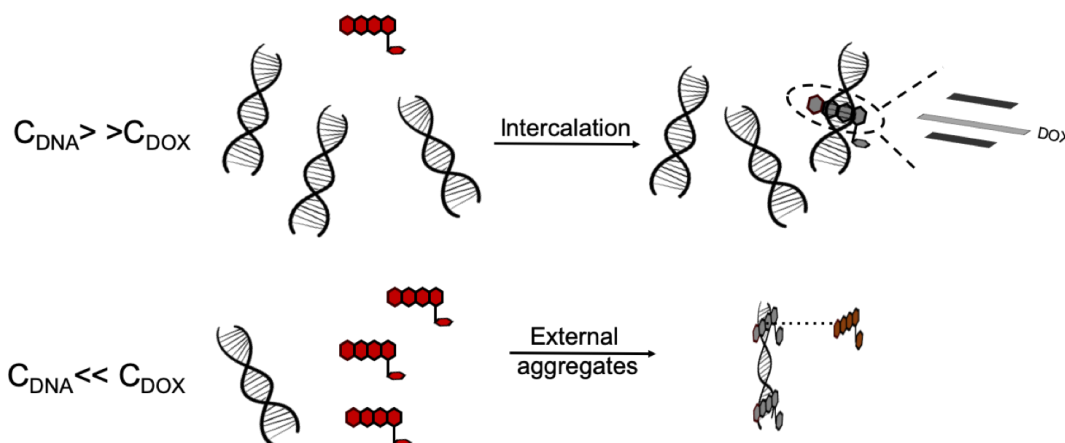


Figure 3.4: Two types of reactions are involved in DOX-DNA interaction. When the DNA concentration is larger than DOX concentration, DOX molecules react with DNA mainly through intercalation. When DOX concentration is larger than DNA concentration, DOX molecules overhang on DNA and form external aggregates with the previously formed DOX-DNA complexes.

If there are two types of complexes formed in DOX-DNA interaction, the  $K$  value determined by FCS method is not reliable anymore— since the fitting model (see equation 1.39) in FCS analysis does not correspond to the formation of external aggregates. However, we should not neglect that DOX-(DOX-DNA) complexes also contribute to the fluctuations of fluorescent signals in FCS measurement, because they are fluorescent. In this case, the  $K$  determined by FCS method reflects DOX average affinity in the two reactions. Though we can analyze the ACF curve with a new fitting model (for instance, a 3-component model), we can not differentiate the contribution from DOX-DNA complexes and DOX-(DOX-DNA) complexes very well, because the two

complexes have a similar diffusion coefficient, their contribution in fluorescence fluctuations could be similar. In this case, we need to use a more sensitive method to distinguish the fluorescent signals from complexes DOX-DNA and complexes DOX-(DOX-DNA).

To solve the issue mentioned above, we applied the single-MB analysis method to determine the  $K$  for DOX-DNA interaction. The single-MB method is based on analyzing the MB change of fluorescent molecules in reaction, it can even monitor one photon difference from molecule to molecule. As DOX-DNA complexes and DOX-(DOX-DNA) complexes have different MB, by using the single-MB analysis method, we can differentiate the fluorescence signals from the two complexes properly. Consequently, we can determine DOX affinity in the two types of reactions separately.

### 3.2.2 Equilibrium constants determination with single-MB analysis method

#### A. Proof of two equilibrium states in DOX–DNA interaction

By monitoring the MB change of DOX in reaction, we confirmed that there are 2 types of reactions in DOX-DNA interaction (see figure 3.5). In experiment, we kept a constant concentration of DOX (40 nM) and we varied DNA concentrations (40-400 nM). We plotted the MB of DOX as a function of DOX to DNA concentration ratio ( $R = \frac{C_{DOX}}{C_{DNA}}$ ). By fitting the curve with a linear function, we divided the MB change of DOX into two regimes. We also determined the cross-over point of the two regimes ( $R = 0.43 \pm 0.03$ ) in DOX-DNA (pUC 19) interaction. To check whether the MB change of DOX is related to DNA types or not, we determined the R in the interactions between DOX and different types of DNA: from the very short 20 bp to the

very long 48502 bp DNA. On the average, the R was  $0.39 \pm 0.05$ , agreed with the previous reported number 0.35 [14].

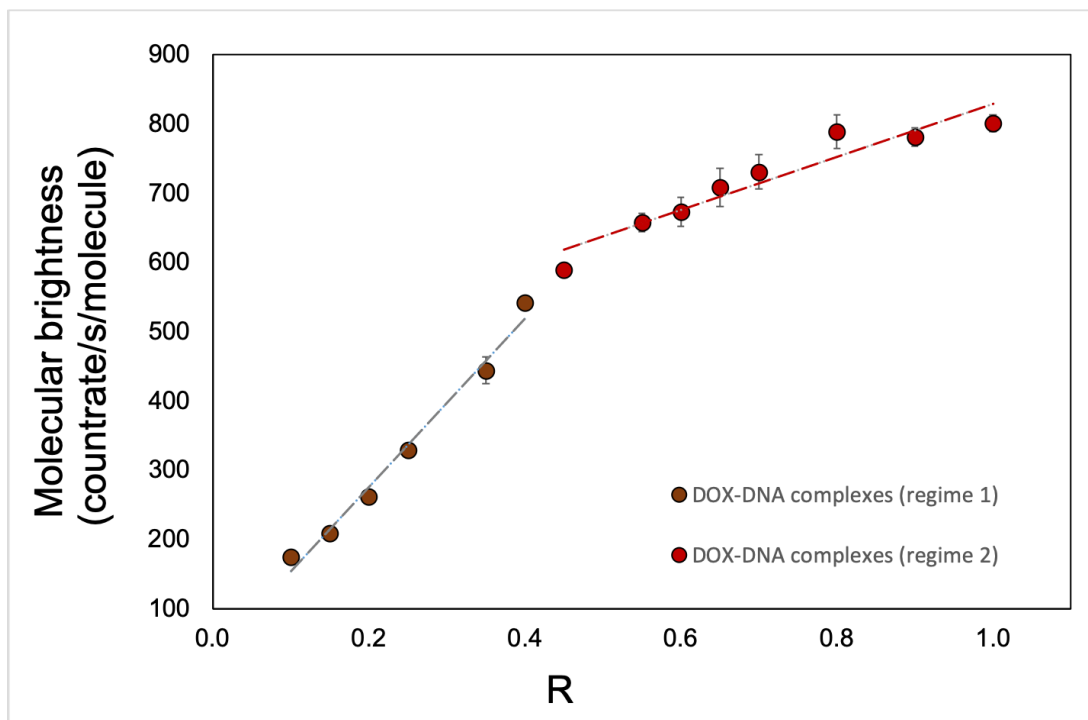


Figure 3.5: The average MB change of DOX in a specific reaction with pUC 19 DNA. With the increase of R, it is possible to determine the two regimes where DOX has different trends in MB change. The MB of unbound DOX molecules ( $\alpha$ ) was 1159 counts/s/molecule in this specific measurement.

As each DOX can bind with 3.1 bp on DNA chain, we expected to reach the saturation of available binding sites when R was 0.32. Thus, we focused on the regime where  $0 < R \leq 1$  to determine the MB of DOX in each type of reaction. We set the intercept of the linear fitting in regime 1 as the MB of DOX-DNA complexes ( $\gamma_1$ ). Also, we set the intercept in regime 2 as the MB of DOX-(DOX-DNA) complexes ( $\gamma_2$ ). By dividing  $\alpha$  with  $\gamma_1$  or  $\gamma_2$ , we calculated how much DOX changed their initial MB in reaction. On the average, DOX changed  $16.56 \pm 10.70$  folds of their initial MB in forming

DOX-DNA complexes. To form DOX-(DOX-DNA) complexes, DOX changed  $2.45 \pm 0.50$  folds of their initial MB. The alteration of DOX MB in each type of reaction is presented in figure 3.6.

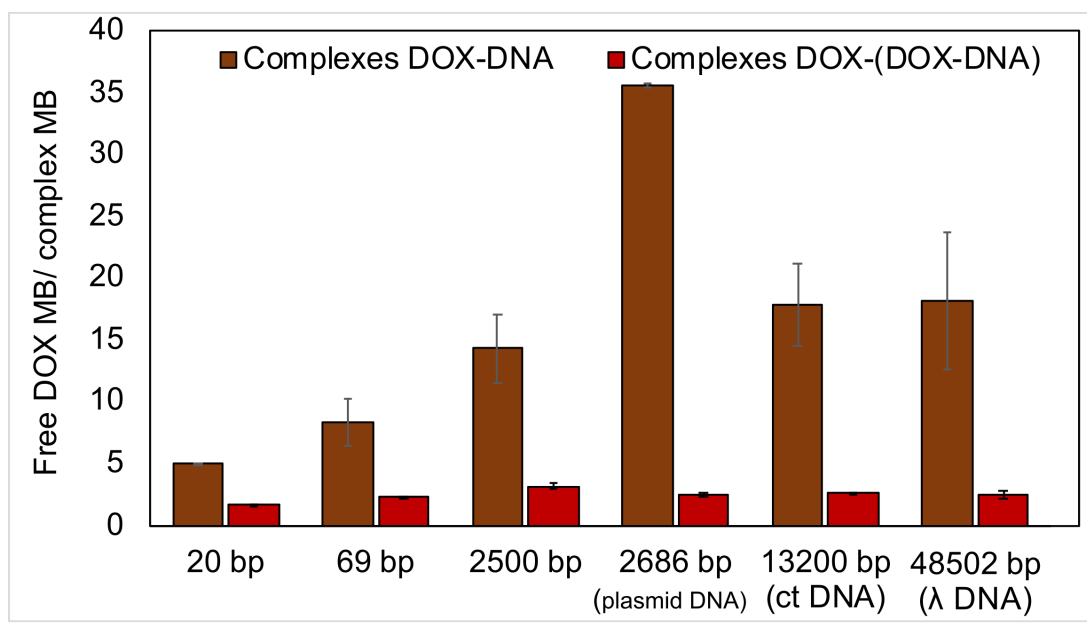


Figure 3.6: The MB change of DOX in forming different types of complexes. The DNA used in reaction varied in length and structure.

In intercalation, there is a correlation between DNA length and DOX MB change, the longer the DNA, the more significant the MB change. An exception is circular plasmid DNA. In the reaction with plasmid DNA, DOX changed 37-fold of its initial MB. In the formation of DOX-(DOX-DNA) complexes, DOX MB change was similar irrespective of DNA lengths or structures. To explain the MB change of DOX in reactions, we proposed the possible mechanisms as follows (see figure 3.7).

**a. The probability of light absorption by DOX molecules**

The number of photons detected in confocal volume is related to the light absorbed by DOX molecules. While the probability of light absorption is decided by the angle between the transition dipole moment of DOX molecules and the electric field vector of the excitation light. When the electric field of the excitation light is parallel to the absorption dipole moment of a DOX molecule, the DOX molecule has the greatest chance to absorb a photon. In contrast, when the absorption dipole moment is perpendicular to the electric field of excitation light, the DOX molecule can not be excited. An unbound DOX molecule can rotate fast to have a proper dipole moment for a maximum absorption (see figure 3.7, panel a).

**b. Physical origin of the formed complexes**

Another factor that affects DOX MB change is the physical origin of the formed complexes. The structure of DOX molecules does not allow them to transform into other quenched conformations such as the case of Cy3 dye (trans- to cis-isomerization). Once the complexes are formed, the direction of DOX dipole moment vector depends on the orientation of the attached DNA. Brownian rotation of DNA dictates the dipole vectors of the bound DOX molecules.

When the DOX–DNA complexes are formed, the DOX molecule intercalates into the bp of DNA through  $\pi$ -stacking [106]. Due to the stacking, the motion of DOX aromatic group is fully limited. The quenched DOX molecule can not adjust its dipole moment for a maximum absorption, leading the significant MB change of the DOX molecule. An exception is the circular plasmid DNA. Compared with entangled linear DNA, circular DNA is less prone to twisting or bending, it has less isotropic distribu-

tion of dipole vectors. As a result, less photons are emitted from the DOX molecule on circular DNA. Also, compared with long DNA, a short DNA can adjust its orientation in electric field more easily, it has more isotropic distribution of dipole vectors. Thus, the DOX molecule changes less of its initial MB in the interaction with short DNA (see figure 3.7, panel b).

### c. The rotation of DOX chromophore group

In the formation of a DOX-(DOX-DNA) complex, the interaction takes place between the aminoglycoside ring of the excess DOX molecule and the formed DOX-DNA complex. Since the tetracenequinone chromophore group of the excess DOX has not participated in interaction, it can rotate freely to have a parallel orientation with the electric field. Thus, more photons are emitted from the freely rotating DOX molecules. As a result, DOX only slightly change their initial MB in electrostatic binding (see figure 3.7, panel c).

## B. Equilibrium constants determination for the interactions between DOX and different types of DNA

With equation 1.48 and 1.52, we determined  $K_1$  and  $K_2$  in DOX-DNA interactions respectively. We display the  $K$  fitting for a specific reaction in figure 3.8, panel a. We also display the equilibrium constants for the interactions between DOX and different types of DNA in figure 3.8, panel b. On the average,  $K_1$  was  $(8.3 \pm 1.2) \times 10^7 \text{ M}^{-1}$  in the formation of DOX-DNA complexes, while  $K_2$  was  $(2.0 \pm 0.5) \times 10^6 \text{ M}^{-1}$  in the formation of DOX-(DOX-DNA) complexes (parameters in detail are listed in appendix B.2).  $K_1$  was around 40 times larger than  $K_2$ , whereas in Gracia's report, the difference is 200 times [14]. This discrepancy could result from the ionic strength

in our measuring conditions. In previous reports about DOX-DNA interactions, when the sodium concentration increases from 2.5 mM to 63 mM, the  $K$  value decreases from  $10^8 \text{ M}^{-1}$  to  $10^7 \text{ M}^{-1}$  [14, 16]. The weaker the ionic strength, the larger the  $K$  value. Since the ionic strength in our measurement was four times stronger than that in Garcia's report [14], it is reasonable for us to have a five times smaller  $K$  than them.

The length or the structure of DNA does not affect the  $K$  values, except for the  $K$  obtained in the reaction with 20 bp DNA (see figure 3.8, panel b). It can be resulted by the sensitivity of the used approaches. The single-MB analysis method is based on collecting the direct signal from the reaction pool, thus, we can monitor the single photon change in reaction. In comparison, FCS method is not based on observing the single-MB change in each reaction (even for long DNA), it is based on the analysis of the fluctuations of fluorescence signals. Thus, the signals from the components with different MB are averaged by the correlation function.

### **C. Equilibrium constants of interactions between DNA and DOX analogs with single-MB analysis**

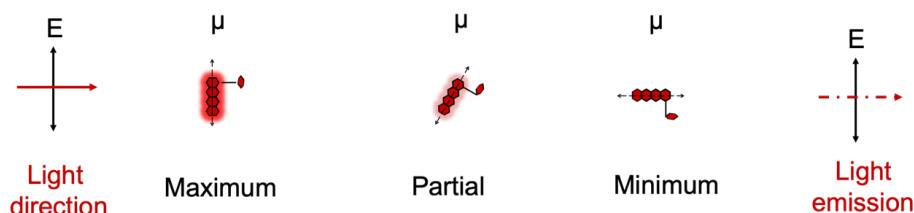
Next, we monitored the MB change of each anthracycline in the interactions with DNA. The results prove that the 2-reaction mechanism is also present for DOX analogs (see figure 3.9). All DOX analogs showed a similar trend in MB change as DOX: a significant MB change (averagely,  $8.7 \pm 3.1$  folds) in forming DOX-DNA complexes, while a slight MB change (averagely,  $2.1 \pm 0.3$  folds) in forming DOX-(DOX-DNA) complexes.

Also, we determined the R for DNR-, EPR- and IDR-DNA interactions with a value of 0.3, 0.4, and 0.3 respectively. Next, we determined  $K_1$  and  $K_2$  for DOX analogs. We have presented the results in figure 3.10. In the formation of anthracycline-DNA

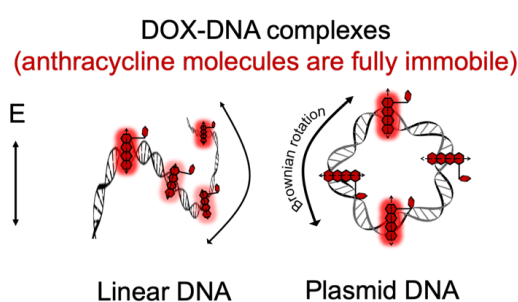
complexes,  $K_1$  were  $(7.8 \pm 0.2) \times 10^7 \text{ M}^{-1}$ ,  $(7.7 \pm 1.1) \times 10^7 \text{ M}^{-1}$ ,  $(7.5 \pm 0.9) \times 10^7 \text{ M}^{-1}$ , and  $(4.8 \pm 0.2) \times 10^7 \text{ M}^{-1}$  in DOX-, DNR-, EPR-, and IDR-DNA interaction respectively. While in the formation of anthracycline-(anthracycline-DNA) complexes,  $K_2$  were  $(2.1 \pm 0.4) \times 10^6 \text{ M}^{-1}$ ,  $(9.8 \pm 1.0) \times 10^5 \text{ M}^{-1}$ ,  $(1.6 \pm 0.0) \times 10^6 \text{ M}^{-1}$ , and  $(1.5 \pm 0.1) \times 10^6 \text{ M}^{-1}$  for DOX, DNR, EPR, and IDR respectively. Parameters in detail are listed in appendix B.2.

To be noticed, as there are limited references stating the bp number each anthracycline requires to form one anthracycline-DNA complex, in curve fitting, we set the number of binding sites for DNR, EPR, and IDR with  $4.3 \pm 0.4$ ,  $2.9 \pm 0.5$ , and  $3.5 \pm 0.7$  respectively. These values were in good agreement with the reported 2-4 bp per binding site for anthracyclines [42, 103, 107, 108].

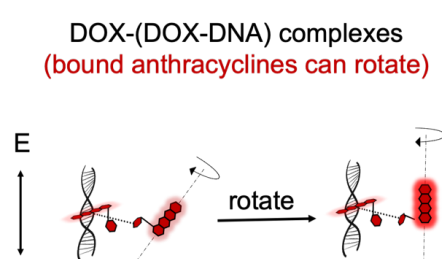
## a. The probability of light absorption by DOX



## b. The physical origin of the formed complexes



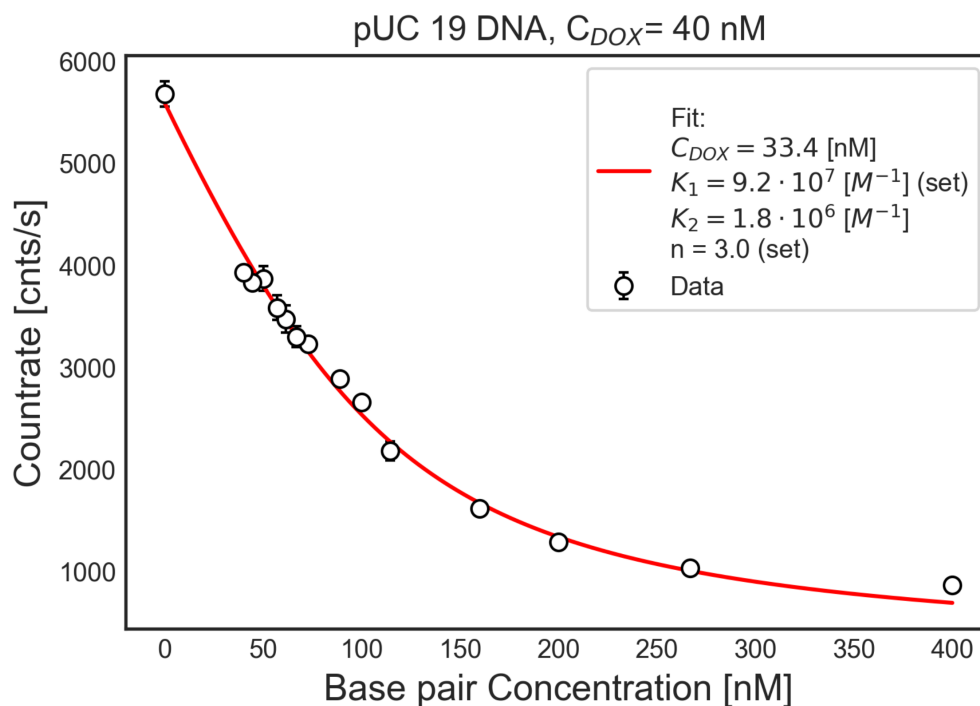
## c. The rotation of DOX chromophore group



E: electric field;  $\mu$ : transition dipole moment

Figure 3.7: Possible mechanisms of DOX MB change in DOX-DNA interaction. a. The probability of light absorption. The photon absorption probability of a DOX molecule depends on the angle between the transition dipole moment of the DOX molecule and the electric field vector of the excitation light. Frequent emission is possible from an unbound DOX molecule because it has a fast rotation. After binding with DNA, the energy levels of a DOX molecule are affected by the DNA, hence, the MB of a DOX molecule changes. b. The physical origin of the formed complexes. In intercalation, compared with entangled linear DNA, circular DNA is less prone to twisting or bending, it has less isotropic distribution of dipole vectors. As a result, less photons are emitted from the DOX bound on plasmid DNA. c. In the formation of DOX-(DOX-DNA) complexes, the MB change of a bound DOX molecule is less dependent on DNA structure, because the chromophore group of the DOX molecule is not in reaction. Thus, the chromophore group of the DOX has more freedom to rotate for a maximum absorption in electric field. As a result, more photons are detected in the formation of DOX-(DOX-DNA) complexes.

a



b

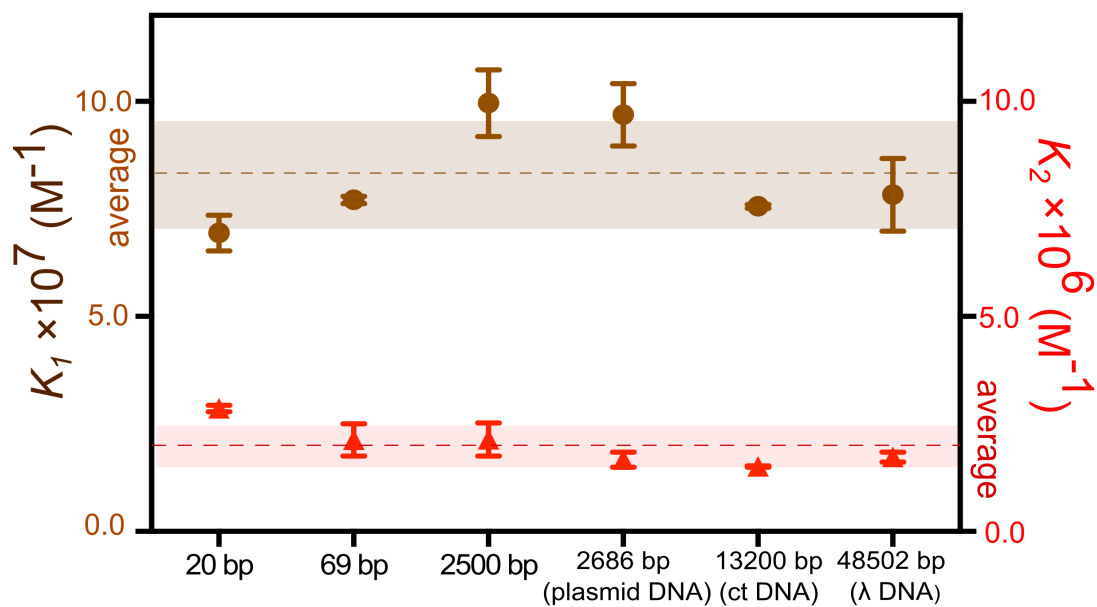


Figure 3.8: Equilibrium constants determination for DOX-DNA interaction. a. Equilibrium constants determined in a specific DOX-DNA (pUC 19) interaction with the 2-reaction model. b. Equilibrium constants determination for interactions between DOX and different types of DNA with the 2-reaction model.

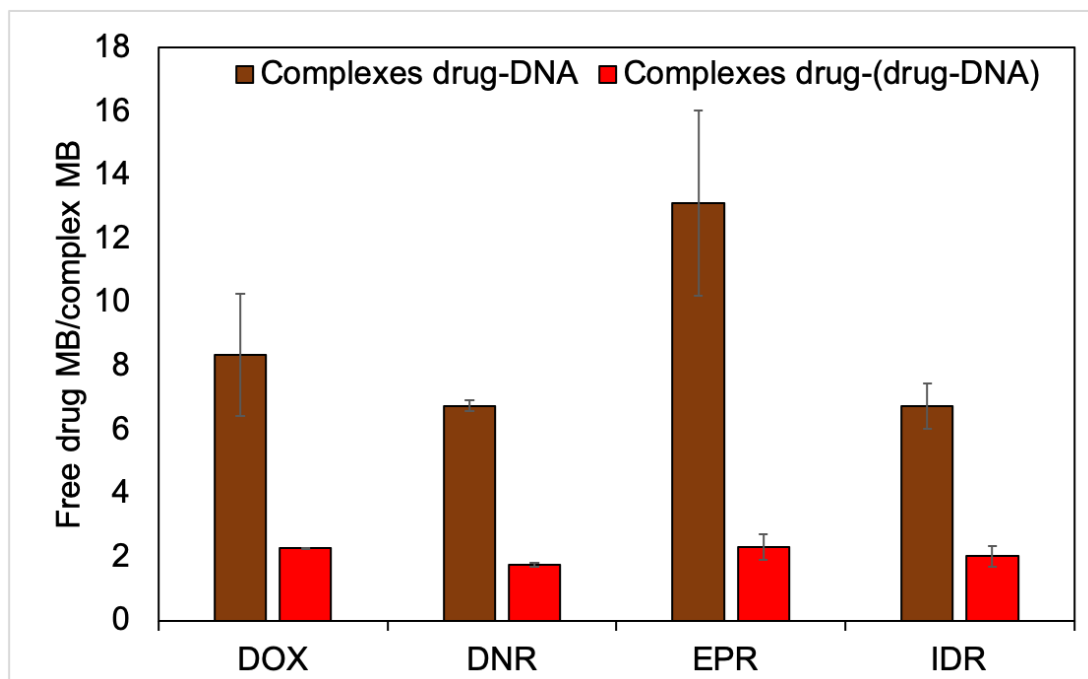


Figure 3.9: MB change of anthracyclines in the formation of each type of complex.

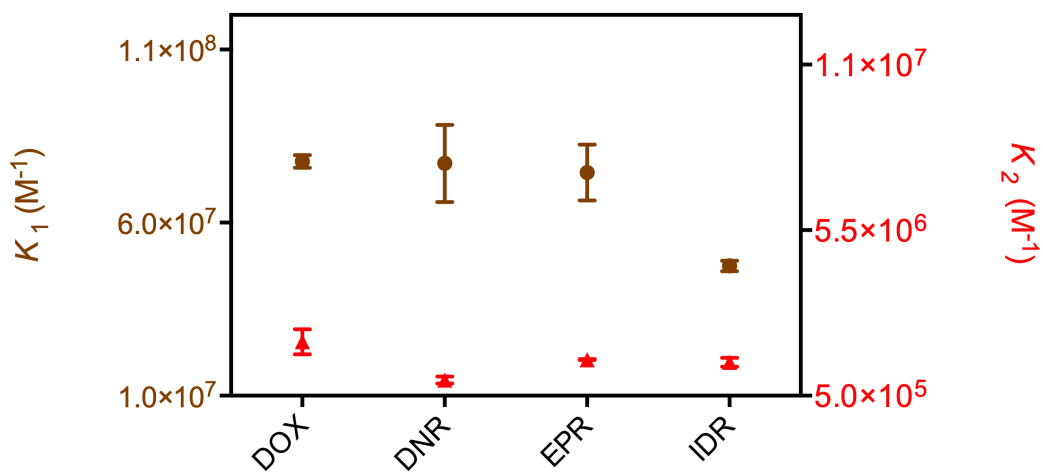


Figure 3.10: Equilibrium constants in the interactions between anthracyclines and DNA.

### 3.3 Summary

1. By using FCS method, we can determine the  $K$  values for anthracycline-DNA interactions. However, if two types of interactions are present in anthracycline-DNA interaction, the  $K$  value determined by FCS method is not accurate, because it is the averaged value of the two types of reactions. With the single-MB analysis method, the  $K$  values of the two types of interactions can be determined separately, because it is based on detecting the single photon change of anthracycline molecules in reactions.
2. With FCS method, we determined the association constants of anthracycline-DNA interactions at nanomolar level. The  $K$  value in DOX-DNA interaction was independent of DNA types. DOX (DNR and EPR showed a similar affinity as DOX in the interaction DNA, the  $K$  value for these anthracyclines was at the order of  $10^6 \text{ M}^{-1}$  in aqueous solution.
3. We applied the single-MB analysis method to determine the  $K$  in anthracycline-DNA interactions. We confirmed that there were two types of reactions (intercalation and electrostatic binding) in anthracycline-DNA interactions, and we explained the possible mechanisms of the two reactions in terms of anthracycline MB change in reactions. The anthracycline affinity in intercalation was 50 times stronger than that in electrostatic binding. The  $K$  of intercalation was at the order of  $10^7 \text{ M}^{-1}$ , while it was at the order of  $10^6 \text{ M}^{-1}$  in electrostatic binding. Besides, the  $K$  were independent of DNA lengths or structures. Moreover, we confirmed that all of the four anthracyclines showed the 2-reaction mechanism in the interaction with DNA, and all of them shared a similar affinity in the binding with DNA.
4. The two reactions occurred at the same time in anthracycline-DNA interactions. The dominant reaction depended on anthracycline to DNA concentration ratio. To

### 3. EQUILIBRIUM CONSTANTS DETERMINATION IN AQUEOUS SOLUTION 63

monitor the electrostatic binding, a sensitive method was required, because the MB change of anthracyclines was not as obvious as that in intercalation.

# Equilibrium constants determination in single living cells

---

From the previous chapter, we know all of the four anthracyclines have a similar affinity in the interaction with DNA in aqueous solution. In this chapter, we chose DOX as the representative and we directly determined the  $K$  of DOX-DNA interaction in the nucleus of single living cells (because 99% of DNA is located in nucleus [109]). More specifically (see figure 4.1): 1 h before experiment, we let DOX diffuse [110] into cells. With the confocal microscopy, we located the nucleus part of the single-cell. Next, we selected a region of interest (ROI) in cell nucleus, set the confocal at the ROI, and collected the fluorescence intensity within the confocal volume over a period of time  $t$  under FCS mode. Finally, by fitting the fluorescence decay with the mono-exponential function, we got the fraction of bound and unbound DOX molecules, and we determined the  $K$  value for DOX-DNA interaction.

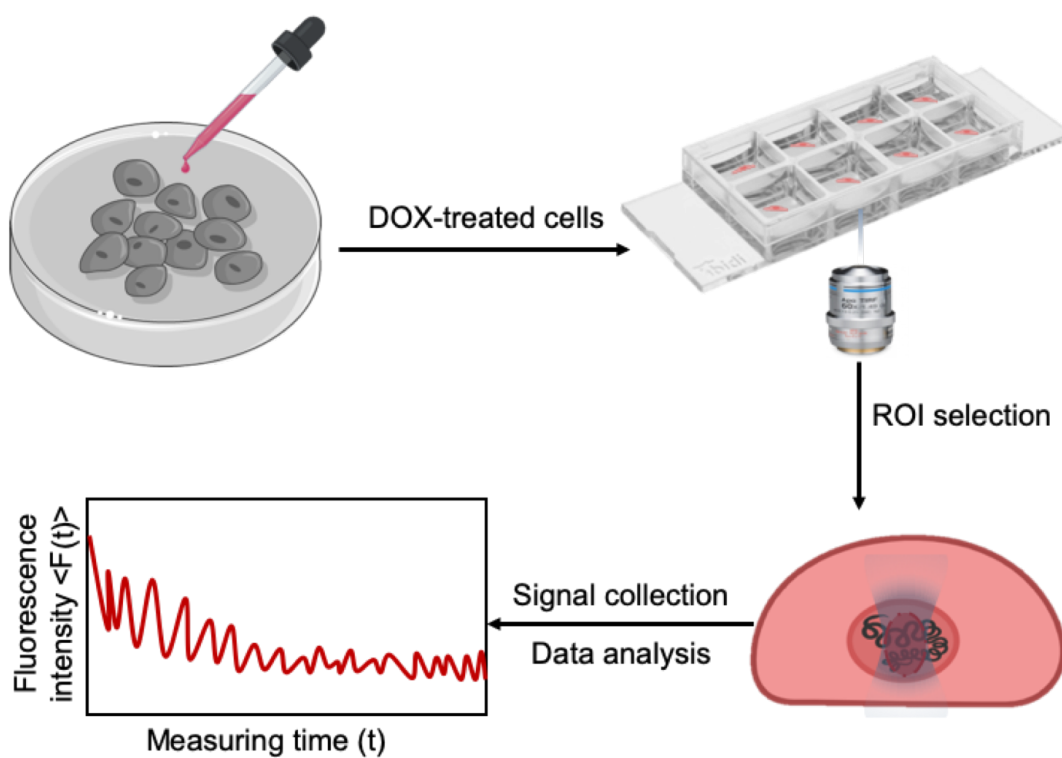


Figure 4.1: Working flow of equilibrium constant determination in single living cells.

## 4.1 Materials, instruments, methods, and working flow

### 4.1.1 Materials

#### A. DOX

The preparation of DOX solution was the same way as that in section 2.1.1.

## B. Cells

HeLa cells were cultured in Dulbecco's modified Eagle's medium (DMEM) with 10% fetal bovine serum (FBS), 100 mg mL<sup>-1</sup> penicillin, 100 mg mL<sup>-1</sup> streptomycin and 2 mM L-glutamine. Cells were maintained at 37°C in a 5% CO<sub>2</sub> humidified atmosphere. One day before experiment, we sub-cultured cells on the 8-well glass-bottom plate for 24 h. The total volume of culture media in the well was 300 μL, the confluence of the cells was around 70%. 1 h before experiment, we replaced the culture media with 270 μL phosphate buffered saline (PBS) buffer containing magnesium and calcium ions and 30 μL DOX solution with a concentration of 300 nM. Fibroblast cells were cultured, maintained and treated with DOX the same way as HeLa cells. HeLa cells were obtained from American Type Culture Collection (ATCC), Manassas, USA; human skin fibroblasts were obtained from Coriell Institute for Medical Research, USA; DMEM, penicillin, streptomycin, L-glutamine and PBS buffer were purchased from Sigma-Aldrich Inc, USA; FBS was purchased from Gibco™, USA.

## C. Reference dye

The stock solution of Rhodamine 110 was prepared the same way as that was in section 3.1.1. To avoid the refractive index mismatch [111], each time before measurement, the 1 nM working solution was acquired by diluting the stock solution into 2.5%<sub>wt</sub> glucose. Glucose was purchased from Sigma-Aldrich Inc, USA.

## D. DNA

pUC 19 DNA was prepared the same way as that in section 3.1.1.

### 4.1.2 Instruments

The instrument settings were the same as that were in section 3.1.2. The temperature was set at  $36 \pm 0.5$  °C in experiment.

### 4.1.3 Methods

Fluorescence decay fitting for the photobleached anthracyclines and single-MB analysis method.

### 4.1.4 Working flow

Each experiment was preceded by a calibration of Rhodamine 110 in 2.5%<sub>wt</sub> glucose. Before recording the fluorescent signals from cells, we checked cell state according to its morphology under confocal mode. Then, under FCS mode, we selected a random point in the nucleus of single-cell as ROI, and we recorded the fluorescence intensity of each ROI for 90-120 s. The background signals were acquired from cells without being treated with DOX for 45 s. The fluorescent signals of 50 cells were recorded in total, those cells with a fluctuating intensity curve were discarded. The control of the system and preliminary data analysis were dealt with the software Symphotime 64. Further data analysis was dealt with Gnuplot (version 4.5). To compare the results in cells and in aqueous solution, we also determined the  $K$  when DOX was reacting with DNA by single-MB analysis method at 36°C.

## 4.2 Results and discussions

### 4.2.1 Cell selection

The apoptosis of a cell can lead the degradation of nuclear DNA [112], further altering the topological state of genomic DNA [113]. As a result, the equilibrium of DOX-DNA interaction is affected and the binding affinity of DOX to DNA can be changed [63]. To accurately determine the  $K$  value in cells, we only collected the fluorescent signals from those living cells. We evaluated the survival of a cell according to its morphology (see figure 4.2). Compared with a cell free of DOX (panel a), an alive cell absorbed DOX (panel b) emitted more fluorescence. While a dead cell with DOX (panel c) was smaller in size and round or oval in shape than an alive cell [114]. In experiment, we measured the background signals from a random ROI (white cross) in cell nucleus as it was in panel a. Then, we calculated the fraction of bound and unbound DOX by measuring the fluorescence intensity from a random ROI (white cross) in cell nucleus as it was in panel b.

### 4.2.2 Equilibrium constants determination in single living cells

In figure 4.3, we illustrate the fluorescence decay fitting in a specific measurement in the nucleus of a HeLa cell. The initial fluorescence intensity was 1.24 kcnts, it decayed to 1/e of its initial intensity at 23.76 s, and kept stable at 0.89 kcnts. By excluding the background signal (0.48 kcnts), we got the ratio of bound DOX and unbound DOX ( $\frac{\langle F(t) \rangle_{DOX-DNA}^{eq}}{\langle F(t) \rangle_{DOX}^{eq}}$ ) with a number of  $\frac{0.35}{0.89-0.48} = 0.86$ .

On the average, the ratio of bound and unbound DOX molecules in HeLa cells was  $1.0 \pm 0.6$ , while it was  $1.0 \pm 0.7$  in fibroblast cells (see table 4.1). As figure 3.6 shows,

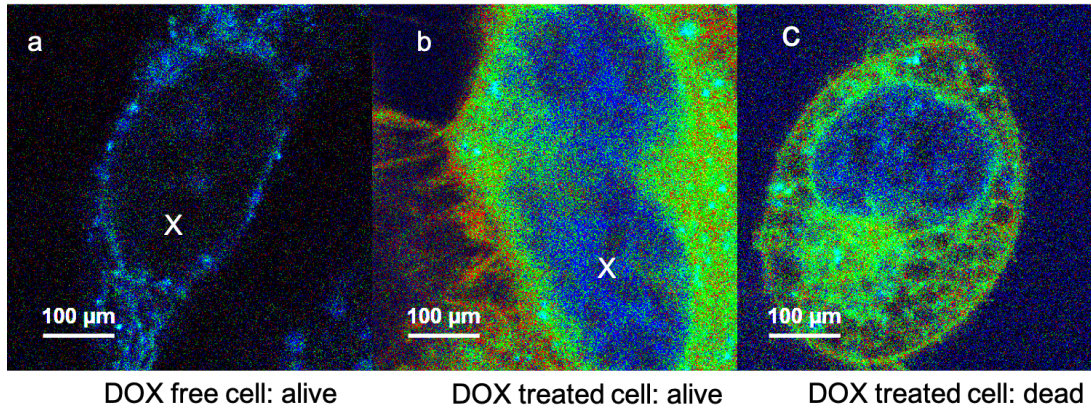


Figure 4.2: The morphology of HeLa cells at different conditions. a. A living cell without DOX. b. Two adjacent living cells with DOX. c. A dead cell with DOX. Compared with the cell without DOX (panel a), a cell with DOX emitted more fluorescence (panel b and c). Compared with living cells (panel b), the cell under apoptosis (panel c) was smaller in size and round or oval in shape. In experiment, we measured the background signal from a cell as in panel a, and we determined the equilibrium constant from a cell as in panel b.

DOX only has 1/16.6-fold of its initial MB when it is intercalating into the bp of DNA, thus, we fixed the parameter  $\frac{MB_{DOX}}{MB_{DOX-DNA}}$  with a number of 16.6. Also, in nucleus, only 1% of the genomic DNA can bind with drug specifically [115, 116], thus, the available DNA concentration ( $C_{DNA}^{eq}$ ) in interaction was 2-order smaller than that we calculated in appendix B.3. Finally, with equation 1.54, we determined the  $K$  with a value of  $(1.5 \pm 0.9) \times 10^5 \text{ M}^{-1}$  in HeLa cells, while it was  $(1.7 \pm 1.1) \times 10^5 \text{ M}^{-1}$  in fibroblast cells.

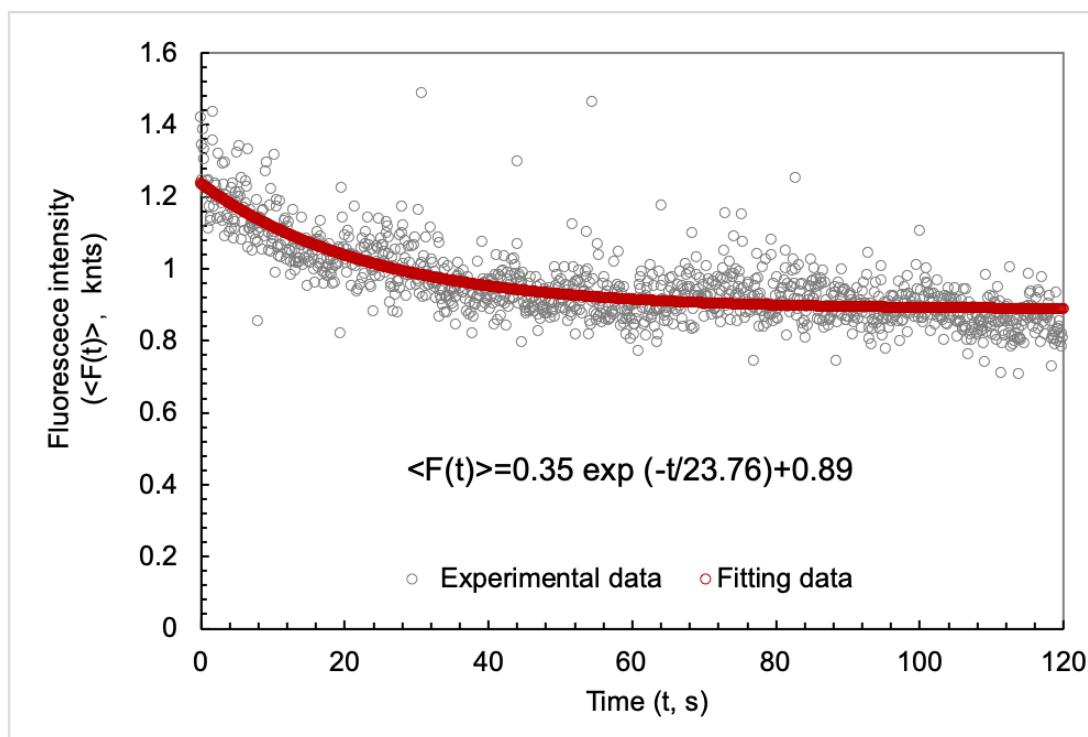


Figure 4.3: The fluorescence decay fitting in a specific measurement in a HeLa cell.

Table 4.1: Critical parameters fitting in equilibrium constants determination in single cells.

Cell lines	Number of cells	$\frac{\langle F(t) \rangle_{DOX-DNA}^{eq}}{\langle F(t) \rangle_{DOX}^{eq}}$	$\frac{MB_{DOX}}{MB_{DOX-DNA}}$	$C_{DNA}^{eq}$ ( $\times 10^{-5} \text{ M}$ )	$K$ ( $\times 10^5 \text{ M}^{-1}$ )
HeLa	25	$1.0 \pm 0.6$	16.6	8.0	$1.5 \pm 0.9$
Fibroblast	29	$1.0 \pm 0.7$	16.6	10.0	$1.7 \pm 1.1$

### 4.2.3 Possible mechanisms for the smaller equilibrium constants determined in cells

Compared with the equilibrium constants determined in aqueous solution at 36°C by single-MB analysis method, the  $K$  determined in single-cells were 1-2 orders smaller (see figure 4.4).

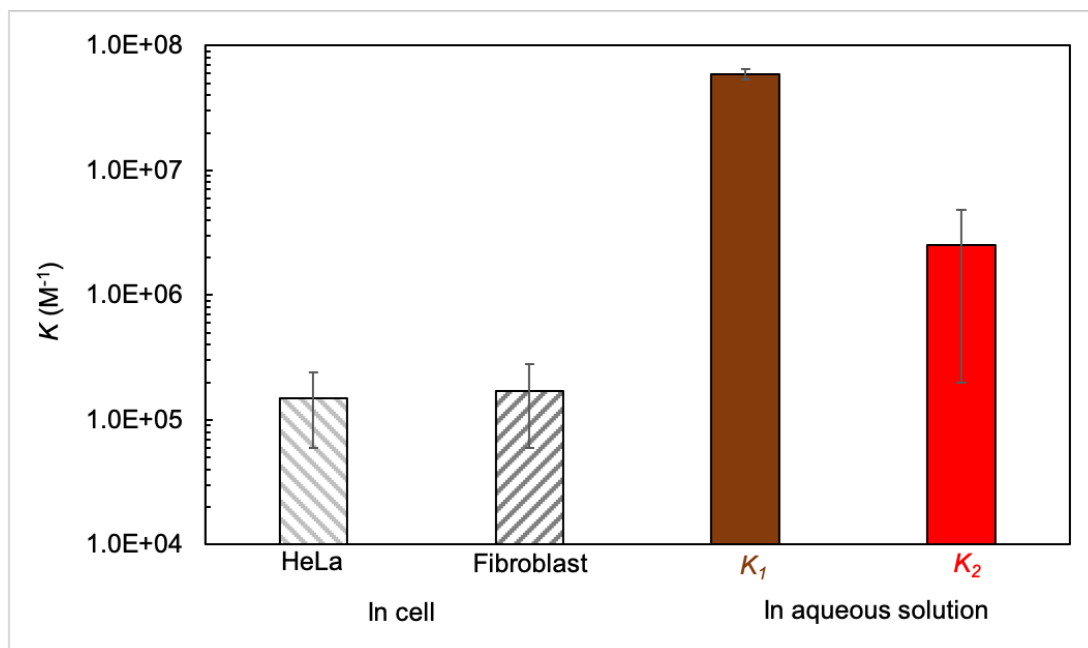


Figure 4.4: Equilibrium constants determined in single-cells and in aqueous solution at 36°C.

However, we have expected that DOX has a similar affinity to DNA in both nucleus and aqueous solution. In other words, the  $K$  determined in nucleus should be in the order of  $10^6$ - $10^7$   $M^{-1}$ . On one hand, according to Bubak's report [117], a probe with a diameter between 2.6-150 nm migrates freely in the 150 nm-wide interchromosomal channel. As a DOX molecule has a diameter of 2.6 nm [118], it can diffuse freely in nucleus. Thus, the fluorescence properties of a DOX molecule in nucleus should be the same as it is in water (no photobleaching for unbound-DOX in nucleus). On the other hand, as the hydrodynamic radius of genomic DNA ( $r_{\text{genomic DNA}} = 243$  nm [119]) is much larger than DOX ( $r_{\text{DOX}} = 1.3$  nm [118]), according to Minton's point of view [63], the binding event of DOX to DNA in nucleus should be same as it is in water. Because the excluded volume of DNA to background molecules remains the same. Based on these facts, we proposed three possible mechanisms to explain the

smaller  $K$  determined in nucleus.

### **A. Hindrance of histones**

Compared with the naked DNA in aqueous solution, DNA in nucleus is wrapped with histones and called as nucleosomal DNA. In previous reports, researchers have found that the affinity of anthracyclines to nucleosomes is lower than naked DNA, because the tails of the core histones can impede drug binding. As a result, both the free energy and the  $K$  of anthracycline-DNA interaction decrease [120, 121].

### **B. Perturbation of side reactions**

On one hand, to maintain the supercoiling state in eukaryotic cells, nucleosomal DNA will react with topoisomerase around through covalent or non-covalent forces [122, 123, 124, 125]. On the other hand, nucleosomal DNA can react with enzymes to repair the damage induced by drugs (chemical stress). For instance, p53 protein-DNA interaction [126], DNase II-DNA interaction [127] and poly (ADPribose) polymerase 1-DNA interaction [128] in DNA repair. If the side reactions are not negligible (see figure 1.4, side reactions), then, the association constant of anthracycline-DNA interaction is not only decided by the kinetics of anthracycline-DNA interaction, but also by the side reactions (see equation 1.13). Thus, it is reasonable for us to have a smaller  $K$  in cells.

### **C. Ionic strength of nucleus**

According to previous reports [129, 130], the nucleus of a living cell contains 0.1 M  $K^+$ , 12 mM  $Na^+$ , 0.5-1 mM  $Mg^{2+}$ , and  $Ca^{2+}$  on  $\mu M$  level. In contrast, for the

measurement in aqueous solution, we maintained the physiological environment with 10 mM Na<sup>+</sup>. Since the ionic strength in nucleus is 10 times higher than that in aqueous solution, and the higher the ionic strength, the lower the  $K$  [14, 16], it is reasonable for us to get a 1-order smaller  $K$  from cellular measurement.

In table 4.1, we also noticed that the  $K$  determined in cells varied 50%. We have proposed two mechanisms to explain such a large deviation.

#### **A. Partitioning between microenvironments**

In nucleus, the genomic DNA is separated into several domains by the background macromolecules, such as the nucleous, speckles, cajal bodies and promyelocytic leukemia protein (PML) bodies (see figure 4.5) [131, 132]. Since the microenvironment of each domain is different, the energy required to transfer DNA to a transition state differs. As a result, the  $K$  in each domain is decided by the fraction of the total system volume occupied by each microenvironment (see equation 1.15), it is reasonable for us to get a diverse  $K$  at different locations in cell nucleus.

#### **B. Heterogeneous distribution of genomic DNA**

As we illustrate in figure 4.5, genomic DNA distributes heterogeneously in the nucleus, leading more accessible DNA on membrane than that at remote distance from the surface [62]. As a result, a rapid association of anthracycline to DNA occurs on the membrane part, it is reasonable for us to have a  $K$  with a deviation of 50% from cell measurements.

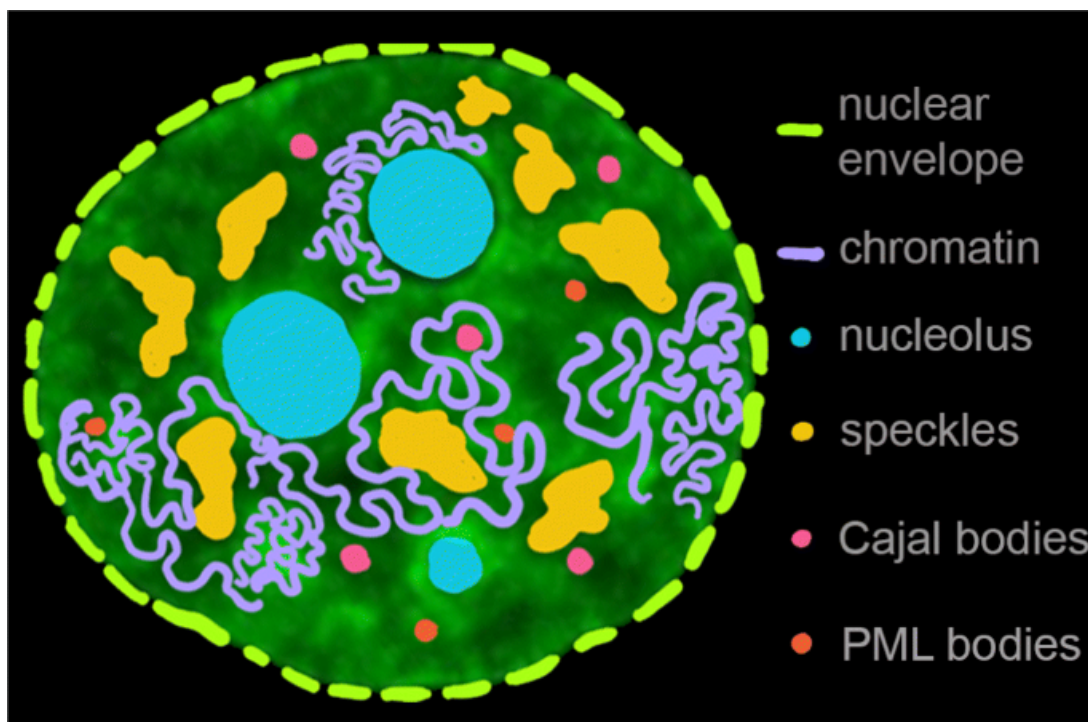


Figure 4.5: The organization of genomic DNA in nucleus. It is heterogeneously distributed, accompanied by different types and numbers of background macromolecules (such as nucleolus, speckles, Cajal bodies and PML bodies). The graph is from Zidovska [131].

#### 4.2.4 Spatial equilibrium constants determination within an individual cell

Though the intratumor heterogeneity of cancer cells can lead the heterogeneous distribution of anthracyclines within an individual cell [133], scientists are still unclear whether the anthracycline affinity is affected by the heterogeneity of cancer cells or not. Thus, we determined the equilibrium constants of DOX-DNA interaction at the nanomolar level at 10 different locations within one cell, 4 cells in total (see figure 4.6). On the average, the  $K$  was  $(1.7 \pm 0.8) \times 10^5 \text{ M}^{-1}$  from ROI to ROI, similar as the  $K$

determined from a random ROI in single cells. It means the affinity of DOX to DNA is not affected by the heterogeneity of cancer cells.

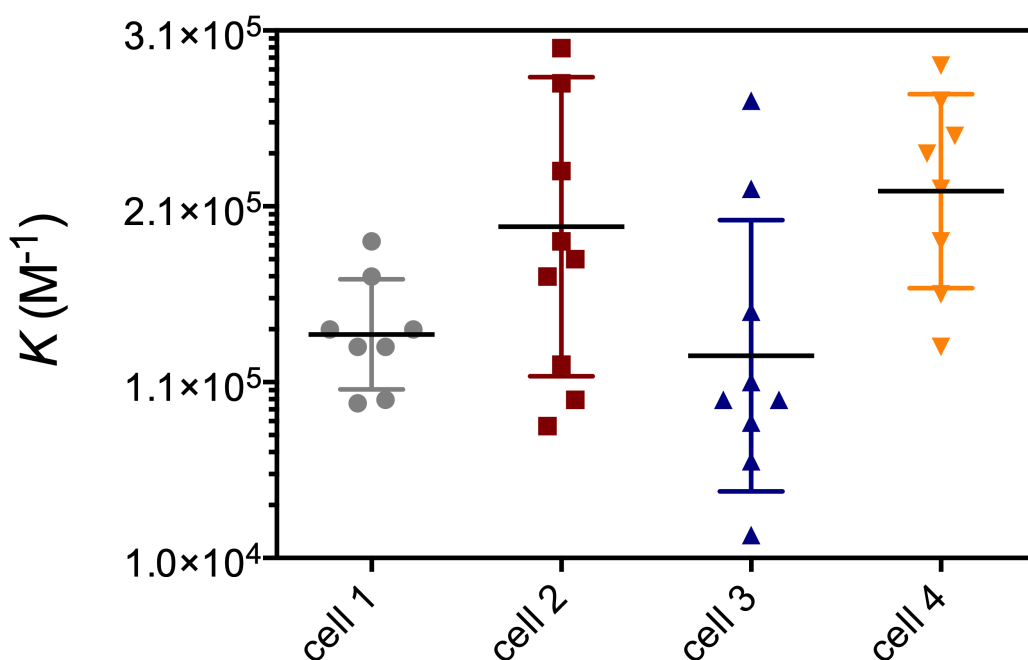


Figure 4.6: Equilibrium constants mapping in single cells.

### 4.3 Summary

1. We developed a method based on the photon bleaching of slow diffusion compounds to determine the  $K$  for DOX-DNA interaction in single living cells.
2. The  $K$  value determined in single living cells is 1-2 orders smaller than that is in aqueous solution. We proposed three mechanisms (hindrance of histones, side reactions and ionic strength) to explain the smaller  $K$  determined in cells. We also explained the 50% error in  $K$  determination could be resulted by the heterogeneous

distribution of **DNA** in nucleus.

3. To check whether the intratumor heterogeneity can affect the affinity of anthracyclines or not, we determined the  $K$  at different locations within one cell. We found the affinity of anthracycline is affected by the intratumor heterogeneity of cancer cells.

4. **DOX** has a similar affinity in healthy and in cancer cells, it is a non-specific anti-cancer drug for all cells in terms of its kinetics.

## Conclusions

---

In this work, we mainly used three different methods based on fluorescence properties of anthracyclines to determine the equilibrium constants in anthracycline-DNA interactions.

In chapter 2, by **Uv-Vis** spectroscopies, we showed anthracyclines had no self-aggregation at micromolar level. When the working concentrations of anthracyclines are below 100  $\mu\text{M}$ , the dimerization of anthracyclines does not compete with anthracycline-DNA interactions, the  $K$  values of anthracycline-DNA interactions are not altered by the self-aggregation process of anthracyclines.

In chapter 3, we determined the association constants in aqueous solution. With **FCS** method, we determined the  $K$  for anthracycline-DNA interactions at nanomolar level. It was at order of  $10^6 \text{ M}^{-1}$ . The  $K$  values were independent of DNA structures. We also found **DOX** analogs shared a similar affinity with **DOX** in the interactions with **DNA**. However, if two types of reactions are present in **DOX**-DNA interactions, the  $K$  determined by **FCS** method is not reliable. Because the  $K$  determined by **FCS** method reflects **DOX** average affinity in the two reactions. With the single-**MB** analysis method, we confirmed that there were two types of reactions in **DOX**-DNA interactions. We proposed the two action mechanisms of **DOX** (intercalation and electrostatic binding)

based on **DOX MB** change in reactions. We also determined the affinity of anthracyclines to **DNA** in intercalation and in electrostatic binding on single molecule level. The association constant of intercalation was at the order of  $10^7 \text{ M}^{-1}$ , while it was  $10^6 \text{ M}^{-1}$  in electrostatic binding. The affinity of intercalation and electrostatic binding differed 40 times. Moreover, we confirmed that the affinity of anthracyclines to **DNA** was independent of **DNA** lengths and structures. Besides, we found all of the four anthracyclines shared a similar affinity to **DNA**.

In chapter 4, we developed a method based on the bleaching of immobilized fluorescent molecules to determine the equilibrium constant in the nucleus of single living cells. The association constant of DOX-DNA interaction was at the order of  $10^5 \text{ M}^{-1}$  in cell nucleus. For the smaller  $K$  in cell measurement, we proposed three possible mechanisms (hindrance of histones, side reactions, and ionic strength). We also found the affinity of **DOX** differed 50% from cell to cell, it could be resulted by the intratumor heterogeneity of cancer cells. In addition, by determining the equilibrium constants within single cell at different locations, we found the the affinity of **DOX** differed about 50% from location to location. In addition, we confirmed that **DOX** was a non-specific anticancer drug to cells in terms of its affinity. We suggested to notice the vitality of healthy cells in cancer treatment, because **DOX** killed cancer cells and healthy cells equivalently in terms of its kinetics.

## Outlook

---

In the future, we still have several work to do to study the kinetics of anthracycline-DNA interactions.

1. To verify the  $K$  determined in cells. Currently, we still need to verify whether the  $K$  determined in cells was correct or not. The obstacle is that we do not know how much the genomic DNA had participated in reaction. To precisely control the DNA concentration in cells, we have mimicked the crowded nucleus environment by using crowders. However, currently, we can only limit the diffusion of DNA in gel cavity, the rotation of DNA in gel cavity is still a problem. With the development of microfluidic techniques, in the future, we can perform anthracycline-DNA interactions in the crowded synthetic cells by a well-controlled manner [74].
2. How the background macromolecules will alter the equilibrium and kinetics of anthracycline-DNA interactions in cells? Though we have proposed some possibilities which may decrease the  $K$  in cells, we have not verified them yet, especially in a quantitatively way. For instance, what is the critical topoisomerase concentration to alter the equilibrium of anthracycline-DNA interaction? To analyze the impact of side reactions, we can introduce some fluorescent proteins to anthracycline-DNA solutions and determine the equilibrium constants of anthracycline-DNA interactions.

3. How does the DNA structure affect the equilibrium and association constant of anthracycline-DNA interaction in cells? Although Minton has pointed out the small molecules (drugs) binding by macromolecules (DNA) will not be affected in crowded environment due to the unchanged excluded volume of background molecules, it is based on the fact that the state DNA remains the same during reaction. In reality, once genomic DNA feels chemical stress (for instance, anthracyclines), it changes its structure from supercoiling to unwind mode or even to be small pieces. In this case, both the excluded volume to background molecules and the entropy of the system change, the free energy of anthracycline-DNA interaction will change consequently. To qualify or quantify the impact the DNA structure change on anthracycline-DNA interactions, we can use X-ray crystallography [134] or cryogenic electron microscopy to analyze DNA structure in reactions.

4. Enhance the signal to noise ratio for natural anthracyclines. The low quantum yield of anthracyclines has limited the application of fluorescent methods to determine the  $K$ , especially in sub-nanomolar range. We have tried to magnify the fluorescent signal of anthracyclines by attaching a fluorescent dye on them. However, the purity of the new compound is still a problem in practice.

5. Determine the affinity of anthracyclines encapsulated in nano-delivery systems. Currently, multiple drug resistance and cardiotoxicity of anthracyclines have become sever problems to patients. To overcome these issues, researchers have developed anthracycline nano-delivery systems [135]. However, whether the affinity of anthracyclines is affected in these delivery systems or not is still unknown, especially in *in vivo* studies [136]. To have an efficient use of these delivery systems, we need to determine the  $K$  in advance.

6. How do the cells choose their fate under chemical stress? When cells feel the

chemical stress from anthracyclines, they start either repair machinery or programmed death. Will the cell directly choose to be dead if the anthracycline-DNA interaction is too strong (for instance,  $10^7 \text{ M}^{-1}$ )? Or will they struggle for a while by interacting with repair enzymes? To quantify the impact the chemical stress brings on cell fate, we can induce the chemical stress to cells by using a series of anthracyclines with different affinities.

# Bibliography

- [1] E. Espinosa, P. Zamora, J. Feliu, and M. González Barón, “Classification of anticancer drugs - A new system based on therapeutic targets,” *Cancer Treatment Reviews*, vol. 29, no. 6, pp. 515–523, 2003.
- [2] S. Zhu, L. Yan, X. Ji, and W. Lu, “Conformational diversity of anthracycline anticancer antibiotics: A density functional theory calculation,” *Journal of Molecular Structure: THEOCHEM*, vol. 951, no. 1-3, pp. 60–68, 2010.
- [3] P. Shaul, M. Frenkel, E. B. Goldstein, L. Mittelman, A. Grunwald, Y. Ebenstein, I. Tsarfaty, and M. Fridman, “The and cytotoxic activity,” *ACS Medicinal Chemistry Letters*, vol. 4, no. 3, pp. 323–328, 2013.
- [4] P. Venkatesh and A. Kasi, “Anthracyclines,” pp. 1–8, 2020.
- [5] A. A. Almaqwashy, T. Paramanathan, I. Rouzina, and M. C. Williams, “Mechanisms of small molecule-DNA interactions probed by single-molecule force spectroscopy,” *Nucleic Acids Research*, vol. 44, no. 9, pp. 3971–3988, 2016.
- [6] M. F. Brana, M. Cacho, A. Gradillas, B. de Pascual-Teresa, and A. Ramos, “Intercalators as Anticancer Drugs,” *Current Pharmaceutical Design*, vol. 7, no. 17, 2005.
- [7] M. Sirajuddin, S. Ali, and A. Badshah, “Drug-DNA interactions and their study by UV-Visible, fluorescence spectroscopies and cyclic voltametry,” *Journal*

- of Photochemistry and Photobiology B: Biology*, vol. 124, pp. 1–19, 2013. [Online]. Available: <http://dx.doi.org/10.1016/j.jphotobiol.2013.03.013>
- [8] D. Agudelo, P. Bourassa, G. Bérubé, and H. A. Tajmir-Riahi, “Intercalation of antitumor drug doxorubicin and its analogue by DNA duplex: Structural features and biological implications,” *International Journal of Biological Macromolecules*, vol. 66, pp. 144–150, 2014.
- [9] C. Ozluer and H. E. S. Kara, “In vitro DNA binding studies of anticancer drug idarubicin using spectroscopic techniques,” *Journal of Photochemistry and Photobiology B: Biology*, vol. 138, pp. 36–42, 2014. [Online]. Available: <http://dx.doi.org/10.1016/j.jphotobiol.2014.05.015>
- [10] M. Denel-Bobrowska and A. Marczak, “Structural modifications in the sugar moiety as a key to improving the anticancer effectiveness of doxorubicin,” *Life Sciences*, vol. 178, pp. 1–8, 2017. [Online]. Available: <http://dx.doi.org/10.1016/j.lfs.2017.04.009>
- [11] S. Bhaduri, N. Ranjan, and D. P. Arya, “An overview of recent advances in duplex DNA recognition by small molecules,” *Beilstein Journal of Organic Chemistry*, vol. 14, pp. 1051–1086, 2018.
- [12] B. Jawad, L. Poudel, R. Podgornik, N. F. Steinmetz, and W. Y. Ching, “Molecular mechanism and binding free energy of doxorubicin intercalation in DNA,” *Physical Chemistry Chemical Physics*, vol. 21, no. 7, pp. 3877–3893, 2019.
- [13] M. B. Martins-Teixeira and I. Carvalho, “Antitumour Anthracyclines: Progress and Perspectives,” *ChemMedChem*, vol. 15, no. 11, pp. 933–948, 2020.

- [14] C. Pérez-Arnaiz, N. Busto, J. M. Leal, and B. García, “New insights into the mechanism of the DNA/doxorubicin interaction,” *Journal of Physical Chemistry B*, vol. 118, no. 5, pp. 1288–1295, 2014.
- [15] Z. Chen, G. Liu, M. Chen, X. Chen, M. Wu, and X. Chen, “An Instrument-Based Screening Assay for DNA-Targeted Anticancer Drugs Using Resonance Light Scattering,” *Combinatorial Chemistry High Throughput Screening*, vol. 13, no. 5, pp. 383–392, 2010.
- [16] S. S. Tartakoff, J. M. Finan, E. J. Curtis, H. M. Anchukaitis, D. J. Couture, and S. Glazier, “Investigations into the DNA-binding mode of doxorubicinone,” *Organic and Biomolecular Chemistry*, vol. 17, no. 7, pp. 1992–1998, 2019.
- [17] A. Kaczorowska, W. Lamperska, K. Fraczkowska, J. Masajada, S. Drobczyński, M. Sobas, T. Wróbel, K. Chybicka, R. Tarkowski, S. Kraszewski, H. Podbielska, W. Kałas, and M. Kopaczyńska, “Profound nanoscale structural and biomechanical changes in DNA helix upon treatment with anthracycline drugs,” *International Journal of Molecular Sciences*, vol. 21, no. 11, pp. 1–14, 2020.
- [18] J. B. Chaires, S. Satyanarayana, D. Suh, I. Fokt, T. Przewloka, and W. Priebe, “Parsing the free energy of anthracycline antibiotic binding to DNA,” *Biochemistry*, vol. 35, no. 7, 1996.
- [19] M. S. Salahudeen and P. S. Nishtala, “An overview of pharmacodynamic modelling, ligand-binding approach and its application in clinical practice,” *Saudi Pharmaceutical Journal*, vol. 25, no. 2, pp. 165–175, 2017. [Online]. Available: <http://dx.doi.org/10.1016/j.jsps.2016.07.002>

- [20] F. Keller and A. Hann, “Clinical pharmacodynamics: Principles of drug response and alterations in kidney disease,” *Clinical Journal of the American Society of Nephrology*, vol. 13, no. 9, pp. 1413–1420, 2018.
- [21] J. Wang, Z. Guo, Y. Fu, Z. Wu, C. Huang, C. Zheng, P. A. Shar, Z. Wang, , W. Xiao, and Y. Wang, “Weak-binding molecules are not drugs?-toward a systematic strategy for finding effective weak-binding drugs,” *Briefings in Bioinformatics*, vol. 18, no. 2, pp. 321–332, 2017.
- [22] V. Kairys, L. Baranauskiene, M. Kazlauskiene, D. Matulis, and E. Kazlauskas, “Binding affinity in drug design: experimental and computational techniques,” *Expert Opinion on Drug Discovery*, vol. 14, no. 8, pp. 755–768, 2019.
- [23] M. Airoidi, G. Barone, G. Gennaro, A. M. Giuliani, and M. Giustini, “Interaction of doxorubicin with polynucleotides. a spectroscopic study,” *Biochemistry*, vol. 53, no. 13, pp. 2197–2207, 2014.
- [24] T. D. Pollard, “MBOC technical perspective: A guide to simple and informative binding assays,” *Molecular Biology of the Cell*, vol. 21, no. 23, pp. 4061–4067, 2010.
- [25] P. Schwille and E. Haustein, “Fluorescence correlation spectroscopy. An introduction to its concepts and applications,” *Doi:10.1002/Lpor.200910041*, pp. 1–33, 2001. [Online]. Available: <http://scholar.google.com/scholar?hl=en&btnG=Search&q=intitle:Fluorescence+correlation+spectroscopy+An+introduction+to+its+concepts+and+applications#0>

- [26] K. Bielec, G. Bubak, T. Kalwarczyk, and R. Holyst, "Analysis of Brightness of a Single Fluorophore for Quantitative Characterization of Biochemical Reactions," *Journal of Physical Chemistry B*, vol. 124, no. 10, pp. 1941–1948, 2020.
- [27] I. Haq, B. Z. Chowdhry, and T. C. Jenkins, "Calorimetric techniques in the study of high-order DNA-drug interactions," *Methods in Enzymology*, vol. 340, no. 1988, pp. 109–149, 2001.
- [28] R. M. Kenney, K. E. Buxton, and S. Glazier, "Investigating the impacts of DNA binding mode and sequence on thermodynamic quantities and water exchange values for two small molecule drugs," *Biophysical Chemistry*, vol. 216, pp. 9–18, 2016. [Online]. Available: <http://dx.doi.org/10.1016/j.bpc.2016.05.002>
- [29] W. Ma, L. Yang, and L. He, "Overview of the detection methods for equilibrium dissociation constant KD of drug-receptor interaction," *Journal of Pharmaceutical Analysis*, vol. 8, no. 3, pp. 147–152, 2018. [Online]. Available: <http://dx.doi.org/10.1016/j.jpha.2018.05.001>
- [30] K. Butowska, K. Żamojć, M. Kogut, W. Kozak, D. Wyrzykowski, W. Wiczak, J. Czub, J. Piosik, and J. Rak, "The product of matrix metalloproteinase cleavage of doxorubicin conjugate for anticancer drug delivery: Calorimetric, spectroscopic, and molecular dynamics studies on peptide–doxorubicin binding to DNA," *International Journal of Molecular Sciences*, vol. 21, no. 18, pp. 1–17, 2020.
- [31] F. Barceló, D. Capó, and J. Portugal, "Thermodynamic characterization of the multivalent binding of chartreusin to DNA," *Nucleic Acids Research*, vol. 30, no. 20, pp. 4567–4573, 2002.

- [32] S. Kelly and N. Price, "The Use of Circular Dichroism in the Investigation of Protein Structure and Function," *Current Protein Peptide Science*, vol. 1, no. 4, pp. 349–384, 2005.
- [33] S. Sass, W. F. Stöcklein, A. Klevesath, J. Hurpin, M. Menger, and C. Hille, "Binding affinity data of DNA aptamers for therapeutic anthracyclines from microscale thermophoresis and surface plasmon resonance spectroscopy," *Analyst*, vol. 144, no. 20, pp. 6064–6073, 2019.
- [34] E. Helmerhorst, D. J. Chandler, M. Nussio, and C. D. Mamotte, "Real-time and label-free bio-sensing of molecular interactions by surface plasmon resonance: A laboratory medicine perspective," *Clinical Biochemist Reviews*, vol. 33, no. 4, pp. 161–173, 2012.
- [35] R. F. Pasternack and P. J. Collings, "Resonance light scattering: A new technique for studying chromophore aggregation," *Science*, vol. 269, no. 5226, pp. 935–939, 1995.
- [36] Z. Chen, G. Liu, M. Chen, X. Chen, M. Wu, and X. Chen, "An Instrument-Based Screening Assay for DNA-Targeted Anticancer Drugs Using Resonance Light Scattering," *Combinatorial Chemistry High Throughput Screening*, vol. 13, no. 5, pp. 383–392, 2010.
- [37] Z. Chen, Y. Peng, M. Chen, X. Chen, and G. Zhang, "DNA as a target for anti-cancer compounds screening directly by resonance light scattering technique," *Analyst*, vol. 135, no. 10, pp. 2653–2660, 2010.
- [38] Z. Chen, S. Qian, X. Chen, J. Chen, G. Zhang, and G. Zeng, "Investigation on the interaction between anthracyclines and DNA in the presence of paclitaxel

- by resonance light scattering technique,” *Microchimica Acta*, vol. 177, no. 1-2, pp. 67–73, 2012.
- [39] Z. Chen, G. Zhang, X. Chen, and W. Gao, “A resonance light-scattering off-on system for studies of the selective interaction between adriamycin and DNA,” *Analytical and Bioanalytical Chemistry*, vol. 402, no. 6, pp. 2163–2171, 2012.
- [40] H. Yu, J. Ren, J. B. Chaires, and X. Qu, “Hydration of drug-DNA complexes: Greater water uptake for adriamycin compared to daunomycin,” *Journal of Medicinal Chemistry*, vol. 51, no. 19, pp. 5909–5911, 2008.
- [41] S. Charak, D. K. Jangir, G. Tyagi, and R. Mehrotra, “Interaction studies of Epirubicin with DNA using spectroscopic techniques,” *Journal of Molecular Structure*, vol. 1000, no. 1-3, pp. 150–154, 2011.
- [42] P. F. Fouzia, A. Nasima, R. Qureshi, J. Nowsherwan, A. Sultan, B. Nosheen, and H. Rafique, “Electrochemical, spectroscopic and theoretical monitoring of anthracyclines’ interactions with DNA and ascorbic acid by adopting two routes: Cancer cell line studies,” *PLoS ONE*, vol. 13, no. 10, pp. 1–19, 2018.
- [43] Z. Mirzaei-Kalar, A. Yavari, and A. Jouyban, “Increasing DNA binding affinity of doxorubicin by loading on Fe<sub>3</sub>O<sub>4</sub> nanoparticles: A multi-spectroscopic study,” *Spectrochimica Acta - Part A: Molecular and Biomolecular Spectroscopy*, vol. 229, p. 117985, 2020. [Online]. Available: <https://doi.org/10.1016/j.saa.2019.117985>
- [44] R. Hajian, E. Ekhlesi, and R. Daneshvar, “Spectroscopic and electrochemical studies on the interaction of epirubicin with fish sperm DNA,” *E-Journal of Chemistry*, vol. 9, no. 3, pp. 1587–1598, 2012.

- [45] L. D. S. Biomoloculaire, F. D. Pharmacie, and C. Analitica, “Quantitative study of doxorubicin in living cell nuclei by microspectrofluorometry Mauro Gigli a , b ., Silvia M . Doglia c , a , Jean M . Millot a , Luigi Valentini b and Michel Manfait a,” *Drugs*, vol. 950, pp. 13–20, 1988.
- [46] V. Rizzo, N. Sacchi, and M. Menozzi, “Kinetic Studies of Anthracycline-DNA Interaction by Fluorescence Stopped Flow Confirm a Complex Association Mechanism,” *Biochemistry*, vol. 28, no. 1, pp. 274–282, 1989.
- [47] X. Zhang, A. Poniewierski, K. Sozański, Y. Zhou, A. Brzozowska-Elliott, and R. Holyst, “Fluorescence correlation spectroscopy for multiple-site equilibrium binding: A case of doxorubicin-DNA interaction,” *Physical Chemistry Chemical Physics*, vol. 21, no. 3, pp. 1572–1577, 2019.
- [48] H. C. Yeh, C. M. Puleo, T. C. Lim, Y. P. Ho, P. E. Giza, R. C. C. Huang, and T. H. Wang, “A microfluidic-FCS platform for investigation on the dissociation of Sp1-DNA complex by doxorubicin,” *Nucleic Acids Research*, vol. 34, no. 21, pp. 1–9, 2006.
- [49] A. Michelman-Ribeiro, D. Mazza, T. Rosales, T. J. Stasevich, H. Boukari, V. Rishi, C. Vinson, J. R. Knutson, and J. G. McNally, “Direct measurement of association and dissociation rates of DNA binding in live cells by fluorescence correlation spectroscopy,” *Biophysical Journal*, vol. 97, no. 1, pp. 337–346, 2009. [Online]. Available: <http://dx.doi.org/10.1016/j.bpj.2009.04.027>
- [50] H. Deschout, K. Raemdonck, J. Demeester, S. C. De Smedt, and K. Braeckmans, “FRAP in pharmaceutical research: Practical guidelines and applications in drug delivery,” *Pharmaceutical Research*, vol. 31, no. 2, pp. 255–270, 2014.

- [51] A. Delon, Y. Usson, J. Derouard, T. Biben, and C. Souchier, "Continuous photobleaching in vesicles and living cells: A measure of diffusion and compartmentation," *Biophysical Journal*, vol. 90, no. 7, pp. 2548–2562, 2006.
- [52] C. Hodges, R. P. Kafle, and J.-C. Meiners, "Quantitative fluorescence correlation spectroscopy on DNA in living cells," *Single Molecule Spectroscopy and Superresolution Imaging X*, vol. 10071, p. 1007102, 2017.
- [53] P. S. Guin and S. Das, "Exploration of Electrochemical Intermediates of the Anticancer Drug Doxorubicin Hydrochloride Using Cyclic Voltammetry and Simulation Studies with an Evaluation for Its Interaction with DNA," *International Journal of Electrochemistry*, vol. 2014, pp. 1–8, 2014.
- [54] N. Elgrishi, K. J. Rountree, B. D. McCarthy, E. S. Rountree, T. T. Eisenhart, and J. L. Dempsey, "A Practical Beginner's Guide to Cyclic Voltammetry," *Journal of Chemical Education*, vol. 95, no. 2, pp. 197–206, 2018.
- [55] J. Monzó, I. Insua, F. Fernandez-Trillo, and P. Rodriguez, "Fundamentals, achievements and challenges in the electrochemical sensing of pathogens," *Analyst*, vol. 140, no. 21, pp. 7116–7128, 2015.
- [56] K. Zia, T. Siddiqui, S. Ali, I. Farooq, M. S. Zafar, and Z. Khurshid, "Nuclear Magnetic Resonance Spectroscopy for Medical and Dental Applications: A Comprehensive Review," *European Journal of Dentistry*, vol. 13, no. 1, pp. 124–128, 2019.
- [57] A. R. Rubio, N. Busto, J. M. Leal, and B. García, "Doxorubicin binds to duplex RNA with higher affinity than ctDNA and favours the isothermal denaturation of triplex RNA," *RSC Advances*, vol. 6, no. 103, pp. 101 142–101 152, 2016.

- [58] B. Doughty, Y. Rao, S. W. Kazer, S. J. Kwok, N. J. Turro, and K. B. Eisenthal, "Binding of the anti-cancer drug daunomycin to DNA probed by second harmonic generation," *Journal of Physical Chemistry B*, vol. 117, no. 49, pp. 15 285–15 289, 2013.
- [59] S. Charak and R. Mehrotra, "Structural investigation of idarubicin-DNA interaction: Spectroscopic and molecular docking study," *International Journal of Biological Macromolecules*, vol. 60, pp. 213–218, 2013.
- [60] R. Hancock, "Crowding , Entropic Forces , and Confinement : Crucial Factors b c," vol. 83, no. 4, pp. 326–337, 2018.
- [61] Y. Hata, T. Sawada, and T. Serizawa, "Macromolecular crowding for materials-directed controlled self-assembly," *Journal of Materials Chemistry B*, vol. 6, no. 40, pp. 6344–6359, 2018.
- [62] G. Rivas and A. P. Minton, "Toward an understanding of biochemical equilibria within living cells," *Biophysical Reviews*, vol. 10, no. 2, pp. 241–253, 2018.
- [63] A. P. Minton, "How can biochemical reactions within cells differ from those in test tubes?" *Journal of Cell Science*, vol. 119, no. 14, pp. 2863–2869, 2006.
- [64] A. P. Minton, "The Influence of Macromolecular Crowding and Macromolecular Confinement on Biochemical Reactions in Physiological Media," *Journal of Biological Chemistry*, vol. 276, no. 14, pp. 10 577–10 580, 2001.
- [65] M. Gao, C. Held, S. Patra, L. Arns, G. Sadowski, and R. Winter, "Crowders and Cosolvents—Major Contributors to the Cellular Milieu and Efficient Means to Counteract Environmental Stresses," *ChemPhysChem*, vol. 18, no. 21, pp. 2951–2972, 2017.

- [66] I. M. Kuznetsova, B. Y. Zaslavsky, L. Breydo, K. K. Turoverov, and V. N. Uversky, “Beyond the excluded volume effects: Mechanistic complexity of the crowded milieu,” *Molecules*, vol. 20, no. 1, pp. 1377–1409, 2015.
- [67] T. Lebeaupin, R. Smith, and S. Huet, “The Multiple Effects of Molecular Crowding in the Cell Nucleus,” *Nuclear Architecture and Dynamics*, pp. 209–232, 2018.
- [68] H. X. Zhou, G. Rivas, and A. P. Minton, “Macromolecular crowding and confinement: Biochemical, biophysical, and potential physiological consequences,” *Annual Review of Biophysics*, vol. 37, pp. 375–397, 2008.
- [69] G. Rivas and A. P. Minton, “Macromolecular Crowding In Vitro, In Vivo, and In Between,” *Trends in Biochemical Sciences*, vol. 41, no. 11, pp. 970–981, 2016. [Online]. Available: <http://dx.doi.org/10.1016/j.tibs.2016.08.013>
- [70] A. P. Minton, “Macromolecular crowding,” *Current Biology*, vol. 16, no. 8, pp. 269–271, 2006.
- [71] Y. Phillip, E. Sherman, G. Haran, and G. Schreiber, “Common crowding agents have only a small effect on protein-protein interactions,” *Biophysical Journal*, vol. 97, no. 3, pp. 875–885, 2009. [Online]. Available: <http://dx.doi.org/10.1016/j.bpj.2009.05.026>
- [72] Y. L. Zhou, J. M. Liao, J. Chen, and Y. Liang, “Macromolecular crowding enhances the binding of superoxide dismutase to xanthine oxidase: Implications for protein-protein interactions in intracellular environments,” *International Journal of Biochemistry and Cell Biology*, vol. 38, no. 11, pp. 1986–1994, 2006.

- [73] T. Díaz-López, C. Dávila-Fajardo, F. Blaesing, M. P. Lillo, and R. Giraldo, “Early Events in the Binding of the pPS10 Replication Protein RepA to Single Iteron and Operator DNA Sequences,” *Journal of Molecular Biology*, vol. 364, no. 5, pp. 909–920, 2006.
- [74] E. Sokolova, E. Spruijt, M. M. Hansen, E. Dubuc, J. Groen, V. Chokkalingam, A. Piruska, H. A. Heus, and W. T. Huck, “Enhanced transcription rates in membrane-free protocells formed by coacervation of cell lysate,” *Proceedings of the National Academy of Sciences of the United States of America*, vol. 110, no. 29, pp. 11 692–11 697, 2013.
- [75] B. Monterroso, B. Reija, M. Jiménez, S. Zorrilla, and G. Rivas, “Charged molecules modulate the volume exclusion effects exerted by crowders on FtsZ polymerization,” *PLoS ONE*, vol. 11, no. 2, pp. 1–14, 2016.
- [76] D. M. Jameson, “Introduction to fluorescence,” *Introduction to Fluorescence*, pp. 1–286, 2014.
- [77] N. S. H. Motlagh, P. Parvin, F. Ghasemi, and F. Atyabi, “Fluorescence properties of several chemotherapy drugs: doxorubicin, paclitaxel and bleomycin,” *Biomedical Optics Express*, vol. 7, no. 6, p. 2400, 2016.
- [78] S. Shah, A. Chandra, A. Kaur, N. Sabnis, A. Lacko, R. Fudala, I. Gryczynski, F. Worth, F. Worth, F. Worth, and F. Worth, “Fluorescence properties of doxorubicin in PBS buffer and PVA films,” pp. 65–69, 2018.
- [79] R. Hajian, N. Shams, and M. Mohagheghian, “Study on the interaction between doxorubicin and deoxyribonucleic acid with the use of methylene blue as a

- probe,” *Journal of the Brazilian Chemical Society*, vol. 20, no. 8, pp. 1399–1405, 2009.
- [80] E. Firouzi Niaki, T. Van Acker, L. Imre, P. Nánási, S. Tarapcsák, Z. Bacsó, F. Vanhaecke, and G. Szabó, “Interactions of Cisplatin and Daunorubicin at the Chromatin Level,” *Scientific Reports*, vol. 10, no. 1, pp. 1–12, 2020.
- [81] A. Aranega and H. Boulaiz, “Cellular and Molecular Biology: Foreword,” *Cellular and Molecular Biology*, vol. 51, no. 1, p. 1, 2005.
- [82] J. Ries and P. Schwille, “New concepts for fluorescence correlation spectroscopy on membranes,” *Physical Chemistry Chemical Physics*, vol. 10, no. 24, pp. 3487–3497, 2008.
- [83] D. Satsoura, B. Leber, D. W. Andrews, and C. Fradin, “Circumvention of fluorophore photobleaching in fluorescence fluctuation experiments: A beam scanning approach,” *ChemPhysChem*, vol. 8, no. 6, pp. 834–848, 2007.
- [84] J. Ries, M. Bayer, G. Csúcs, R. Dirkx, M. Solimena, H. Ewers, and P. Schwille, “Automated suppression of sample-related artifacts in Fluorescence Correlation Spectroscopy,” *Optics Express*, vol. 18, no. 11, p. 11073, 2010.
- [85] B. Stefanska and D. J. MacEwan, “Preface,” *Methods in Pharmacology and Toxicology*, no. December, pp. V–VII, 2017.
- [86] A. Gupta, J. Sankaran, and T. Wohland, “Fluorescence correlation spectroscopy: The technique and its applications in soft matter,” *Physical Sciences Reviews*, vol. 4, no. 4, pp. 1–18, 2019.

- [87] E. L. Elson, “Fluorescence correlation spectroscopy: Past, present, future,” *Biophysical Journal*, vol. 101, no. 12, pp. 2855–2870, 2011. [Online]. Available: <http://dx.doi.org/10.1016/j.bpj.2011.11.012>
- [88] P. Ferrand, J. Wenger, H. Rigneault, P. Ferrand, J. Wenger, H. R. Fluorescence, C. Spectroscopy, and P. Ferrand, “Fluorescence Correlation Spectroscopy To cite this version : HAL Id : hal-00624663 Fluorescence Correlation Spectroscopy,” 2015.
- [89] N. Amecke, “Fluorescence correlation spectroscopy,” *Methods in Molecular Biology*, vol. 1251, pp. 135–150, 2014.
- [90] Y. Jiang, B. Xu, A. Melnykov, G. M. Genin, and E. L. Elson, “Fluorescence Correlation Spectroscopy and Photon Counting Histograms in Finite, Bounded Domains,” *Biophysical Journal*, vol. 119, no. 2, pp. 265–273, 2020. [Online]. Available: <https://doi.org/10.1016/j.bpj.2020.05.032>
- [91] D. A. Gewirtz, “A critical evaluation of the mechanisms of action proposed for the antitumor effects of the anthracycline antibiotics adriamycin and daunorubicin,” *Biochemical Pharmacology*, vol. 57, no. 7, pp. 727–741, 1999.
- [92] C. Kleusch, C. Monzel, K. C. Sridhar, B. Hoffmann, A. Csiszár, and R. Merkel, “Fluorescence correlation spectroscopy reveals interaction of some microdomain-associated lipids with cellular focal adhesion sites,” *International Journal of Molecular Sciences*, vol. 21, no. 21, pp. 1–18, 2020.
- [93] M. Wachsmuth, T. Weidemann, G. Müller, U. W. Hoffmann-Rohrer, T. A. Knoch, W. Waldeck, and J. Langowski, “Analyzing intracellular binding and

- diffusion with continuous fluorescence photobleaching,” *Biophysical Journal*, vol. 84, no. 5, pp. 3353–3363, 2003.
- [94] E. S. Misteli and Tom, “Mobility and immobility of chromatin in transcription and genome stability Evi,” *Curr Opin Genet Dev.*, vol. 17, no. 5, pp. 435–442, 2007.
- [95] R. Peters, “Fluorescence Photobleaching Techniques Reiner Peters The,” in *Fluorescence Microscopy: From Principles to Biological Applications, Second Edition*, 2017, pp. 339–363.
- [96] A. Delon, Y. Usson, J. Derouard, T. Biben, and C. Souchier, “Photobleaching, mobility, and compartmentalisation: Inferences in fluorescence correlation spectroscopy,” *Journal of Fluorescence*, vol. 14, no. 3, pp. 255–267, 2004.
- [97] C. Hodges, R. P. Kafle, J. D. Hoff, and J. C. Meiners, “Fluorescence Correlation Spectroscopy with Photobleaching Correction in Slowly Diffusing Systems,” *Journal of Fluorescence*, vol. 28, no. 2, pp. 505–511, 2018.
- [98] J. S. Lewis, Z. Barani, A. S. Magana, and F. Kargar, “ce pte d M us pt,” pp. 0–31, 2019.
- [99] S. Chen, Y. L. Yu, and J. H. Wang, “Inner filter effect-based fluorescent sensing systems: A review,” *Analytica Chimica Acta*, vol. 999, pp. 13–26, 2018. [Online]. Available: <https://doi.org/10.1016/j.aca.2017.10.026>
- [100] P. Changenet-Barret, T. Gustavsson, D. Markovitsi, I. Manet, and S. Monti, “Unravelling molecular mechanisms in the fluorescence spectra of doxorubicin in aqueous solution by femtosecond fluorescence spectroscopy,” *Physical Chemistry Chemical Physics*, vol. 15, no. 8, pp. 2937–2944, 2013.

- [101] M. Than Htun, “Photophysical study on daunorubicin by fluorescence spectroscopy,” *Journal of Luminescence*, vol. 129, no. 4, pp. 344–348, 2009.
- [102] S. D. Hettiarachchi, R. M. Graham, K. J. Mintz, Y. Zhou, S. Vanni, Z. Peng, and R. M. Leblanc, “Triple conjugated carbon dots as a nano-drug delivery model for glioblastoma brain tumors,” *Nanoscale*, vol. 11, no. 13, pp. 6192–6205, 2019.
- [103] F. Barcelo, J. Martorell, F. Gavilanes, and J. M. Gonzalez-Ros, “Equilibrium binding of daunomycin and adriamycin to calf thymus DNA,” *Biochemical Pharmacology*, vol. 37, no. 11, pp. 2133–2138, 1988.
- [104] L. Song, V. H. Ho, C. Chen, Z. Yang, D. Liu, R. Chen, and D. Zhou, “Efficient, pH-Triggered Drug Delivery Using a pH-Responsive DNA-Conjugated Gold Nanoparticle,” *Advanced Healthcare Materials*, vol. 2, no. 2, pp. 275–280, 2013.
- [105] P. Mohan and N. Rapoport, “Doxorubicin as a Molecular Nanotheranostic Agent.pdf,” vol. 7, no. 6, pp. 1959–1973, 2010.
- [106] Y. Wang and Z. Xu, “Interaction mechanism of doxorubicin and SWCNT: Protonation and diameter effects on drug loading and releasing,” *RSC Advances*, vol. 6, no. 1, pp. 314–322, 2015.
- [107] S. R. Byrn and G. D. Dolch, “Analysis of binding of daunorubicin and doxorubicin to DNA using computerized curve-fitting procedures,” *Journal of Pharmaceutical Sciences*, vol. 67, no. 5, pp. 688–693, 1978.

- [108] G. Gołuński, A. Borowik, A. Lipińska, M. Romanik, N. Derewońko, A. Woźwodzka, and J. Piosik, "Pentoxifylline affects idarubicin binding to DNA," *Bioorganic Chemistry*, vol. 65, pp. 118–125, 2016.
- [109] J. W. Taanman, "The mitochondrial genome: Structure, transcription, translation and replication," *Biochimica et Biophysica Acta - Bioenergetics*, vol. 1410, no. 2, pp. 103–123, 1999.
- [110] T. Lei, S. Srinivasan, Y. Tang, R. Manchanda, A. Nagesetti, A. Fernandez-Fernandez, and A. J. McGoron, "Comparing cellular uptake and cytotoxicity of targeted drug carriers in cancer cell lines with different drug resistance mechanisms," *Nanomedicine: Nanotechnology, Biology, and Medicine*, vol. 7, no. 3, pp. 324–332, 2011. [Online]. Available: <http://dx.doi.org/10.1016/j.nano.2010.11.004>
- [111] T. Kalwarczyk, K. Kwapiszewska, K. Szczepanski, K. Sozanski, J. Szymanski, B. Michalska, P. Patalas-Krawczyk, J. Duszynski, and R. Holyst, "Apparent Anomalous Diffusion in the Cytoplasm of Human Cells: The Effect of Probes' Polydispersity," *Journal of Physical Chemistry B*, vol. 121, no. 42, pp. 9831–9837, 2017.
- [112] R. Jones, "Cellular and Nuclear Degradation during Apoptosis," *Bone*, vol. 23, no. 1, pp. 1–7, 2014. [Online]. Available: <https://www.ncbi.nlm.nih.gov/pmc/articles/PMC3624763/pdf/nihms412728.pdf>
- [113] F. Yang, S. S. Teves, C. J. Kemp, and S. Henikoff, "Doxorubicin, DNA torsion, and chromatin dynamics," *Biochimica et Biophysica Acta - Reviews on Cancer*, vol. 1845, no. 1, pp. 84–89, 2014. [Online]. Available: <http://dx.doi.org/10.1016/j.bbcan.2013.12.002>

- [114] Z. Farhane, F. Bonnier, O. Howe, A. Casey, and H. J. Byrne, “Doxorubicin kinetics and effects on lung cancer cell lines using in vitro Raman microspectroscopy: binding signatures, drug resistance and DNA repair,” *Journal of Biophotonics*, vol. 11, no. 1, 2018.
- [115] M. Kellis, B. Wold, M. P. Snyder, B. E. Bernstein, A. Kundaje, G. K. Marinov, L. D. Ward, E. Birney, G. E. Crawford, J. Dekker, I. Dunham, L. L. Elnitski, P. J. Farnham, E. A. Feingold, M. Gerstein, M. C. Giddings, D. M. Gilbert, T. R. Gingeras, E. D. Green, R. Guigo, T. Hubbard, J. Kent, J. D. Lieb, R. M. Myers, M. J. Pazin, B. Ren, J. A. Stamatoyannopoulos, Z. Weng, K. P. White, and R. C. Hardison, “Defining functional DNA elements in the human genome,” *Proceedings of the National Academy of Sciences of the United States of America*, vol. 111, no. 17, pp. 6131–6138, 2014.
- [116] V. Elgart, J. R. Lin, and J. Loscalzo, “Determinants of drug-target interactions at the single cell level,” *PLoS Computational Biology*, vol. 14, no. 12, pp. 1–23, 2018.
- [117] G. Bubak, K. Kwapiszewska, T. Kalwarczyk, K. Bielec, T. Andryszewski, M. Iwan, S. Bubak, and R. Hołyst, “Quantifying Nanoscale Viscosity and Structures of Living Cells Nucleus from Mobility Measurements,” *The Journal of Physical Chemistry Letters*, pp. 294–301, 2020.
- [118] A. Jagusiak, K. Chlopaś, G. Zemanek, P. Wolski, and T. Panczyk, “Controlled release of doxorubicin from the drug delivery formulation composed of single-walled carbon nanotubes and congo red: A molecular dynamics study and dynamic light scattering analysis,” *Pharmaceutics*, vol. 12, no. 7, pp. 1–21, 2020.

- [119] M. Wachsmuth, T. A. Knoch, and K. Rippe, “Dynamic properties of independent chromatin domains measured by correlation spectroscopy in living cells,” *Epigenetics and Chromatin*, vol. 9, no. 1, pp. 1–20, 2016.
- [120] A. Rabbani, R. M. Finn, A. A. Thambirajah, and J. Ausió, “Binding of antitumor antibiotic daunomycin to histones in chromatin and in solution,” *Biochemistry*, vol. 43, no. 51, pp. 16 497–16 504, 2004.
- [121] H. Fritzsche, U. Wähnert, J. B. Chaires, N. Dattagupta, F. B. Schlessinger, and D. M. Crothers, “Anthracycline Antibiotics. Interaction with DNA and Nucleosomes and Inhibition of DNA Synthesis,” *Biochemistry*, vol. 26, no. 7, pp. 1996–2000, 1987.
- [122] S. M. Mirkin, “DNA Topology: Fundamentals,” *Encyclopedia of Life Sciences*, no. c, pp. 1–11, 2001.
- [123] A. Manuscript, “Europe PMC Funders Group Investigating DNA supercoiling in eukaryotic genomes,” vol. 16, no. 6, pp. 379–389, 2017.
- [124] M. R. Redinbo, L. Stewart, P. Kuhn, J. J. Champoux, and W. G. Hol, “Crystal structures of human topoisomerase I in covalent and noncovalent complexes with DNA,” *Science*, vol. 279, no. 5356, pp. 1504–1513, 1998.
- [125] B. Pogorelcnik, A. Perdih, and T. Solmajer, “Recent Developments of DNA Poisons - Human DNA Topoisomerase IIalpha; Inhibitors - as Anticancer Agents,” *Current Pharmaceutical Design*, vol. 19, no. 13, pp. 2474–2488, 2013.
- [126] F. He, W. Borchers, T. Song, X. Wei, M. Das, L. Chen, G. W. Daughdrill, and J. Chen, “Interaction between p53 N terminus and core domain regulates specific and nonspecific DNA binding,” *Proceedings of the National Academy*

- of Sciences of the United States of America*, vol. 116, no. 18, pp. 8859–8868, 2019.
- [127] K. Kawane, K. Motani, and S. Nagata, “DNA degradation and its defects,” *Cold Spring Harbor Perspectives in Biology*, vol. 6, no. 6, 2014.
- [128] S. Singh, D. K. Makwana, T. Buckley, A. Agrawal, S. V. Koduru, and A. K. Tiwari, “Clinical significance of PARP-1 inhibitors in cancer chemotherapy,” *Translational Clinical Biology*, vol. 1, no. 1, p. 10, 2013.
- [129] K. Rippe, “Dynamic organization of the cell nucleus,” *Current Opinion in Genetics and Development*, vol. 17, no. 5, pp. 373–380, 2007.
- [130] B. Liu, B. Poolman, and A. J. Boersma, “Ionic Strength Sensing in Living Cells,” *ACS Chemical Biology*, vol. 12, no. 10, pp. 2510–2514, 2017.
- [131] A. Zidovska, “The rich inner life of the cell nucleus: dynamic organization, active flows, and emergent rheology,” *Biophysical Reviews*, vol. 12, no. 5, pp. 1093–1106, 2020.
- [132] S. Wang, J.-h. Su, B. J. Beliveau, B. Bintu, J. R. Moffitt, and C.-t. Wu, “Single Chromosomes,” vol. 544, no. 2011, pp. 2955–2960, 2016.
- [133] S. Garattini, I. Fuso Nerini, and M. D’Incalci, “Not only tumor but also therapy heterogeneity,” *Annals of Oncology*, vol. 29, no. 1, pp. 13–18, 2018.
- [134] Z. B. Starkewolf, L. Miyachi, J. Wong, and T. Guo, “X-ray triggered release of doxorubicin from nanoparticle drug carriers for cancer therapy,” *Chemical Communications*, vol. 49, no. 25, pp. 2545–2547, 2013.

- [135] P. Ma and R. J. Mumper, “Anthracycline nano-delivery systems to overcome multiple drug resistance: A comprehensive review,” *Nano Today*, vol. 8, no. 3, pp. 313–331, 2013.
- [136] V. Kumar, S. Palazzolo, S. Bayda, G. Corona, G. Toffoli, and F. Rizzolio, “DNA nanotechnology for cancer therapy,” *Theranostics*, vol. 6, no. 5, pp. 710–725, 2016.
- [137] J. J. Landry, P. T. Pyl, T. Rausch, T. Zichner, M. M. Tekkedil, A. M. Stütz, A. Jauch, R. S. Aiyar, G. Pau, N. Delhomme, J. Gagneur, J. O. Korb, W. Huber, and L. M. Steinmetz, “The genomic and transcriptomic landscape of a hela cell line,” *G3: Genes, Genomes, Genetics*, vol. 3, no. 8, pp. 1213–1224, 2013.

## List of abbreviations

---

<b>ACF</b>	autocorrelation curve
<b>ANT</b>	anthracycline
<b>APDs</b>	avalanche photodiodes
<b>ATCC</b>	American Type Culture Collection
<b>bp</b>	base pair
<b>CD</b>	circular dichroism spectroscopy
<b>CP</b>	continuous fluorescence photobleaching
<b>ct</b>	calf thymus
<b>CV</b>	cyclic voltammetry
<b>D</b>	diffusion coefficient
<b>DMEM</b>	Dulbecco's modified Eagle's medium
<b>DNA</b>	deoxyribonucleic acid
<b>DNR</b>	daunorubicin hydrochloride

<b>DOX</b>	doxorubicin hydrochloride
<b>DSC</b>	differential scanning calorimetry
<b>EG</b>	ethylene glycol
<b>EPR</b>	epirubicin hydrochloride
<b>eq</b>	equilibrium state
<b>FBS</b>	fetal bovine serum
<b>FCS</b>	fluorescence correlation spectroscopy
<b>FLIP</b>	fluorescence loss in photobleaching
<b>FRAP</b>	fluorescence recovery after photobleaching
<b>GFP</b>	green fluorescent protein
<b>IDR</b>	idarubicin hydrochloride
<b>ITC</b>	isothermal titration calorimetry
<b>K</b>	equilibrium constant
<b>LSM</b>	Laser Scanning Microscopes
<b>MB</b>	molecule brightness
<b>NA</b>	numerical aperture
<b>NMR</b>	nuclear magnetic resonance spectroscopy
<b>PBS</b>	phosphate buffered saline

<b>PDI</b> s	protein-DNA interactions
<b>PEG</b>	polyethylene glycol
<b>PML</b>	promyelocytic leukemia protein
<b>PPI</b> s	protein-protein interactions
<b>RLS</b>	resonance light scattering spectroscopy
<b>ROI</b>	region of interest
<b>SPR</b>	surface plasmon resonance spectroscopy
<b>TCSPC</b>	Time-correlated single photon counting
<b>Uv-Vis</b>	UV-Visible

# Parameters in a typical measurement

---

## B.1 Equilibrium constants determination with FCS method

In this section, we illustrate the critical parameters used in a typical measurement with FCS method. All of the anthracyclines were measured under the similar experimental conditions (i.e. emission filters, excitation laser power), thus the parameters were comparable.

Table B.1: Critical parameters used in a typical measurement for different anthracyclines.

Anthracyclines	$V_{\text{eff}}$ (fL)	$n$	$N_{\text{ANT}}$	$D_{\text{ANT}}$ ( $\times 10^{-10} \text{ m}^2 \cdot \text{s}^{-1}$ )	$D_{\text{ANT-DNA}}$ ( $\times 10^{-10} \text{ m}^2 \cdot \text{s}^{-1}$ )	$\text{MB}_{\text{ANT}}$ (cnts)	$\text{MB}_{\text{ANT-DNA}}$ (cnts)
DOX-DNA (plasmid DNA)	0.24	866.5	4.9	403	5.8	1158.6	175.0
DOX-DNA (2500 bp)	0.29	806.5	6.2	422	3.8	1001.6	171.6
DNR-DNA (2500 bp)	0.24	806.5	5.7	384	4.9	753.8	115.8
EPR-DNA (2500 bp)	0.23	806.5	5.7	418	3.7	741.0	78.9

## B.2 Equilibrium constants determination with single-MB analysis method

In this section, we illustrated the critical parameters acquired in a typical measurement with MB analysis method. All of the anthracyclines were measured under the same experimental conditions (i.e. emission filters, excitation laser power), thus the obtained MB parameters for each component are comparable. Take DOX-DNA interaction as an example: first of all, we calibrated the size of the confocal volume ( $V_{eff}$ ) by using the standard calibration dye–rhodamine 110 with FCS method. Then, we let DOX molecules diffuse in and out of the confocal volume, and we recorded the photon count rate of DOX molecules ( $\langle F(t) \rangle_{DOX}$ ) over time  $t$ . By fitting the ACF of DOX molecules, we knew the number of DOX molecules ( $N_{DOX}$ ). The MB of DOX ( $\alpha$ ) was calculated by dividing  $\langle F(t) \rangle_{DOX}$  with  $N_{DOX}$  ( $\alpha = \frac{\langle F(t) \rangle_{DOX}}{N_{DOX}}$ ). Similarly, we recorded the photon count rate for DOX-DNA complexes ( $\langle F(t) \rangle_{DOX-DNA}$ ) and DOX-(DOX-DNA) complexes ( $\langle F(t) \rangle_{DOX-(DOX-DNA)}$ ) respectively. By dividing  $\langle F(t) \rangle_{DOX-DNA}$  and  $\langle F(t) \rangle_{DOX-(DOX-DNA)}$  with  $N_{DOX}$  separately, we got the MB of DOX-DNA complexes ( $\gamma_1$ ) and DOX-(DOX-DNA) complexes ( $\gamma_2$ ) respectively. We acquired these parameters for DNR, EPR, and IDR the same way as DOX.

Table B.2: Critical parameters used in a typical single MB analysis method.

<b>Anthracyclines</b>	<b><math>V_{eff}</math> (fL)</b>	<b><math>N_{ANT}</math></b>	<b><math>\alpha</math> (cnts)</b>	<b><math>\gamma_1</math> (cnts)</b>	<b><math>\gamma_2</math> (cnts)</b>
DOX	0.28	5.5	1020.4	93.3	447.5
DNR	0.28	7.7	586.0	85.4	328.8
EPR	0.30	8.1	679.2	44.8	336.3
IDR	0.24	4.5	993.9	137.2	434.4

### B.3 DNA concentration calculation in the single cells

We calculated the available DNA (actually bp) concentration in nucleus of single cells according to the formula [116]:

$$C_{DNA} = \frac{N_{bp}}{V_{nucleus} \cdot N_A} \quad (\text{B.1})$$

where  $N_{bp}$  is the number of bp in nucleus,  $V_{nucleus}$  is the volume of nucleus, and  $N_A$  is the Avogadro number. Human genome contains  $3.1 \times 10^9$  bp/haploid genome. A HeLa cell is hypertriploid [137], one cell should contain  $9.3 \times 10^9$  bp, while a fibroblast cell is diploid, one cell should contain  $6.2 \times 10^9$  bp. Since each 3.1 bp form a binding site, the available bp number in a HeLa cell should be  $3.1 \times 10^9$  bp while a fibroblast cell contains  $2.0 \times 10^9$  bp. The final DNA concentration of each type of cell is listed in table B.3.

Table B.3: Base pair concentration calculation in single cells.

Cell lines	Available bp number ( $10^9$ )	$V_{nucleus}$ ( $10^{-13}$ L)	$C_{DNA}$ ( $10^{-3}$ M)
HeLa	3.1	6.9	8.0
Fibroblast	2.0	5.0	10.0